smartLipids and smartCrystals for improved dermal delivery of anti-pollution actives

Inaugural-Dissertation
to obtain the academic degree
Doctor rerum naturalium (Dr. rer. nat.)

submitted to the Department of Biology, Chemistry and Pharmacy
at Freie Universität Berlin

by

Daniel Köpke

2019

The work was performed under the supervision of Prof. Dr. Rainer H. Müller at the Institute of Pharmacy, Freie Universität Berlin from September 2016 to December 2019.

1st Reviewer:	Prof. Dr. Rainer H. Müller
2nd Reviewer:	Prof. Dr. Michael Dittgen

Date of defense: 14 Feb. 2020

You can never know everything and part of what you know is always wrong. Perhaps even the most important part. A portion of wisdom lies in knowing that. A portion of courage lies in going on anyway.

James Oliver Rigney, Jr.

Table of contents

1. Introduction 1
1.1. Health concerns by air pollution 1
1.2. Barrier function of the skin 1
1.3. Impaired barrier function 2
1.4. Pharmacological effects of pollutants on skin 3
1.4.1. Particulate matter 4
1.4.2. AhR-mediated reactive oxygen species 4
1.4.3. UV/ozone 5
1.5. Anti-pollution strategies 5
1.5.1. Skin barrier reinforcement 5
1.5.2. Antioxidants 6
1.5.3. Aryl hydrocarbon receptor antagonists 6
1.5.4. Symptomatic therapy 7
1.5.4.1. Anti-inflammatory drugs 7
1.5.4.2. Collagen homeostasis 7
1.5.4.3. Pigmentation 7
1.6. smartLipids 8
1.6.1. History of smartLipids 8
1.6.1.1. Solid lipid nanoparticles (SLN) 8
1.6.1.2. Nanostructured lipid carriers (NLC) 9
1.6.1.3. smartLipids 9
1.6.1.4. Advantages of lipid nanoparticles of all generations 10
1.6.2. smartLipids 2nd skin 11
1.6.2.1. Natural lipid composition in the human SC 11
1.6.2.2. smartLipids 2nd skin Q10 13
1.6.3. PER smartLipids 13

Table of contents

1.7. smartCrystals 14
1.7.1. History of smartCrystals 14
1.7.1.1. nanocrystals 14
1.7.1.2. smartCrystals 15
1.7.2. Symurban smartCrystals 16
1.8. Production of smartLipids and smartCrystals 17
1.8.1. High pressure homogenization 17
1.8.2. Wet bead milling 18
1.9. Particle size analysis 19
1.9.1. Laser diffraction 19
1.9.2. Photon correlation spectroscopy 20
1.9.3. Light microscopy 20
1.10. Aims of the thesis 22
1.11. References 24
2. Development of smartLipids 2nd skin to reinforce impaired skin lipid barrier 33
Abstract 33
2.1. Introduction 34
2.2. Materials and methods 36
2.2.1. Materials 36
2.2.2. Methods 37
2.2.2.1. Production of smartLipids 2nd skin 37
2.2.2.2. Characterization of smartLipids 2nd skin 38
2.2.2.2.1 Production of smartLipids suspensions 38
2.2.2.2.2 Melting behavior 38
2.3. Results and Discussion 39
2.3.1. Composition of lipid mixture 39

2.3.2. Surfactant screening 40
2.3.3. Preservation of smartLipids 2nd skin 43
2.3.4. Loading with model active coenzyme Q10 44
2.4. Conclusion 45
2.5. References 46
3. Inverse loading method for the production of smartLipids loaded with whitening agent phenylethyl resorcinol 49
Abstract 49
3.1. Introduction 50
3.2. Materials and methods 51
3.2.1. Materials 51
3.2.2. Lipid screening 52
3.2.3. Production of PER loaded lipid nanoparticles on lab scale 52
3.2.4. Production of PER loaded lipid nanoparticles on large scale 53
3.2.5. Particle size analysis 53
3.2.6. Determination of encapsulation efficacy 53
3.3. Results and discussion 54
3.3.1. Definition of requirements to the new formulations 54
3.3.2. Lipid screening and inverse loading method 55
3.3.3. Inverse loading of PER into lipid matrices 56
3.3.4. Production of PER lipid nanoparticles 58
3.3.5. Characterisation of best 3 formulations 61
3.3.6. Increase of particle content 62
3.3.7. Establishment of large-scale production on LAB 60 63
3.4. Conclusion 66
3.5. References 67

4. Phenylethyl resorcinol smartLipids for skin brightening – increased loading & chemical stability 69

4.1. Abstract 69

5. Determination of crystallinity of PER smartLipids 89
5.1. Introduction 89
5.2. Materials and methods 90
5.2.1. Materials 90
5.2.2. Methods 91
5.2.2.1. Production of analyzed materials 91
5.2.2.2. Differential scanning calorimetry 91
5.2.2.3. X-ray crystallography 92
5.3. Results and discussion 93
5.3.1. Differential scanning calorimetry 93
5.3.2. X-ray crystallography 96
5.4. Conclusion 98
5.5. References 98
6. Formulation of anti-pollution agent Symurban as smartCrystals for increased saturation solubility and improved dermal bioavailability 99
6.1. Abstract 99
6.2. Introduction 100
6.3. Materials and methods 103
6.3.1. Materials 103
6.3.2. Production of Symurban smartCrystals 104
6.3.2.1. High pressure homogenization 104
6.3.2.2. Bead mill 104
6.3.3. Particle characterization 104
6.3.3.1.1 Photon correlation spectroscopy (PCS) 104
6.3.3.1.2 Laser diffraction (LD) 105
6.3.3.1.3 Light microscopy 105
6.3.4. Gas chromatography–mass spectrometry (GC-MS) 105

6.3.5. Determination of saturation solubility 106
6.3.6. *in vivo* skin penetration study 106
6.4. Results and discussion 107
6.4.1. Production method of Symurban smartCrystals 107
6.4.2. Screening of surfactants 109
6.4.3. Storage stability of Symurban smartCrystals 111
6.4.4. Saturation solubility 113
6.4.5. *In vivo* skin penetration profile 115
6.5. Conclusion 117
6.6. References 117
7. Summary 121
8. Zusammenfassung 123
9. Abbreviations 125
10. List of publications 127
11. Curriculum Vitae 131

1. Introduction

1.1. Health concerns by air pollution

Modern society and technological progress provides a lot of benefits to the individual humans, such as effective health care, easy and quick transport to any place in the world, any imaginable nutrition, consumables and, generally, all kinds of other conveniences. But the flipside of this coin is that environmental consequences of human behavior is not always considered when people want to have their individual needs satisfied. Beside the exploitation of the earth's resources, air pollution is thereupon certainly one of the severest consequences from modern people's lifestyle in the western world.

The world health organization (WHO) defines pollution as "contamination of the environment by any agent that modifies the natural characteristics of the atmosphere. Pollutants of major public health concern include particulate matter (PM), carbon monoxide, ozone, nitrogen dioxide and sulfur dioxide" (WHO, 2019). A special focus lies on PM, as the WHO evaluates it as the biggest health risk (WHO, 2019). PM can carry toxic organic substances, such as polycyclic and halogenated aromatic hydrocarbon, that derive from incomplete burning of organic materials (Alomirah et al., 2011) and initiate a variety of toxic pharmacological processes (cf. chapter 1.4.1).

According to the WHO, every year more than 4 million people die early from the consequences of outdoor air pollution (Li et al., 2019). Especially particulate pollution usually is associated to cardiovascular and respiratory diseases (Brunekreef and Holgate, 2002; Manojkumar and Srimuruganandam, 2019; Seaton et al., 1995) and sometimes even to cancer (Pope et al., 2002; White et al., 2019). Therefore it is one of the most serious modern health issues.

1.2. Barrier function of the skin

While the cardiovascular and respiratory effects of air pollution are well-studied, the effects to other organs such as the skin have been underestimated. As the biggest organ having the most contact to the environment and therefore also to pollutants, it has long time been barely in the focus of research. This might be the case because the healthy (i.e. undamaged) skin is an effective barrier against exogenous hazards.

The outer epidermis is a complexly composed system that generates diverse protective and defensive mechanisms, e.g. the protection from water loss (Elias and Menon, 1991),

antimicrobial activity (Oren et al., 2003), antioxidant activity (Korkina, 2016) and protection against UV radiation (Pearse and Marks, 1983). The outermost barrier, the stratum corneum (SC) is composed of multiple layers of anucleate corneocytes and lamellar layers of lipids being composed of ceramides, cholesterol and free fatty acids (Elias and Menon, 1991).

A critical peculiarity of the SC lipids is its crystalline structure. The SC lipids are secreted from the stratum granulosum in form of so-called lamellar bodies, which play a critical role in the barrier function of the skin (Coderch et al., 2003; Elias and Wakefield, 2014; Feingold, 2012). This liquid crystalline structure requires a respective quantitative composition of the SC lipids. With the "brick and mortar" composition of the stratum corneum (Nemes and Steinert, 1999) it functions as passive diffusion barrier in both directions: for preventing the skin from dehydration but also keeping hydrophilic and lipophilic toxins (i.e. pollutants) off the skin (Wickett and Visscher, 2006).

1.3. Impaired barrier function

The healthy natural skin lipid barrier can be damaged by diverse various factors, e.g. mechanical strain, overly frequent washing, application of ethanol-based or harsh skin care products, excessive solar exposure, genetics or the age of the skin. For example a sodium dodecyl sulphate-treated skin took more than two weeks until the transepithelial water loss (TEWL) and skin hydration were fully recovered (Wilhelm et al., 1994). A damaged skin barrier is also associated to various skin diseases, e.g. atopic dermatitis (Cork et al., 2009; Yamamoto et al., 1991), psoriasis (Harding, 2004; Motta S. et al., 1994), rosacea (Ní Raghallaigh et al., 2012) dry skin (Rawlings, 2003) and winter xerosis (Harding, 2004). Differences in the SC lipid profile, e.g. in atopic dermatitis, proofed to impair the formation of the characteristic lamellar bodies, reducing the density of package of the corneocytes and thus impair the impermeability of the skin barrier (Coderch et al., 2003; Elias and Wakefield, 2014; Feingold, 2012).

Further, studies show that the penetration of lipophilic model substances like estradiol (Essa et al., 2003) or nicotinic acid ester (Gehring et al., 1997) is increased when the skin barrier is deliberately damaged by electroporation (Essa et al., 2003) or degreasing the skin with organic solvent (Gehring et al., 1997). Thus, damaged skin leads to an increased penetration of air pollutants, e.g. polycyclic aromatic and halogenated hydrocarbon (PAH und HAH) from airborne PM. PM itself proofed to penetrate into the epidermal tissue being deliberately damaged (Jin et al., 2018). This leads to inflammatory response and expression of matrix

metallopeptidases (MMP), leading to collagen degradation (Jin et al., 2018). All in all, the exposure to PM proofed to disrupt the stratum corneum integrity (Pan et al., 2015). Therefore, the exposure of damaged skin to a polluted surrounding like it is present in most urban regions in the world (WHO, 2019), might lead to a "vicious circle" that requires therapeutic intervention.

1.4. Pharmacological effects of pollutants on skin

Recent studies show, that dermal diseases and skin aging are associated to air pollution. A variety of pharmacological mechanisms has been discovered, describing how substances that derive from airborne pollution particles can damage the skin (Kim et al., 2016). Air pollution is a complex phenomenon. Therefore only the most relevant aspects of the pollution pharmacology are discussed in the following to give a better understanding of pollution-induced processes in the skin, that are to be controlled by the developed technologies. A brief and simplified overview over these processes and potential intervention points are given in Fig. 1.

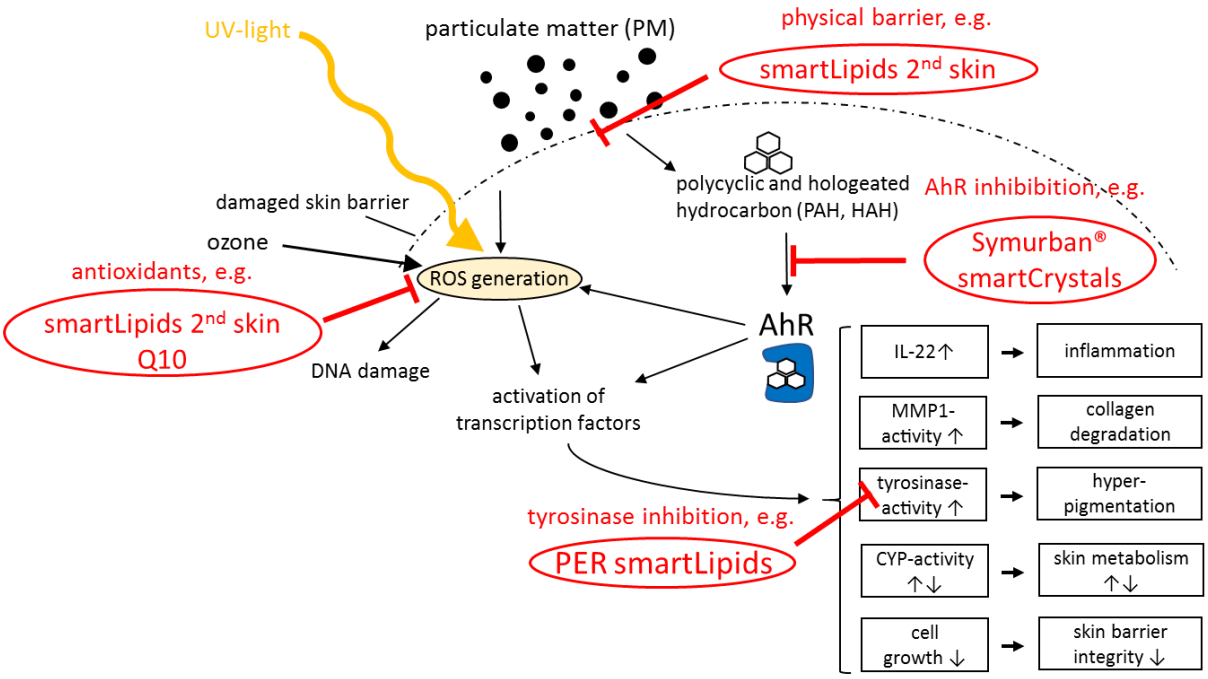

Fig. 1: Simplified overview over pollution-induced skin pharmacology shows 4 anti-pollution strategies for which a galenic solution was to be developed in this thesis. Figure was modified after (Kim et al., 2016).

1.4.1. Particulate matter

According to the WHO, PM "affects more people than any other pollutant" (WHO, 2019). PM is usually classified after its particle size into $PM_{0.1}$ (<0.1 µm), $PM_{2.5}$, (< 2.5 µm) and PM_{10} (2.5-10 µm) whereas the chemical composition is not further defined (Kampa and Castanas, 2008). However, besides harmless materials of mineral origin (e.g. metal carbonates, silicates and oxides), PM also contains organic components with hazardous potential, e.g. PAH and HAH. PAH and HAH originate from incomplete burning of organic material and are transported by airborne fine dust particles (Alomirah et al., 2011). More or less independent from the PM particle size, PM-originated PAH and HAH are able to penetrate the skin. When penetrated, PAH and HAH bind to the aryl hydrocarbon receptor (AhR) (Denison and Heath-Pagliuso, 1998; Denison and Nagy, 2003; Hankinson, 1995; Marlowe and Puga, 2005), a specific ligand-activated transcription factor activating various pharmacological processes, e.g. interleukin- and TNFα-mediated inflammation (Esser et al., 2009; Kim et al., 2014; Stockinger et al., 2014; Veldhoen et al., 2008; Xue et al., 2018), collagen degradation by matrix metallopeptidases (Ono et al., 2013; Qiao et al., 2017), pigmentation disorders by melanogenesis (Luecke et al., 2010; Nakamura et al., 2013) or reduced skin barrier integrity and delayed skin repair by reduced keratinocyte proliferation (Haas et al., 2016) (Fig. 1).

1.4.2. AhR-mediated reactive oxygen species

The activation of the AhR also activates the CYP-metabolism which for itself leads to the production of reactive oxygen species (ROS) and thus causes oxidative stress in the tissue (Dietrich, 2016; Fujii-Kuriyama and Mimura, 2005; Kim et al., 2016). This oxidative stress will further trigger the activation of the mentioned pharmacological processes (Poljšak et al., 2012; Rinnerthaler et al., 2015). The AhR proofed to be associated to various skin diseases, such as vitiligo (Behfarjam and Jadali, 2018), psoriasis (Beránek et al., 2018; Kim et al., 2014) scleroderma (Noakes, 2017), neurodermatitis (Hidaka et al., 2017) and acne vulgaris (Fabbrocini et al., 2015). Further, the promotion of dermal carcinogenesis is discussed (Kolluri et al., 2017; Matsumoto et al., 2007; Xue et al., 2018). Therefore both, the AhR-activity and the intercellular ROS levels seem to be the central elements in the pollution-pharmacology and thus allow an effective therapeutic intervention.

1.4.3. UV/ozone

UV radiation activates the melanogenetic pathway by the activation of the melanocortin 1 receptor and following release of melanocyte stimulating hormone. This way, melanocyte proliferation and the production of enzymes from the melanogenetic pathway (e.g. tyrosinase, tyrosinase-related protein-1 and 2) is activated (D'Mello et al., 2016; Riley, 2003; Videira et al., 2013). These enzymes convert L-tyrosine into pheomelanin (red-yellow) and eumelanin (brown-black). Increased UV-strain to the skin, e.g. by a damaged ozone content in the atmosphere thus may lead to pigmentation disorders.

On the other hand, ozone itself is considered to be air pollutant and can cause skin-damage. Ozone induces ROS, damages lipids by lipid peroxidation in the SC and thereby weakens the integrity of the lipid barrier. Inflammatory response and carcinogenesis can be the consequence (Cotovio et al., 2001; Thiele et al., 1997; Valacchi et al., 2002). Ozone also interferes with the AhR and induces CYP1A1, CYP1A2 and CYP1B1-mediated inflammatory response in the skin (Afaq et al., 2009), and sensitizes the skin against UV-induced tanning (Jux et al., 2011). Hence, ozone is leading to increased ROS-levels in the skin.

1.5. Anti-pollution strategies

1.5.1. Skin barrier reinforcement

One strategy is the strengthening of the natural skin barrier. The application of a silk polypeptide film on the skin proofed to reduce the absorption of fine carbon particles and reduced the TEWL (Schlay and Slootta, 2016). Similar effects could be observed by applying ceramides to the skin, normalizing the TEWL of sodium dodecyl sulphate damaged skin (Evonik Nutrition & Care GmbH, 2019). Also a electroporation- or solvent-damaged skin could be re-protected against penetration of lipophilic model drugs by phospholipid liposomes and a mixture of ceramides, cholesterol and free fatty acids (Essa et al., 2003; Gehring et al., 1997). However, incomplete or incorrect skin lipid mixtures might yield abnormal lamellar bodies (Coderch et al., 2003; Lodén and Raány, 2000), which impairs the skin integrity and even decline the resistance of the skin against pollutants in the long run. Therefore, for optimal reinforcement of a natural and effective anti-pollution skin barrier, it is important to use a lipid mixture, which is composed like the lipid mixture in the SC.

1.5.2. Antioxidants

As described in chapter 1.4.2 and shown in Fig. 1, ROS play an essential role in the anti-pollution and anti-aging pharmacology. An imbalance in the oxidant- and antioxidant system can be caused not only by AhR activation (Dietrich, 2016; Fujii-Kuriyama and Mimura, 2005), but also by other pollutants like ozone (Cotovio et al., 2001; Valacchi et al., 2002) but also by UV-light (Rittié and Fisher, 2002; Wenk et al., 2001). Therefore, either the production of ROS can be minimized, e.g. by the application of sunscreens (Mistry, 2017) or antioxidants can effectively be used in anti-pollution formulations to scavenge ROS present in the skin, and prevent the skin from inflammation, altered skin metabolism or post-inflammatory pigmentation (Juliano and Magrini, 2018; Mistry, 2017; Valacchi et al., 2016). However, many antioxidants like coenzyme Q10 (Sun et al., 2012), flavonoids like hesperidin (Romero et al., 2015), quercitin (Hatahet et al., 2016) or rutin (Pyo et al., 2016) are poorly soluble and thus poorly bioavailable in the skin. Therefore, an appropriate technological solution must be applied to reach an effective antioxidant concentration in the skin.

1.5.3. Aryl hydrocarbon receptor antagonists

A completely different approach it the use of active substances that inhibit the AhR. As discussed in chapter 1.4.1, the AhR plays an important role in the pollution-mediated regulation of ageing processes. There are several chemicals antagonizing the AhR, such as StemRegenin 1 (Boitano et al., 2010), 6,2',4'-Trimethoxyflavone (Murray et al., 2010), GNF351 (Smith et al., 2011) or CH-223191 (Kim et al., 2006), and thus might be interesting in preventing or treating anti-pollution induced damages. Nevertheless, all of these substances are developed for experimental purposes. None of these substances can be used in pharma or cosmetics because they are too expensive and/or are not regulatorily accepted for this purpose. In Contrast, Symurban (INCI: Benzylidene Dimethoxydimethylindanone) is also a competitive inhibitor of the AhR (Haarmann-Stemmann et al., 2015; Qiao et al., 2017; Tigges et al., 2014) and is regulatorily accepted and distributed by the company Symrise for pollution prevention. However, Symurban is also poorly soluble in water and thus requires an appropriate technological solution for sufficient dermal bioavailability.

1.5.4. Symptomatic therapy

It is also possible to treat the symptomatic pollution effects directly. As discussed in chapter 1.4.1, inflammatory response and redness, loss of elasticity and wrinkles by collagen degradation and irregular pigmentation by the induction of melanogenesis belong to the most important dermal clinical effects of air pollution.

1.5.4.1. *Anti-inflammatory drugs*

Inflammatory response to pollution can be controlled by the application of anti-inflammatory drugs. Some plant extracts and vegetable oils for example proved to have anti-inflammatory properties (Lin et al., 2017) and could thus be beneficial as adjuvants for anti-pollution formulae. Highly potent anti-inflammatory therapy, e.g. by glucocorticoids inhibits keratinocyte growth, can cause atrophy of the skin barrier and should thus be used reluctantly (Chedid, 1996). Therefore, a milder, indirect reduction of inflammatory response, e.g. by antioxidants (cf. chapter 1.5.2) is preferable in most cases.

1.5.4.2. *Collagen homeostasis*

The collagen degradation by MMP-1 and other MMP's is challenging to antagonize. Currently there are currently no cosmetic or pharmaceutical solutions directly using this pathway. But the collagen synthesis in the fibroblasts can be stimulated by some actives. Some highly specific oligopeptides have been developed to modulate the dermal collagen synthesis (Fields et al., 2009; Reddy et al., 2012). Introducing a lipophilic moiety such as a palmitic acid acylation, allows the formulation of a prodrug with sufficient dermal bioavailability. This way, pollution induced collagen degradation may be compensated. However, these highly specific oligopeptides (e.g. palmitoyl-tripeptide-1 (pal-GHK) or palmitoyl-pentapeptide-4 (pal-KTTKS)) are not easy to synthetize and thus comparatively expensive, limiting their field of application.

1.5.4.3. *Pigmentation*

The treatment of depigmentation disorders is a mayor challenge to the cosmetic market. Hydroquinone (HQ) alone or in combination with tretinoin and glucocorticoids were longtime regarded to be the gold standard treatment, being very effective but also causing many serious side effects and HQ was even suspected to cause cancer (Zhu and Gao, 2008). For good

reason HQ is only available on prescription and is no longer regulatorily accepted in cosmetic products distributed in the EU (European Parliament, 2009) and also in many other countries. Natural alternatives like kojic acid, arbutin, flavonoids or glabridin are traditionally used for whitening and assessed in their whitening activity by tyrosinase activity or in cell culture experiments. However, for most of them there is no clinical evidence for being effective in whitening at all (Solano et al., 2006). Some synthetic and semisynthetic actives have been developed showing clinically approved whitening effect, e.g. 4n-butylresorcinol (Huh et al., 2010; Kolbe et al., 2013), phenylethyl resorcinol (Vielhaber et al., 2007) or thiamidol (Arrowitz et al., 2019). Beside their poor bioavailability, all these active ingredients have in common, that they have a phenolic moiety in their chemical structure and thus are susceptible to oxidative and photodegradation. Therefore, an appropriate technological solution is again required.

1.6. smartLipids

1.6.1. History of smartLipids

1.6.1.1. *Solid lipid nanoparticles (SLN)*

The first generation of lipid nanoparticles, called solid lipid nanoparticles (SLN), was developed in 1991 (Gasco, 1991; Müller et al., 2000). They are composed of solid lipids (e.g. triglycerides, waxes) with a particle size of approximately 50 nm to 1000 nm (Müller et al., 2000), dispersed in an aqueous surfactant solution. Like prior nanoparticulate formulation approaches, such as nanoemulsions or liposomes, SLN can be produced with high pressure homogenization (cf. chapter 1.8.1.). Using lipids with a melting point between approximately 40 °C and 90 °C, the SLN can be manufactured in melted state by heating the lipids above their melting point in the manufacturing process. After cooling the product to room temperature, the nanosized lipid drops solidify and yield a long-term stable nanosuspension, which can be produced with minimum technical effort.

SLN can further be loaded with pharmaceutical or cosmetic actives, which then will be protected from chemical degradation, show increased dermal penetration as well as controlled drug release (Müller et al., 2000)(cf. chapter 1.6.1.4).

1.6.1.2. *Nanostructured lipid carriers (NLC)*

A disadvantage of the SLN is the high crystallinity of the lipid matrix, which considerably restricted the loading capacity and storage stability of the particles. Polymorphic transitions alter the solubility of the active ingredients in the lipid matrix, which can cause the active ingredient to be expelled from the particle during the storage process. This problem was partially solved in the second generation lipid nanoparticles, the NLC, which was developed in 1999 (Jenning et al., 2002, 2014; Müller et al., 2002). In contrast to SLN, only consisting of a single highly purified solid lipid in its matrix, NLC contain a blend of a solid and a liquid lipid (Müller et al., 2002; Müller et al., 2007). Since the solubility of cosmetic and pharmaceutical active ingredients in liquid lipid is often higher, NLC often allow significantly higher active loading than SLN. In addition, the incorporation of oil impairs the formation of regular crystal structures, which reduces polymorphic transitions and thus increases storage stability (Müller et al., 2002).

1.6.1.3. *smartLipids*

The third and latest generation of submicron lipid particles, the smartLipids was developed in 2014 (Müller et al., 2014; Ruick, 2015) and further improved the lipid suspensions in terms of loading capacity and storage stability. smartLipids are composed of a complex blend of up to 10 single lipid components including solid and liquid lipids. Due to its chaotic lipid structure, the crystallinity of the lipid particle is further decreased, allowing long-term storage with little or no polymorphic transitions, comprising the expel of the incorporated active (Ding et al., 2017; Müller et al., 2019; Ruick, 2015). The loading capacity for incorporated actives was further increased, which was demonstrated for three active examples in Fig. 2. This high active loading is not only interesting from a commercial perspective (higher loading of the particle concentrate means less smartLipids concentrate needs to be homogenized and thus lower costs for the manufacturer), but also might lead to higher active penetration: As smartLipids form an occlusive film on the skin (cf. chapter 1.6.2) having direct contact with the SC, the active concentration in the film (i.e. the active concentration in the lipid particle) will determine the penetration rate for the active. Thus, higher penetration can be predicted for smartLipids.

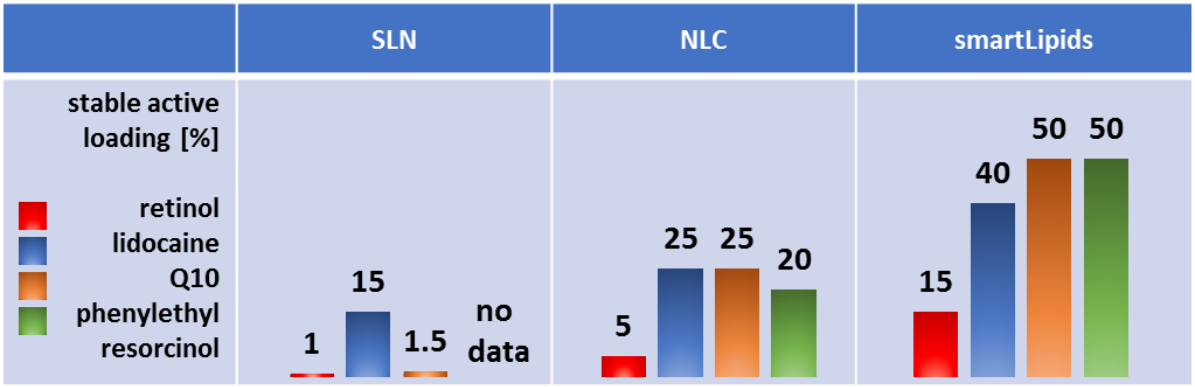

Fig. 2: Comparison of maximum loading capacities of retinol, lidocaine and phenylethyl resorcinol in SLN, NLC and smartLipids (Figure modified after (Müller et al., 2019))

1.6.1.4. *Advantages of lipid nanoparticles of all generations*

The lipid matrix of SLN, NLC and smartLipids is composed of natural ingredients like triglycerides, waxes, fatty acids and -alcohols, ceramides, etc. In contrast to for example polymeric nanoparticles, no toxic solvent or monomer residues are present in the particles. Therefore, they are regulatorily accepted for pharmaceutical, but also for cosmetic application. In many cases, so-called ECOCERT ingredients can be used for the stabilization of the particles. They are free of petrochemicals, GMO-free, free of skin-damaging and ecological questionable polyethylene glycol and are produced from renewable resources and with environmentally friendly processes (Groupe ECOCERT, 2019). In times when people are rising consciousness for aspects like ecology and sustainability, this is of particular importance for marketing and consumers' acceptance.

Due to the submicron particle size, SLN, NLC and smartLipids have an enormously increased surface area. Consequently, the particles adhere to the skin surface and form a thin, durable and occlusive film (Müller et al., 2013b; Müller et al., 2019). This film is able to repair and reinforce a damaged skin lipid film, normalize TEWL and skin hydration and provide an anti-pollution effect (Müller et al., 2013b; Müller et al., 2019).

Active ingredients are incorporated into SLN, NLC or smartLipids by dissolving them in the melted lipid matrix during the manufacturing process. Due to high loading of the particles and direct contact between the particle film and the skin, a high concentration gradient between the formulation and the target tissue and thus a high active flux into the skin (cf. chapter 1.7.1.1) can be predicted (Müller et al., 2007). The advanced penetration rate is further supported by the occlusion effect of SLN, NLC and smartLipids (Müller et al., 2013b; Müller et al., 2019; Pardeike, 2009).

Firmly encapsulated in the lipid particle, actives being susceptible to oxidation can be protected, because oxygen is mainly present in the aqueous phase and is thus kept separated from the active (Jenning and Gohla, 2001; Junyaprasert et al., 2009; Müller et al., 2000, 2000; Souto et al., 2007). Also light-sensitive actives can be chemically protected (Durand et al., 2010; Fan et al., 2014; Jenning and Gohla, 2001; Müller et al., 2000; Pardeike et al., 2009), because, similar to nanoparticulate TiO_2, submicron lipid particles scatter light. This way, not only a sunscreen effect can be achieved by the particles themselves (Wissing, 2003), but also actives incorporated into the particle are less strained by light exposure. Thus, not only high physical but also chemical stability of incorporated actives can be achieved.

1.6.2. smartLipids 2nd skin

As described in chapter 1.3, a damaged skin lipid barrier leads to an increased penetration of pollution-originated toxins into the skin, again weakening the skin and leading to a vicious circle. A repair of the natural skin lipids barrier might be an effective strategy to break out of this circle (cf. chapter 1.4.2.1). To reestablish a healthy, functional and effective skin barrier, it is important to adapt the qualitative and quantitative composition of the lipids in the human SC. However, this lipid mixture has a very rigid consistency, is poorly spreadable and poorly adhesive to the skin. Both problems might be overcome by the formulation of this lipid mixture as submicron lipid particles suspension, i.e. as smartLipids (Müller et al., 2013b). This suspension was called “smartLipids 2nd skin” (in the literature also described as ““Second Skin SmartLipids®”, “Second-Skin SmartLipids®” or “S3L”).

1.6.2.1. *Natural lipid composition in the human SC*

The lipids in the human SC are qualitatively composed of ceramides, cholesterol and free fatty acids (Boncheva, 2014; van Smeden and Bouwstra, 2016; Weerheim and Ponec, 2001; Wertz, 2013). The quantitative composition varies widely, depending on various factors, e.g. the extraction method used (Bonté et al., 1995), the age, gender or ethnicity of the examined subject (Jungersted et al., 2010), the climate conditions of the study, the depth in the skin and body part investigated (Weerheim and Ponec, 2001). The minim overall quantitative content of ceramides was claimed to be 16 % (Motta, 1994), whereas the maximum concentration was 70% (Deffond et al., 1986).

Ceramides are commercially available e.g. by the company Evonik as “Ceramide III/IIIB” and “Ceramide VI”. These products alone proofed to reinforce the natural skin lipid barrier when applied to the skin (Evonik Nutrition & Care GmbH, 2019). Therefore, the overall ceramide content in smartLipids 2nd skin was defined to be 70%. Ceramide III/IIIB and Ceramide VI differ in the type of substituted fatty acid, i.e. Ceramide III/IIIB is substituted with a non-hydroxy-fatty acid, whereas Ceramide VI features an α-hydroxy-fatty acid. After van Smeden et al., these two Ceramide-types are present in the human SC in a 1:1.7 ratio (van Smeden et al., 2014). This ratio was also adapted for smartLipids 2nd skin.

Also the free fatty acids quantitative composition was inspired after literature data. The free fatty acids include representatives with saturated and unsaturated chains and with a carbon chain length (even- and odd-numbered) of C16-C28 (Nicollier et al., 1986). Especially very long-chain (> C22) and odd-numbered fatty acids are only commercially available in small amounts for analytical purpose and are very expensive (e.g. montanic acid, C28: 1 g = 300 €). After they are only present in a small amount (in addition < 2.5% of the total lipid mass) and thus should not affect the barrier properties, all odd-numbered and very long-chain free fatty acids (> C22) were left out of the smartLipids 2nd skin mixture.

The overall composition of the smartLipids 2nd skin bulk lipid is: Ceramide IIIB 44.1 %, Ceramide VI 25.9 %, cholesterol 15.0 %, stearic acid 3.3 %, behenic acid 3.1 %, oleic acid 2.7 %, palmitic acid 2.6 %, linoleic acid 2.0 %, and arachidic acid 1.4 % (Fig. 3).

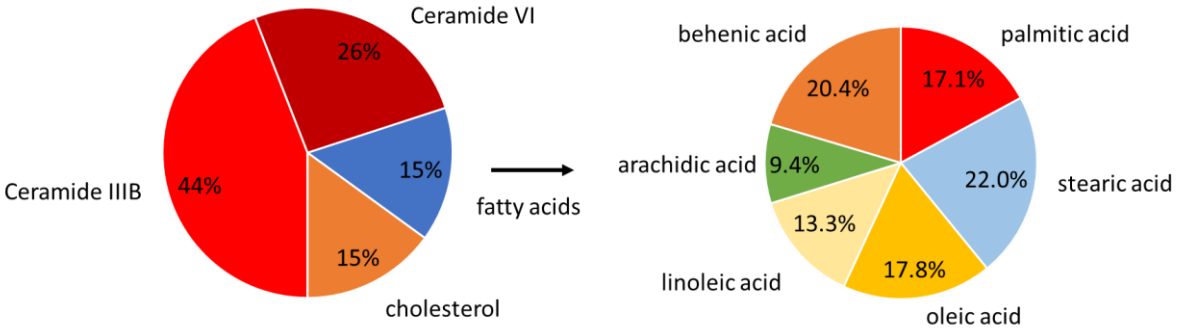

Fig. 3: The quantitative composition of smartLipids 2nd skin bulk lipid is inspired by composition of the lipids in the human stratum corneum as it is described in the literature.

smartLipids 2nd skin contain 9 different lipid components (7 solids and 2 liquids) and thus comply the definition of smartLipids. Thus, high active loading, long-term stability and deep skin penetration of incorporated actives can be predicted.

1.6.2.2. *smartLipids 2nd skin Q10*

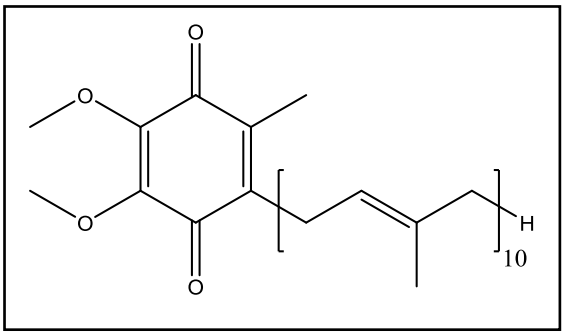

Fig. 4: Chemical structure of coenzyme Q10 (ubiquinone)

Beside its ability to reinforce the natural skin lipids barrier, smartLipids 2nd skin can be loaded with various cosmetic and pharmaceutical actives. As model active, coenzyme Q10 (chemical structure in Fig. 4) was selected.

When penetrated into the epidermis it's an effective antioxidant (Knott et al., 2015), reduces, wrinkle depth and UVA damages (Zhou et al., 2010). Coenzyme Q10 enhances the dermal elastin production, is has an anti-inflammatory effect by IL-1α- inhibition and reduces melanin production in vitro (Zhang et al., 2012). Beside the poor clinical data availability, it is an antioxidant being popularly used as an over the counter cosmetic product (Allemann and Baumann, 2008). Due to its lipophilic character and its popular use, it has been used as model active for the loading of smartLipids 2nd skin.

1.6.3. PER smartLipids

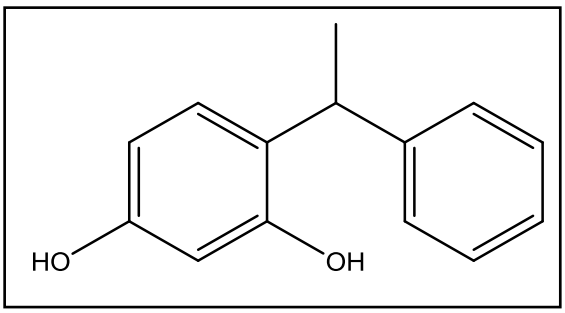

Fig. 5: Chemical structure of PER (phenylethyl resorcinol)

As already described in chapter 1.5.4.3, melasma and other pigmentation disorders are prevalent pollution effects. Whitening itself is anyway very widespread in cosmetics. The worldwide whitening market is valued by over 4 million US$ (2017), annually growing by 6.5% and is predicted to double by 2024 (GlobeNewswire.com, 2019). Phenylethyl resorcinol (4-(1-phenylethyl)1,3-ben-zenediol, PER, chemical structure in Fig. 5) is a very effective active ingredient for skin whitening. Already a concentration of 0.5% in a cosmetic product leads to a clinically effective depigmentation. PER is slightly soluble in water (4 mg/mL) and susceptive for photodegradation. Embedding PER in submicron lipid particles increases the chemical stability (Fan et al., 2014) as well as the in vitro effectiveness of PER (Kim et al., 2017). With focus on anti-pollution, PER-smartLipids can – similar to smartLipids 2nd skin – reinforce the function of the protective natural skin barrier and contribute to maintaining healthy skin by protecting it from exogenous toxins.

PER incorporated in lipid nanoparticles is already described in the literature. However, the published formulations are still far away from market maturity: So far, published formulations use excipients with polyethylene glycol in their chemical structure. Apart from being ecologically questionable and not skin-friendly, they form insoluble chelates with PER impairing the dermal penetration of PER (cf. chapter 3). Further, formulations still have limited loading capacity, storage stability and have only have been developed for lab scale yet.

1.7. smartCrystals

1.7.1. History of smartCrystals

1.7.1.1. *nanocrystals*

In the 1990s, nanocrystals have been developed as a formulation approach to increase the oral and dermal bioavailability of poorly soluble active ingredients (Müller et al., 1999). They are particles that consist of 100% active ingredient and have a particle sizes between 100 nm and 1000 nm and usually are produced by a top-down process, e.g. high pressure homogenization or wet bead milling. Depending on the active ingredient, these particles can then be applied orally, intravenous or dermally (Shegokar and Müller, 2010).

For oral or dermal application, the resulting increased surface area of the active substance and consequently the dissolution velocity is increased (Hatahet et al., 2016; Shegokar and Müller, 2010; Sun et al., 2012) and the active substance penetrated into the tissue can immediately be replaced by new dissolved active. That means that the dissolution rate of the active ingredient no longer determines the penetration rate in the penetration process.

Even more important is that nanocrystals proofed to have an increased kinetic saturation solubility. The small particle size results in a strong surface curvature. In analogy to the Kelvin equation, which actually describes the vapor pressure of liquids as a function of their particle size, also the “dissolution pressure” of solid particle dispersed in liquid media is increased as the size is reduced below a few micrometer:

$$ln\frac{p}{p_{sat}} = \frac{2 * \gamma * V_m}{r * R * T}$$

With: p – actual vapor pressure, p_{sat} – saturated vapor pressure, γ – liquid/vapor surface tension, V_m – molar volume of the liquid, r – particle radius, R – universal gas constant and T – temperature

This increased saturation solubility for submicron particle size proofed to be valid for a variety of actives, e.g. co-enzyme Q10 (Sun et al., 2012), curcumin (Vidlářová et al., 2016), lovastatin (Nanjwade et al., 2011), nifedipin (Hecq et al., 2005), quercitin (Hatahet et al., 2016) and rutin (Pyo et al., 2016).

The penetration rate of the active can be described after Fick's diffusion law:

$$J = -D * \frac{\Delta c}{\Delta x}$$

With: J – diffusional flux, D – diffusion coefficient, Δc – concentration gradient, Δx – diffusion length

Thus, increasing the saturation solubility of the dissolved active increased the concentration gradient between the formulation and the target tissue (i.e. the skin) and consequently the diffusional flux of the active, the dermal bioavailability. This proofed to be evident for numerous examples of poorly soluble actives (Al Shaal et al., 2010; Hatahet et al., 2016; Pelikh et al., 2018; Pyo et al., 2016; Vidlářová et al., 2016).

1.7.1.2. *smartCrystals*

In 2008, the technology was further developed into the so-called smartCrystals (Keck et al., 2008). Compared to nanocrystals, smartCrystals are produced by combining two production processes, e.g. wet bead milling and high pressure homogenization. By synergistic effects of different processes, smaller particles and higher physical stability can be achieved (Al Shaal et al., 2010; Keck et al., 2008; Pyo et al., 2016). In addition, also effects resulting from the smaller particle size such as higher saturation solubility, antioxidant capacity and higher sun protection factor were described for the poorly soluble active rutin (Müller et al., 2013a). Further, the production process is accelerated and thus the costs can be lowered. Commercially available smartCrystals products have been developed for glycyrrhetinic acid (Mishra et al., 2017), hesperidin (Romero et al., 2015), quercitin (Hatahet et al., 2016), rutin (Pyo et al., 2016) and other. Therefore, smartCrystals seem to be an attractive delivery system for overcoming the poor solubility and dermal bioavailability of Symurban.

1.7.2. Symurban smartCrystals

Symurban (INCI name benzylidene Dimethoxydimethylindanone, chemical structure in Fig. 6) is a synthetic cosmetic active introduced into the market in 2009 by the company Symrise for the protection of the skin from pollution-induced long-term damage.

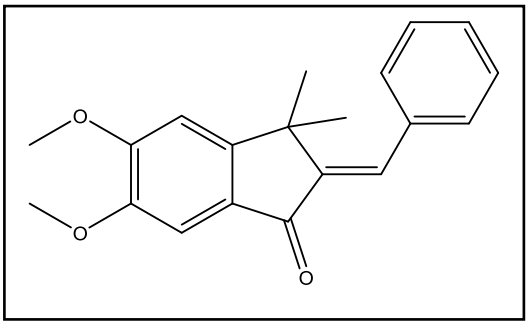

Fig. 6: Chemical structure of Symurban (benzylidene dimethoxydimethylindanone)

Pharmacologically, it is a competitive inhibitor of the AhR (Haarmann-Stemmann et al., 2015; Qiao et al., 2017; Tigges et al., 2014). Thus pollution-components like PAH and HAH can no longer activate this receptor. Consequently, following pharmacological processes, e.g. MMP-1- activation, IL-6 release or activation of the tyrosinase pathway are suppressed and ageing-related processes like collagen degradation, inflammation or hyperpigmentation can be suppressed.

However, Symurban is poorly soluble in water (0.25 µg/mL) and is challenging to formulate in a sufficiently dermally bioavailable form. As it is readily soluble in cosmetics oils, the company Symrise recommends to dissolve it in the oil phase of the cosmetic product. According to Symrise also the use of co-solvents like ethanol can be applied. Many of these Co-solvents are irritating for the skin and damage the lipid barrier in the SC, which is especially problematic because an intact skin barrier is important for effective anti-pollution, as discussed in chapter 1.3. Further, these cosolvents are usually low-molecular substances and penetrate much faster than the actual active molecule and some of them are volatile. Therefore, Symurban might precipitate again on the skin, leading to uncomfortable scratching on the skin and still insufficient dermal bioavailability.

Especially for a cosmetic purpose, higher oil contents are not optimal for the consumers acceptance due to an unpleasant, greasy skin feeling. In addition, O/W systems are predominantly used in cosmetics. Due to the high distribution coefficient (log P = 3.7), Symurban is then predominantly present in the inner oil phase. The bioavailability manly depends on the outer, coherent phase (Nair et al., 2013), which will in the case of lipophilic drugs like Symurban have a low concentration. Thus, this system is not optimal for sufficient dermal bioavailability of Symurban. Therefore, Symurban smartCrystals were to be developed.

1.8. Production of smartLipids and smartCrystals

1.8.1. High pressure homogenization

High pressure homogenization is a common top-down production method for the production of both, nanocrystals and solid lipid nanoparticles and the respective following generations smartCrystals, nanostructured lipid carriers and smartLipids. With this technique, a suspension or emulsion with µm sized particle size will be decreased in particle size by passing the product through a small gap (about 5-25 µm) with enormous high pressure (usually 300-1500 bar). This pressure accelerates the product to very high velocity (200-300 m/s) which than impacts on a metal ring and thereby grinding the particles. Emulsion droplets shear and break down into smaller droplets.

But the main grinding mechanism is the so-called cavitation: According to the law of Bernoulli, the sum of static and dynamic pressure is always constant. The high velocity of the product requires high dynamic pressure and thus a low static pressure. The static pressure in the homogenization gap drops below the vapor pressure of the water. This leads to the formation of water steam bubbles which then collapse again after the product has passed the homogenization gap. The implosion of the water steam bubbles accelerates the particles towards each other and the resulting collision further degrades the particles in size.

The main advantages of high pressure homogenization is that it allows to manufacture nanoparticulate systems with very reproducible particle size and narrow particle size distribution. There is little contamination by abrasion material and also the microbial contamination of the products will be reduced by the homogenization process. The process is easily upscalable, i.e. a product can easily be developed on lab scale and then produced on the industrial scale. It is industrially well established commonly used in food, cosmetic and pharma industry and GMP-aspects like cleanability, validation/qualification can easily be considered. The particle size of the product can be controlled by production parameters, such as temperature, homogenization pressure and number of homogenization cycles.

In this thesis, high pressure homogenization was performed on LAB 40 (APV Systems, Germany) with a batch size of 40 mL for the lab scale discontinuous production and Gaulin LAB 60 (APV Systems, Germany) with a production capacity of 60 kg/h for the industrial scale continuous production.

1.8.2. Wet bead milling

Wet bead milling is also a top-down production method for the production of nanocrystals and smartCrystals. With this process, a raw suspension of the drug or active is grinded by extreme shear forces in a special milling chamber. This milling chamber is filled with beads which are made from ultra-hard ceramics material, e.g. yttria stabilized zirconium dioxide. Due to a rotor-stator-principle and very high rotation velocity (e.g. 2000 rpm), high friction forces between the hard beads and the comparatively soft active particles cause an effective reduction of the active's particle size.

Also wet bead milling is a widespread industrial process for the production of nanoparticles for cosmetics or pharmaceuticals. It is also easily upscalable, allows reproductive particle size and is thus an appropriate method for the manufacturing in the GMP surrounding.

The particle size can be controlled by production parameters, such as stirring speed and time, but also the size of the beads determines the limit particle size of the nanosuspension.

In this thesis, a Bühler PML-2 (Bühler AG, Germany) bead mill was used with a batch size of 120 mL in discontinuous production.

1.9. Particle size analysis

Both smartLipids and smartCrystals are effective mainly through their particle size. The strong adhesion to the epithelium, the light scattering properties and the increased saturation solubility of smartCrystals are only possible by submicron particle size. Therefore, physical stability, i.e. unchanged particle size during storage, was a critical parameter in the galenic development of these technologies. The particle size was therefore determined uniformly using the following methods.

1.9.1. Laser diffraction

A standard-technique for the determination of particle size is laser diffraction (LD). A focused laser light beam hits the surface of particles suspended in aqueous media or in air and is thereby scattered, i.e. refracted in its direction. The scattering angle of the particle depends on the particle size of the suspended particle. Due to interference effects, a particle size-characteristic scattering pattern is the result.

The LD device is equipped with a focal light detector, allowing to detect the intensity of the scattered light as a function of scattering angle. For the detection of light at larger angles, large angle- and back scatter detectors are installed at the side of the LD device.

Two different calculus models can be applied: Fraunhofer and Mie theory. The Fraunhofer theory is the easier and more robust calculus model, but it is only applicable for particles of 50 µm and bigger (ISO 13320, 2009). For smaller particle size, the application of Mie theory is required, which for its part requires the refractive index.

According to the company Malvern, the specification of the refractive index to 2 decimal places is sufficiently enough. For solid particles, this can be done by preparing a dilution series of the particle matter, measuring the refractive index of the solutions, e.g. with a Abbé refractometer, and extrapolating to 100% (Malvern, 2017). By this, a refractive index of 1.46 was determined for the natural skin lipids particles and PER smartLipids, and 1.61 for Symurban. These values were used for the analysis of the respective materials.

LD allows to detect particles between 0.020 and 2000 µm. All LD measurements in this thesis were performed using a Mastersizer 2000 and a Hydro 2000S dispersion unit (Malvern, UK).

1.9.2. Photon correlation spectroscopy

Another technique for the analysis of particle size, especially when particles are in the nano-dimension, is photon correlation spectroscopy (PCS, synonyms: dynamic light scattering or quasi-elastic light scattering). This technique also applies a focused laser light beam on a diluted particle sample, but only uses a side- and backscattering detector. As the particles in the suspension are not static, but will be poked and moved by the dispersion medium molecules, also the intensity of the scattered light will differ as a function of time. Since the kinetic energy of the dispersion media molecules (usually but not necessarily water) is constant, the velocity of the suspended particles and thus the velocity of change in the intensity of the scattered light, depends on the size of the suspended particles.

The intensity of the scattered light as a function of time can be converted into an intensity autocorrelation function. The decay of this autocorrelation function correlates to the diffusion coefficient of the suspended particles after the Einstein-Stokes-equation:

$$D = \frac{k_B * T}{6\pi * \eta * r}$$

With: D – diffusion coefficient, k_B – Boltzmann's constant, T – absolute temperature, η – dynamic viscosity and r – radius of the spherical particle.

Thus, knowing about the dynamic viscosity and the temperature, the diffusion constant can be converted into the hydrodynamic particle size of the particles suspended in the dispersion media and thus the particle size of the sample.

PCS allows to detect particles between 0.3 and 10,000 nm. All PCS measurements in this thesis were performed using a Zetasizer Nano ZS (Malvern, UK).

1.9.3. Light microscopy

LD and PCS both are only indirectly able to detect the size of the particles and require comparatively complex calculus to determine the particle size from the actual raw data. These calculations all assume a spherical particle shape, which can cause problems in case of edged or irregularly shaped particles. Further, both methods require the dilution of the sample, which may bias the measurement because aggregates are loosened or particles may dilute.

The probably most direct method to detect particles is light microscopy (LM). Particles are visualized under the microscope and photographed. Photographing a particle with known dimensions, the number of pixels can be correlated to a length in the microscopic image. By automatic image analysis, the distribution of the EQPC diameter (diameter of a circle of equal

projection area), the feret diameter or other characteristic lengths of the particles can be described.

The maximum resolution d depends on the wavelength of the used light (λ) and the numerical aperture (N_A), a number that characterizes the objective used in the microscope. Considering a wavelength λ of 550 nm (green-yellow light) and a numeric aperture N_A of 1.25 (N_A of the most sensitive objective that was used in this thesis), the maximum resolution is:

$$d = \frac{\lambda}{N_A} = \frac{500\ nm}{1.25} = 440\ nm$$

Thus, light microscopy is not appropriate for the quantitative analysis of smartLipids or smartCrystals, because their target size is near to the limit of detection of LM. However, a qualitative information can still be collected by using LM: Aggregates are easily visible under the microscope and therefore the intensity of aggregation of the sample can be assed. Further, the absence of micrometer-sized particles can be stated by regarding the samples under the microscope.

All LM measurements in this thesis were performed using a BA 210 microscope (Motic, Germany) using a Moticam 3 camera (Motic, Germany) and objectives with 10x, 40x and 100x magnification and a numeric aperture of 0.25, 0.65 and 1.25, respectively.

1.10. Aims of the thesis

The main focus of this thesis is on the galenic development of innovative submicron delivery systems for modern anti-pollution therapy. Thus, the **general aim of this thesis** is to develop physically and chemically stable smartLipids and smartCrystals formulations for all 4 anti-pollution strategies that are mentioned in the introduction: skin barrier reinforcement, antioxidants, aryl hydrocarbon receptor antagonists and symptomatic therapy. Mechanisms of stabilization are to be discussed were possible.

With smartLipids 2nd skin (cf. Chapter 2), a formulation is to be developed to strengthen the natural skin barrier. The special challenge is the physical stabilization of the complex lipid matrix having pronounced surface activity. Thus, the **first aim** is to develop physically stable smartLipids 2nd skin with long-term physical stability. The **second aim** is to demonstrate the high loading capacity of smartLipids 2nd skin. Therefore, smartLipids 2nd skin are to be loaded with the model drug coenzyme Q10, which is a skin-physiological antioxidant at the same time. Thus, improved dermal delivery of antioxidants is to be tackled by the developments of smartLipids 2nd skin Q10.

PER smartLipids are to be developed for the symptomatic therapy of pollution-induced melasma and pigmentation disorders. PER NLC proofed to increase the chemical stability and in-vitro inhibition of melanogenesis in literature. However, the currently published submicron lipid particle formulations use incompatible excipients, have insufficient loading capacity and storage stability and are not yet developed for industrial production scale. Thus, they are to be further developed to market maturity. In Chapter 3, physically stable smartLipids are to be developed, which is the **third aim** of this thesis. The active PER is a photosensitive active, degrading under the formation of reddish products, which must be prevented to assure consumers' acceptance of the product. Thus, the color stability of PER smartLipids as the **fourth aim** is to be optimized in Chapter 4.

The solid state of PER smartLipids is crucial for the typical effects such as adhesiveness, film formation on the skin and controlled release. Thus, the solid state of PER smartLipids has to be approved, which is the **fifths aim** of this thesis and covered in Chapter 5.

Symurban, a competitive inhibitor of the AhR, allows effective anti-pollution protection in vitro, but is poorly soluble in water and thus poorly dermally bioavailable. In contrast to Q10 and PER, Symurban is not susceptible to pronounced chemical degradation. The increase in dermal bioavailability is more relevant in smartCrystals than in smartLipids. Therefore, physically stable Symurban smartCrystals are to be developed, which is the **sixth aim** of this thesis and covered in Chapter 5. The **seventh and last aim**, is to demonstrate the performance of the Symurban smartCrystals concept by increased saturation solubility and tape tripping experiment.

1.11. References

Afaq, F., Zaid, M.A., Pelle, E., Khan, N., Syed, D.N., Matsui, M.S., Maes, D., Mukhtar, H., 2009. Aryl hydrocarbon receptor is an ozone sensor in human skin. J. Invest. Dermatol. 129 (10), 2396–2403.

Al Shaal, L., Müller, R.H., Shegokar, R., 2010. smartCrystal combination technology: scale up from lab to pilot scale and long term stability. Pharmazie 65 (12), 877–884.

Allemann, B., Baumann, L., 2008. Antioxidants used in skin care formulations. Skin Therapy Lett. 13 (7), 5–9.

Alomirah, H., Al-Zenki, S., Al-Hooti, S., Zaghloul, S., Sawaya, W., Ahmed, N., Kannan, K., 2011. Concentrations and dietary exposure to polycyclic aromatic hydrocarbons (PAHs) from grilled and smoked foods. Food Control 22 (12), 2028–2035.

Arrowitz, C., Schoelermann, A.M., Mann, T., Jiang, L.I., Weber, T., Kolbe, L., 2019. Effective Tyrosinase Inhibition by Thiamidol Results in Significant Improvement of Mild to Moderate Melasma. J. Invest. Dermatol. 139 (8), 1691–1698.e6.

Behfarjam, F., Jadali, Z., 2018. Vitiligo patients show significant up-regulation of aryl hydrocarbon receptor transcription factor. An. Bras. Dermatol. 93 (2), 302–303.

Beránek, M., Fiala, Z., Kremláček, J., Andrýs, C., Krejsek, J., Hamáková, K., Palička, V., Borská, L., 2018. Serum levels of aryl hydrocarbon receptor, cytochromes P450 1A1 and 1B1 in patients with exacerbated psoriasis vulgaris. Folia Biol. (Praha) 64 (3), 97–102.

Boitano, A.E., Wang, J., Romeo, R., Bouchez, L.C., Parker, A.E., Sutton, S.E., Walker, J.R., Flaveny, C.A., Perdew, G.H., Denison, M.S., Schultz, P.G., Cooke, M.P., 2010. Aryl hydrocarbon receptor antagonists promote the expansion of human hematopoietic stem cells. Science 329 (5997), 1345–1348.

Boncheva, M., 2014. The physical chemistry of the stratum corneum lipids. Int. J. Cosmet. Sci. 36 (6), 505–515.

Bonté, F., Pinguet, P., Chevalier, J.M., Meybeck, A., 1995. Analysis of all stratum corneum lipids by automated multiple development high-performance thin-layer chromatography. J. Chromatogr. B., Biomed. Appl. 664 (2), 311–316.

Brunekreef, B., Holgate, S.T., 2002. Air pollution and health. Lancet 360 (9341), 1233–1242.

Chedid, M., 1996. Glucocorticoids inhibit keratinocyte growth factor production in primary dermal fibroblasts. Endocrinology 137 (6), 2232–2237.

Coderch, L., López, O., La Maza, A. de, Parra, J.L., 2003. Ceramides and skin function. Am. J. Clin. Dermatol. 4 (2), 107–129.

Cork, M.J., Danby, S.G., Vasilopoulos, Y., Hadgraft, J., Lane, M.E., Moustafa, M., Guy, R.H., Macgowan, A.L., Tazi-Ahnini, R., Ward, S.J., 2009. Epidermal barrier dysfunction in atopic dermatitis. J. Invest. Dermatol. 129 (8), 1892–1908.

Cotovio, J., Onno, L., Justine, P., Lamure, S., Catroux, P., 2001. Generation of oxidative stress in human cutaneous models following in vitro ozone exposure. Toxicol. Vitro. 15 (4-5), 357–362.

Deffond, D., Saint Leger, D., Leveque, J.L., Agache P, 1986. In vivo measurement of epidermal lipids in man. Bioeng. Skin 2 (1), 71–85.

Denison, M.S., Heath-Pagliuso, S., 1998. The Ah receptor: A regulator of the biochemical and toxicological actions of structurally diverse chemicals. Bull. Environ. Contam. Toxicol. 61 (5), 557–568.

Denison, M.S., Nagy, S.R., 2003. Activation of the aryl hydrocarbon receptor by structurally diverse exogenous and endogenous chemicals. Annu. Rev. Pharmacol. Toxicol. 43, 309–334.

Dietrich, C., 2016. Antioxidant Functions of the Aryl Hydrocarbon Receptor. Stem Cells Int. 2016.

Ding, Y., Pyo, S.M., Müller, R.H., 2017. smartLipids®as third solid lipid nanoparticle generation - stabilization of retinol for dermal application. Pharmazie 72 (12), 728–735.

D'Mello, S.A.N., Finlay, G.J., Baguley, B.C., Askarian-Amiri, M.E., 2016. Signaling pathways in melanogenesis. Int. J. Mol. Sci. 17 (7).

Durand, L., Habran, N., Henschel, V., Amighi, K., 2010. Encapsulation of ethylhexyl methoxycinnamate, a light-sensitive UV filter, in lipid nanoparticles. J. Microencapsul. 27 (8), 714–725.

Elias, P.M., Menon, G.K., 1991. Structural and Lipid Biochemical Correlates of the Epidermal Permeability Barrier, in: Elias, P.M. (Ed.), Skin Lipids, vol. 24. Elsevier, pp. 1–26.

Elias, P.M., Wakefield, J.S., 2014. Mechanisms of abnormal lamellar body secretion and the dysfunctional skin barrier in patients with atopic dermatitis. J. Allergy Clin. Immunol. 134 (4), 781-791.e1.

Essa, E.A., Bonner, M.C., Barry, B.W., 2003. Electroporation and ultradeformable liposomes; human skin barrier repair by phospholipid. J. Control. Release 92 (1-2), 163–172.

Esser, C., Rannug, A., Stockinger, B., 2009. The aryl hydrocarbon receptor in immunity. Trends Immunol. 30 (9), 447–454.

European Parliament, 2009. Regulation (EC) No 1223/2009 of the European Parliament and of the Council of 30 November 2009 on cosmetic products: OJ L 342, 22.12.2009.

Evonik Nutrition & Care GmbH, 2019. Ceramide III / Ceramide IIIB technical information. https://www.ulprospector.com/de/eu/PersonalCare/Detail/1481/52000/Ceramide-III. Accessed 19 November 2019.

Fabbrocini, G., Kaya, G., Caseiro Silverio, P., Vita, V. de, Kaya, A., Fontao, F., Sorg, O., Saurat, J.-H., 2015. Aryl Hydrocarbon Receptor Activation in Acne Vulgaris Skin: A Case Series from the Region of Naples, Italy. Dermatology (Basel) 231 (4), 334–338.

Fan, H., Liu, G., Huang, Y., Li, Y., Xia, Q., 2014. Development of a nanostructured lipid carrier formulation for increasing photo-stability and water solubility of Phenylethyl Resorcinol. Appl. Surf. Sci. 288 (1), 193–200.

Feingold, K.R., 2012. Lamellar bodies: The key to cutaneous barrier function. J. Invest. Dermatol. 132 (8), 1951–1953.

Fields, K., Falla, T.J., Rodan, K., Bush, L., 2009. Bioactive peptides: Signaling the future. J. Cosmet. Dermatol. 8 (1), 8–13.

Fujii-Kuriyama, Y., Mimura, J., 2005. Molecular mechanisms of AhR functions in the regulation of cytochrome P450 genes. Biochem. Biophys. Res. Commun. 338 (1), 311–317.

Gasco, M.R., 1991. U.S. Patent No. 5250236: Method for producing solid lipid microspheres having a narrow size distribution. U.S. Patent and Trademark Office.

Gehring, W., Wenz, J., Gloor, M., 1997. Influence of topically applied ceramide/phospholipid mixture on the barrier function of intact skin, atopic skin and experimentally induced barrier damage. Int. J. Cosmetic Sci. 19 (4), 143–156.

GlobeNewswire.com, 2019. Global skin lightening products market will reach USD 8,895 million by 2024: zion market research. https://www.globenewswire.com/news-release/2019/01/10/1685903/0/en/Global-Skin-Lightening-Products-Market-Will-Reach-USD-8-895-Million-By-2024-Zion-Market-Research.html. Accessed 7 December 2019.

Groupe ECOCERT, 2019. Natural and organic cosmetics. https://www.ecocert.com/en/certification-detail/natural-and-organic-cosmetics-cosmos. Accessed 10 December 2019.

Haarmann-Stemmann, T., Esser, C., Krutmann, J., 2015. The Janus-Faced Role of Aryl Hydrocarbon Receptor Signaling in the Skin: Consequences for Prevention and Treatment of Skin Disorders. J. Invest. Dermatol. 135 (11), 2572–2576.

Haas, K., Weighardt, H., Deenen, R., Köhrer, K., Clausen, B., Zahner, S., Boukamp, P., Bloch, W., Krutmann, J., Esser, C., 2016. Aryl hydrocarbon receptor in keratinocytes is essential for murine skin barrier integrity. J. Invest. Dermatol. 136 (11), 2260–2269.

Hankinson, O., 1995. The aryl hydrocarbon receptor complex. Annu. Rev. Pharmacol. Toxicol. 35, 307–340.

Harding, C.R., 2004. The stratum corneum: Structure and function in health and disease. Dermatol. Ther. 17 Suppl 1, 6–15.

Hatahet, T., Morille, M., Hommoss, A., Dorandeu, C., Müller, R.H., Bégu, S., 2016. Dermal quercetin smartCrystals®: Formulation development, antioxidant activity and cellular safety. Eur. J. Pharm. Biopharm. 102, 51–63.

Hecq, J., Deleers, M., Fanara, D., Vranckx, H., Amighi, K., 2005. Preparation and characterization of nanocrystals for solubility and dissolution rate enhancement of nifedipine. Int. J. Pharm. 299 (1-2), 167–177.

Hidaka, T., Ogawa, E., Kobayashi, E.H., Suzuki, T., Funayama, R., Nagashima, T., Fujimura, T., Aiba, S., Nakayama, K., Okuyama, R., Yamamoto, M., 2017. The aryl hydrocarbon receptor AhR links atopic dermatitis and air pollution via induction of the neurotrophic factor artemin. Nat. Immunol. 18 (1), 64.

Huh, S.Y., Shin, J.-W., Na, J.-I., Huh, C.-H., Youn, S.-W., Park, K.-C., 2010. Efficacy and safety of liposome-encapsulated 4-n-butylresorcinol 0.1% cream for the treatment of melasma: a randomized controlled split-face trial. J. Dermatol. 37 (4), 311–315.

ISO 13320, 2009. Particle size analysis — Laser diffraction methods, 10th ed.

Jenning, V., Gohla, S.H., 2001. Encapsulation of retinoids in solid lipid nanoparticles (SLN). J. Microencapsul. 18 (2), 149–158.

Jenning, V., Lippacher, A., Mäder, K., Müller, R.H., 2002. European patent No. 1176949: Lipidpartikel auf der Basis von Mischungen von flüssigen und festen Lipiden und Verfahren zu ihrer Herstellung. European Patent Office.

Jenning, V., Lippacher, A., Mäder, K., Müller, R.H., 2014. U.S. Patent No. 8663692: Lipid particles on the basis of mixtures of liquid and solid lipids and method for producing same. U.S. Patent and Trademark Office.

Jin, S.-P., Li, Z., Choi, E.K., Lee, S., Kim, Y.K., Seo, E.Y., Chung, J.H., Cho, S., 2018. Urban particulate matter in air pollution penetrates into the barrier-disrupted skin and produces ROS-dependent cutaneous inflammatory response in vivo. J. Dermatol. Sci. 91 (2), 175–183.

Juliano, C., Magrini, G., 2018. Cosmetic Functional Ingredients from Botanical Sources for Anti-Pollution Skincare Products. Cosmetics 5 (1), 19.

Jungersted, J.M., Høgh, J.K., Hellgren, L.I., Jemec, G.B.E., Agner, T., 2010. Ethnicity and stratum corneum ceramides. Br. J. Dermatol. 163 (6), 1169–1173.

Junyaprasert, V.B., Teeranachaideekul, V., Souto, E.B., Boonme, P., Müller, R.H., 2009. Q10-loaded NLC versus nanoemulsions: Stability, rheology and in vitro skin permeation. Int. J. Pharm. 377 (1-2), 207–214.

Jux, B., Kadow, S., Luecke, S., Rannug, A., Krutmann, J., Esser, C., 2011. The aryl hydrocarbon receptor mediates UVB radiation-induced skin tanning. J. Invest. Dermatol. 131 (1), 203–210.

Kampa, M., Castanas, E., 2008. Human health effects of air pollution. Environ. Pollut. 151 (2), 362–367.

Keck, C., Kobierski, S., Mauludin, R., Müller, R.H., 2008. Second generation of drug nanocrystals for delivery of poorly soluble drugs: smartCrystals technology. Dosis 24 (2), 124–128.

Kim, B.-S., Na, Y.-G., Choi, J.-H., Kim, I., Lee, E., Kim, S.-Y., Lee, J.-Y., Cho, C.-W., 2017. The improvement of skin whitening of phenylethyl resorcinol by nanostructured lipid carriers. Nanomaterials (Basel) 7 (9), 241.

Kim, H.O., Kim, J.H., Chung, B.Y., Choi, M.G., Park, C.W., 2014. Increased expression of the aryl hydrocarbon receptor in patients with chronic inflammatory skin diseases. Exp. Dermatol. 23 (4), 278–281.

Kim, K.E., Cho, D., Park, H.J., 2016. Air pollution and skin diseases: Adverse effects of airborne particulate matter on various skin diseases. Life Sci. 152, 126–134.

Kim, S.-H., Henry, E.C., Kim, D.-K., Kim, Y.-H., Shin, K.J., Han, M.S., Lee, T.G., Kang, J.-K., Gasiewicz, T.A., Ryu, S.H., Suh, P.-G., 2006. Novel compound 2-methyl-2H-pyrazole-3-carboxylic acid (2-methyl-4-o-tolylazo-phenyl)-amide (CH-223191) prevents 2,3,7,8-TCDD-induced toxicity by antagonizing the aryl hydrocarbon receptor. Mol. Pharmacol. 69 (6), 1871–1878.

Knott, A., Achterberg, V., Smuda, C., Mielke, H., Sperling, G., Dunckelmann, K., Vogelsang, A., Krüger, A., Schwengler, H., Behtash, M., Kristof, S., Diekmann, H., Eisenberg, T., Berroth, A., Hildebrand, J., Siegner, R., Winnefeld, M., Teuber, F., Fey, S., Möbius, J., Retzer, D., Burkhardt, T., Lüttke, J., Blatt, T., 2015. Topical treatment with coenzyme Q10-containing formulas improves skin's Q10 level and provides antioxidative effects. Biofactors 41 (6), 383–390.

Kolbe, L., Mann, T., Gerwat, W., Batzer, J., Ahlheit, S., Scherner, C., Wenck, H., Stab, F., 2013. 4-n-butylresorcinol, a highly effective tyrosinase inhibitor for the topical treatment of hyperpigmentation. J. Eur. Acad. Dermatol. Venereol. 27 (1), 19–23.

Kolluri, S.K., Jin, U.-H., Safe, S., 2017. Role of the aryl hydrocarbon receptor in carcinogenesis and potential as an anti-cancer drug target. Arch. Toxicol. 91 (7), 2497–2513.

Korkina, L., 2016. Metabolic and redox barriers in the skin exposed to drugs and xenobiotics. Expert Opin. Drug Metab. Toxicol. 12 (4), 377–388.

Li, X., Jin, L., Kan, H., 2019. Air pollution: A global problem needs local fixes. Nature 570 (7762), 437–439.

Lin, T.-K., Zhong, L., Santiago, J.L., 2017. Anti-inflammatory and skin barrier repair effects of topical application of some plant oils. Int. J. Mol. Sci. 19 (1).

Lodén, M., Raány, E.B., 2000. Skin-identical lipids versus petrolatum in the treatment of tape-stripped and detergent-perturbed human skin. Acta. Derm. Venereol. (80), 412–415.

Luecke, S., Backlund, M., Jux, B., Esser, C., Krutmann, J., Rannug, A., 2010. The aryl hydrocarbon receptor (AHR), a novel regulator of human melanogenesis. Pigment Cell Melanoma Res. 23 (6), 828–833.

Malvern, 2017. Rapid determination of the particle refractive index for laser diffraction particle size calculations. Mavernpanalytical, www.malvernpanalytical.com. https://www.malvernpanalytical.com/en/learn/knowledge-center/technical-notes/TN101104DeterminationParticleRefractiveIndex. Accessed 25 November 2017.

Manojkumar, N., Srimuruganandam, B., 2019. Health effects of particulate matter in major Indian cities. Int. J. Environ. Health Res. 29 (6), 1–13.

Marlowe, J.L., Puga, A., 2005. Aryl hydrocarbon receptor, cell cycle regulation, toxicity, and tumorigenesis. J. Cell. Biochem. 96 (6), 1174–1184.

Matsumoto, Y., Ide, F., Kishi, R., Akutagawa, T., Sakai, S., Nakamura, M., Ishikawa, T., Fujii-Kuriyama, Y., Nakatsuru, Y., 2007. Aryl hydrocarbon receptor plays a significant role in mediating airborne particulate-induced carcinogenesis in mice. Environ. Sci. Technol. 41 (10), 3775–3780.

Mishra, M., Shegokar, R., Gohla, S., Muller, R.H., 2017. Improved skin penetration of hydrophobic glycyrrhetinic acid smart- Crystal® compared to its water soluble salt. Drug Deliv. Lett. 7 (3), 211–218.

Mistry, N., 2017. Guidelines for formulating anti-pollution products. Cosmetics 4 (4), 57.

Motta, S., 1994. Abnormality of water barrier function in psoriasis. Arch. Dermatol. 130 (4), 452.

Motta S., Sesan S., Monti M., Giuliani A., Caputo R., 1994. Interlamellar lipid differences between normal and psoriatic stratum corneum. Acta. Derm. Venereol. Suppl. (Stockh.) (186), 131–132.

Müller, R.H., Becker, R., Kruss, B., Peters, K., 1999. U.S. Patent No. 5858410: Pharmaceutical nanosuspensions for medicament administration as systems with increased saturation solubility and rate of solution. U.S. Patent and Trademark Office.

Müller, R.H., Chen, R., Keck, C.M., 2013a. smartCrystals for consumer care & cosmetics: enhanced dermal delivery of poorly soluble plant actives. Househ. Pers. Care Today 8 (5), 18–23.

Müller, R.H., Mäder, K., Gohla, S.H., 2000. Solid lipid nanoparticles (SLN) for controlled drug delivery – a review of the state of the art. Eur. J. Pharm. Biopharm. 50 (1), 161–177.

Müller, R.H., Olechowski, F., Köpke, D., Pyo, S.M., 2019. SmartLipids: The Third Generation of Solid Submicron Lipid Particles for Dermal Delivery of Actives, in: Cornier, J., Keck, C.M., van de Voorde, M. (Eds.), Nanocosmetics. From Ideas to Products, 1st ed., pp. 141–159.

Müller, R.H., Petersen, R.D., Hommoss, A., Pardeike, J., 2007. Nanostructured lipid carriers (NLC) in cosmetic dermal products. Adv. Drug Deliv. Rev. 59 (6), 522–530.

Müller, R.H., Radtke, M., Wissing, S.A., 2002. Solid lipid nanoparticles (SLN) and nanostructured lipid carriers (NLC) in cosmetic and dermatological preparations. Adv. Drug Deliv. Rev. 54 (Supp. 1), S131-155.

Müller, R.H., Ruick, R., Keck, C.M., 2014. smartLipids - the next generation of lipid nanoparticles by optimized design of particle matrix. DPhG-Jahrestagung, Frankfurt (PT.27).

Müller, R.H., Sinambela, P., Keck, C.M., 2013b. NLC – the invisible dermal patch for moisturizing & skin protection. Euro Cosmetics 6, 20–22.

Murray, I.A., Flaveny, C.A., DiNatale, B.C., Chairo, C.R., Schroeder, J.C., Kusnadi, A., Perdew, G.H., 2010. Antagonism of aryl hydrocarbon receptor signaling by 6,2',4'-trimethoxyflavone. J. Pharmacol. Exp. Ther. 332 (1), 135–144.

Nair, A., Jacob, S., Al-Dhubiab, B., Attimarad, M., Harsha, S., 2013. Basic considerations in the dermatokinetics of topical formulations. Braz. J. Pharm. Sci. 49 (3), 423–434.

Nakamura, M., Ueda, Y., Hayashi, M., Kato, H., Furuhashi, T., Morita, A., 2013. Tobacco smoke-induced skin pigmentation is mediated by the aryl hydrocarbon receptor. Exp. Dermatol. 22 (8), 556–558.

Nanjwade, B.K., Derkar, G.K., Bechra, H.M., Nanjwade, V.K., Manvi, F.V., 2011. Design and characterization of nanocrystals of lovastatin for solubility and dissolution enhancement. J. Nanomedic. Nanotechnol. 2 (2), 1–17.

Nemes, Z., Steinert, P.M., 1999. Bricks and mortar of the epidermal barrier. Exp. Mol. Med. 31 (1), 5–19.

Ní Raghallaigh, S., Bender, K., Lacey, N., Brennan, L., Powell, F.C., 2012. The fatty acid profile of the skin surface lipid layer in papulopustular rosacea. Br. J. Dermatol. 166 (2), 279–287.

Nicollier, M., Massengo, T., Rémy-Martin, J.-P., Laurent, R., Adessi, G.-L., 1986. Free F
fatty acids and fatty acids of triacylglycerols in normal and hyperkeratotic human stratum corneum. J. Investig. Dermatol. 87 (1), 68–71.

Noakes, R., 2017. Dissecting the enigma of scleroderma: possible involvement of the kynurenine pathway. Pteridines 28 (2), 3172.

Ono, Y., Torii, K., Fritsche, E., Shintani, Y., Nishida, E., Nakamura, M., Shirakata, Y., Haarmann-Stemmann, T., Abel, J., Krutmann, J., Morita, A., 2013. Role of the aryl hydrocarbon receptor in tobacco smoke extract-induced matrix metalloproteinase-1 expression. Exp. Dermatol. 22 (5), 349–353.

Oren, A., Ganz, T., Liu, L., Meerloo, T., 2003. In human epidermis, β-defensin 2 is packaged in lamellar bodies. Exp. Mol. Pathol. 74 (2), 180–182.

Pan, T.-L., Wang, P.-W., Aljuffali, I.A., Huang, C.-T., Lee, C.-W., Fang, J.-Y., 2015. The impact of urban particulate pollution on skin barrier function and the subsequent drug absorption. J. Dermatol. Sci. 78 (1), 51–60.

Pardeike, J., 2009. Nanosuspensions and nanostructured lipid carriers for dermal application: Dissertation zur Erlangung des akademischen Grades des Doktors der Naturwissenschaften (Dr. rer. nat.).

Pardeike, J., Hommoss, A., Müller, R.H., 2009. Lipid nanoparticles (SLN, NLC) in cosmetic and pharmaceutical dermal products. Int. J. Pharm. 366 (1-2), 170–184.

Pearse, A.D., Marks, R., 1983. Response of human skin to ultraviolet radiation: Dissociation of erythema and metabolic changes following sunscreen protection. J. Invest. Dermatol. 80 (3), 191–194.

Pelikh, O., Stahr, P.-L., Huang, J., Gerst, M., Scholz, P., Dietrich, H., Geisel, N., Keck, C.M., 2018. Nanocrystals for improved dermal drug delivery. Eur. J. Pharm. Biopharm. 128, 170–178.

Poljšak, B., Dahmane, R.G., Godić, A., 2012. Intrinsic skin aging: The role of oxidative stress. Acta Dermatovenerol. Alp. Pannonica. Adriat. 21 (2), 33–36.

Pope, C.A., Burnett, R.T., Thun, M.J., Calle, E.E., Krewski, D., Ito, K., Thurston, G.D., 2002. Lung cancer, cardiopulmonary mortality, and long-term exposure to fine particulate air pollution. J Am. Med. Assoc. 287 (9), 1132–1141.

Pyo, S., Meinke, M., Keck, C., Müller, R., 2016. Rutin—Increased antioxidant activity and skin penetration by nanocrystal technology (smartCrystals). Cosmetics 3 (1), 9.

Qiao, Y., Li, Q., Du, H.-Y., Wang, Q.-W., Huang, Y., Liu, W., 2017. Airborne polycyclic aromatic hydrocarbons trigger human skin cells aging through aryl hydrocarbon receptor. Biochem. Biophys. Res. Commun. 488 (3), 445–452.

Rawlings, A.V., 2003. Trends in stratum corneum research and the management of dry skin conditions. Int. J. Cosmet. Sci. 25 (1-2), 63–95.

Reddy, B., Jow, T., Hantash, B.M., 2012. Bioactive oligopeptides in dermatology: Part I. Exp. Dermatol. 21 (8), 563–568.

Riley, P.A., 2003. Melanogenesis and melanoma. Pigment Cell Res. 16 (5), 548–552.

Rinnerthaler, M., Bischof, J., Streubel, M.K., Trost, A., Richter, K., 2015. Oxidative stress in aging human skin. Biomolecules 5 (2), 545–589.

Rittié, L., Fisher, G.J., 2002. UV-light-induced signal cascades and skin aging. Ageing Res. Rev. 1 (4), 705–720.

Romero, G.B., Chen, R., Keck, C.M., Müller, R.H., 2015. Industrial concentrates of dermal hesperidin smartCrystals®--production, characterization & long-term stability. Int. J. Pharm. 482 (1-2), 54–60.

Ruick, R., 2015. smartLipids - die neue Generation der Lipidnanopartikel nach SLN und NLC: Dissertation zur Erlangung des akademischen Grades des Doktors der Naturwissenschaften (Dr. rer. nat.). Freie Universiät Berlin.

Schlay, S., Slootta, U., 2016. Efficient skin protection against negative environmental influences by breathable, vegan silk polypeptides. SÖWF journal 142 (4), 14–19.

Seaton, A., Godden, D., MacNee, W., Donaldson, K., 1995. Particulate air pollution and acute health effects. Lancet 345 (8943), 176–178.

Shegokar, R., Müller, R.H., 2010. Nanocrystals: Industrially feasible multifunctional formulation technology for poorly soluble actives. Int. J. Pharm. 399 (1-2), 129–139.

Smith, K.J., Murray, I.A., Tanos, R., Tellew, J., Boitano, A.E., Bisson, W.H., Kolluri, S.K., Cooke, M.P., Perdew, G.H., 2011. Identification of a high-affinity ligand that exhibits complete aryl hydrocarbon receptor antagonism. J. Pharmacol. Exp. Ther. 338 (1), 318–327.

Solano, F., Briganti, S., Picardo, M., Ghanem, G., 2006. Hypopigmenting agents: an updated review on biological, chemical and clinical aspects. Pigment Cell Res. 19 (6), 550–571.

Souto, E.B., Almeida, A.J., Müller, R.H., 2007. Lipid nanoparticles (SLN®, NLC®) for cutaneous drug delivery: structure, protection and skin effects. J. Biomed. Nanotechnol. 3 (4), 317–331.

Stockinger, B., Di Meglio, P., Gialitakis, M., Duarte, J.H., 2014. The aryl hydrocarbon receptor: multitasking in the immune system. Annu. Rev. Immunol. 32, 403–432.

Sun, J., Wang, F., Sui, Y., She, Z., Zhai, W., Wang, C., Deng, Y., 2012. Effect of particle size on solubility, dissolution rate, and oral bioavailability: Evaluation using coenzyme Q_{10} as naked nanocrystals. Int. J. Nanomedicine 7, 5733–5744.

Thiele, J.J., Podda, M., Packer, L., 1997. Tropospheric ozone: An emerging environmental stress to skin. Biol. Chem. 378 (11), 1299–1305.

Tigges, J., Haarmann-Stemmann, T., Vogel, C.F.A., Grindel, A., Hübenthal, U., Brenden, H., Grether-Beck, S., Vielhaber, G., Johncock, W., Krutmann, J., Fritsche, E., 2014. The new aryl hydrocarbon receptor antagonist E/Z-2-benzylindene-5,6-dimethoxy-3,3-dimethylindan-1-one protects against UVB-induced signal transduction. J. Invest. Dermatol. 134 (2), 556–559.

Valacchi, G., Muresan, X.M., Sticozzi, C., Belmonte, G., Pecorelli, A., Cervellati, F., Demaude, J., Krol, Y., Oresajo, C., 2016. Ozone-induced damage in 3D-Skin model is prevented by topical vitamin C and vitamin E compound mixtures application. J. Dermatol. Sci. 82 (3), 209–212.

Valacchi, G., van der Vliet, A., Schock, B.C., Okamoto, T., Obermuller-Jevic, U., Cross, C.E., Packer, L., 2002. Ozone exposure activates oxidative stress responses in murine skin. Toxicology 179 (1-2), 163–170.

van Smeden, J., Bouwstra, J.A., 2016. Stratum corneum lipids: Their role for the skin barrier function in healthy subjects and atopic dermatitis patients. Curr. Probl. Dermatol. 49, 8–26.

van Smeden, J., Janssens, M., Gooris, G.S., Bouwstra, J.A., 2014. The important role of stratum corneum lipids for the cutaneous barrier function. Biochim. Biophys. Acta. 1841 (3), 295–313.

Veldhoen, M., Hirota, K., Westendorf, A.M., Buer, J., Dumoutier, L., Renauld, J.-C., Stockinger, B., 2008. The aryl hydrocarbon receptor links T_H17-cell-mediated autoimmunity to environmental toxins. Nature 453 (7191), 106.

Videira, I.F.d.S., Moura, D.F.L., Magina, S., 2013. Mechanisms regulating melanogenesis. An. Bras. Dermatol. 88 (1), 76–83.

Vidlářová, L., Romero, G.B., Hanuš, J., Štěpánek, F., Müller, R.H., 2016. Nanocrystals for dermal penetration enhancement - Effect of concentration and underlying mechanisms using curcumin as model. Eur. J. Pharm. Biopharm. 104, 216–225.

Vielhaber, G., Schmaus, G., Jacobs, K., Franke, H., Lange, S., Herrmann, M., Joppe, H., Koch, O., 2007. 4-(1-Phenylethyl)1,3-Benzenediol: A new, highly efficient lightening agent. Int. J. Cosmet. Sci. 29 (1), 65–66.

Weerheim, A., Ponec, M., 2001. Determination of stratum corneum lipid profile by tape stripping in combination with high-performance thin-layer chromatography. Arch. Dermatol. Res. 293 (4), 191–199.

Wenk, J., Brenneisen, P., Meewes, C., Wlaschek, M., Peters, T., Blaudschun, R., Ma, W., Kuhr, L., Schneider, L., Scharffetter-Kochanek, K., 2001. UV-induced oxidative stress and photoaging. Curr. Probl. Dermatol. 29, 83–94.

Wertz, P.W., 2013. Current understanding of skin biology pertinent to skin penetration: Skin biochemistry. Skin Pharmacol. Physiol. 26 (4-6), 217–226.

White, A.J., Keller, J.P., Zhao, S., Kaufman, J.D., Sandler, D.P., 2019. Air pollution, clustering of particulate matter components and breast cancer. Cancer Epidemiol. Biomarkers Prev. 28 (3), 624-625.

WHO, 2019. World Health Organization international website. WHO. https://www.who.int/airpollution/en/. Accessed 21 October 2019.

Wickett, R.R., Visscher, M.O., 2006. Structure and function of the epidermal barrier. Am. J. Infect. Control. 34 (10), S98–110.

Wilhelm, K.-P., Freitag, G., Wolff, H.H., 1994. Surfactant-induced skin irritation and skin repair. J. Am. Acad. Dermatol. 30 (6), 944–949.

Wissing, S., 2003. Cosmetic applications for solid lipid nanoparticles (SLN). Int. J. Pharm. 254 (1), 65–68.

Xue, P., Fu, J., Zhou, Y., 2018. The aryl hydrocarbon receptor and tumor immunity. Front. Immunol. 9, 286.

Yamamoto, A., Serizawa, S., Ito, M., Sato, Y., 1991. Stratum corneum lipid abnormalities in atopic dermatitis. Arch. Dermatol. Res. 283 (4), 219–223.

Zhang, M., Dang, L., Guo, F., Wang, X., Zhao, W., Zhao, R., 2012. Coenzyme Q(10) enhances dermal elastin expression, inhibits IL-1α production and melanin synthesis in vitro. Int. J. Cosmet. Sci. 34 (3), 273–279.

Zhou, H., Yue, Y., Liu, G., Li, Y., Zhang, J., Yan, Z., Duan, M., 2010. Characterisation and skin distribution of lecithin-based coenzyme Q10-loaded lipid canocapsules. Nanoscale Res. Lett. 5 (10), 1561–1569.

Zhu, W., Gao, J., 2008. The use of botanical extracts as topical skin-lightening agents for the improvement of skin pigmentation disorders. J. Investig. Dermatol. Symp. Proc. 13 (1), 20–24.

2. Development of smartLipids 2nd skin to reinforce impaired skin lipid barrier[1]

Abstract

If healthy, the natural skin protective barrier provides effective protection against the undesirable permeation of environmental toxins into the skin. The barrier function is essentially carried out by an intact lipid barrier in the stratum corneum. If this barrier is damaged by skin diseases (e.g. atopic dermatitis or psoriasis), excessive washing or other influencing factors, toxins from air pollution can penetrate into the skin and cause irritation, inflammation, collagen degradation and pigmentation disorders. The damaged lipid barrier can be rebuilt by smartLipids 2nd skin. These are submicron lipid particles consisting of a lipid blend that resembles the lipid composition in the human stratum corneum. smartLipids 2nd skin can be loaded with active ingredients, e.g. antioxidants. Due to the complex lipid matrix, smartLipids can be loaded much higher than previous generations of lipid nanoparticles (SLN, NLC). Due to their submicron particle size, smartLipids are highly adhesive and form an occlusive film on the skin. According to this, the penetration of incorporated actives can be distinctly increased. Thus, smartLipids 2nd skin enable a synergistic mechanical and molecular anti-pollution intervention. The particular challenge of this work was to develop a submicron lipid suspension of a complex skin-like lipid blend having all more or less pronounced surface activity. The aim was to achieve with long-term stability of smartLipids 2nd skin with a skin-friendly surfactant and proof the high loading capacity of the model drug coenzyme Q10. A surfactant screening investigating a total of 19 surfactants showed that the submicron lipid suspension could be optimally stabilized with 1.5% Lanette E. After preservation with 3% pentylene glycol, submicron suspensions with a particle size of about 120 nm and a storage stability over one year could be achieved. The loading experiment with the model active coenzyme Q10 showed a loading capacity of 50%, which doubled the previously published maximum loading in NLC (25%) with similar particle size and storage stability of almost one year. Therefore, smartLipids 2nd skin represent an innovative, promising formulation approach for the modern prevention of dermal effects of air pollution.

[1] This chapter is in preparation to be submitted for publication in:

Skin Pharmacology and Physiology

2.1. Introduction

Urban air pollution is regarded as one of the most harmful effects on modern society. The impact of air quality on pulmonary and cardiovascular systems has been well demonstrated in numerous studies (Brunekreef and Holgate, 2002; Manojkumar and Srimuruganandam, 2019; Pope et al., 2002; Seaton et al., 1995). In 2019 the world health organization for example published that 4.2 million deaths by lung cancer, acute lower respiratory infection, stroke, ischemic heart disease and chronic obstructive pulmonary disease can be associated to poor air quality (Li et al., 2019; WHO, 2019). In recent years, more and more other organs became the focus of investigation, for instance the largest human organ being constantly in direct contact with air pollution – the human skin (Kim et al., 2016; Mancebo and Wang, 2015; Puri et al., 2017).

The human skin in healthy condition is able to repel the majority of exogenous toxins. First and foremost, the natural lipid film on skin proved to be essential for the integrity of the skin barrier against air pollutants (Coderch et al., 2003; Elias and Menon, 1991; Feingold, 2012; van Smeden et al., 2014). In vivo studies demonstrated that the penetration of toxic pollutants is particularly high when the natural lipid film is damaged. For example, the penetration rate of lipophilic model substances such as estradiol (Essa et al., 2003) or nicotinic acid ester (Gehring et al., 1997) increased by intentionally damaging the natural lipid barrier. Air pollution is therefore of concern in cases where the lipid barrier of the skin is altered or even damaged. Changes in the skin lipid profile are present in various skin diseases, e.g. neurodermatitis (Cork et al., 2009; Yamamoto et al., 1991), psoriasis (Harding, 2004; Motta et al., 1994) and rosacea (Ní Raghallaigh et al., 2012), but are also present in people with winter xerosis (Harding, 2004) and dry skin (Rawlings, 2003). Hence, this is not only a fringe group phenomenon. For instance, psoriasis affects between 1.3% of the African and 2.5% of the Caucasian population (Gelfand et al., 2005) and also atopic dermatitis has a prevalence between 15-20% in children and 1-3% in adults (Nutten, 2015). The clinical picture of these skin diseases worsens with exposure to high air pollution levels, primarily through the activation of aryl hydrocarbon receptors (AhR), which lead to an increased release of proinflammatory cytokines and matrix metalloproteases, the skin barrier is further weakened (Jin et al., 2018; Pan et al., 2015). Non-treatment of the impaired skin lipid barrier can therefore result in a vicious circle.

The application of ceramides (main component of natural skin lipids) showed reinforcing effect on SDS-damaged skin barrier, proven by increased skin moisture (Evonik Nutrition &

Care GmbH, 2019). Also in atopic dermatitis patients a decrease in transepidermal water loss was observed after the application of ceramides. Further, in 22 out of 24 patients the clinical symptoms were significantly improved, demonstrating well the correlation between lipid barrier function and disease pattern (Chamlin et al., 2002). Besides ceramides, which make up 70% of skin lipids, also cholesterol and fatty acids occur playing an essential role in the formation of an effective skin lipid barrier (Boncheva, 2014; van Smeden and Bouwstra, 2016; Weerheim and Ponec, 2001; Wertz, 2013). In order to obtain the highest protection for impaired skin by diseases e.g. neurodermatitis, psoriasis and rosacea, the aim of this work was to develop a formulation with human skin-identical lipid composition. As dermal delivery system, smartLipids were selected, the third and latest generation of solid lipid nanoparticles. The smartLipids appear to be the ideal delivery system as they exhibit a pronounced skin adhesion and form the desired occlusive film on the skin already at concentrations of 2% and above (Müller et al., 2013; Müller et al., 2019). As this formulation is supposed to protect the skin by covering it like a second skin, it was named “smartLipids 2nd skin”. Another characteristic of smartLipids is the increased encapsulation efficiency of active ingredients compared to solid lipid nanoparticles and nanostructured lipid carriers (Ding et al., 2017; Müller et al., 2019; Ruick, 2015). smartLipids, loaded with an API for the therapy of psoriasis as an example, thus enables a synergetic therapy on physical and molecular level. As the exposure of impaired skin to air pollution results in the formation of reactive oxygen species as an intermediate product (Dietrich, 2016; Fujii-Kuriyama and Mimura, 2005), the antioxidant coenzyme Q10 was used as the model active ingredient.

2.2. Materials and methods

2.2.1. Materials

All materials used in this work are listed in Tab. 1 including trade name, INCI name and manufacturer/distributor. Milli-Q water was freshly produced using a Milli-Q system from Millipore GmbH (Darmstadt, Germany).

Tab. 1: Overview of materials used in this work.

function	trade name	INCI	manufacturer/distributor
natural skin lipids mixture	Ceramide IIIB	Ceramide NP	Evonik Nutrition & Care GmbH, Germany
	Ceramide VI	Ceramide AP	Evonik Nutrition & Care GmbH, Germany
	Cholesterol 95%	Cholesterol	Thermo Fisher (Kandel) GmbH, Germany
	Palmac 98-18	Steratic Acid	Berg + Schmidt GmbH & Co. KG, Germany
	Behenic acid 85%	Behenic Acid	Thermo Fisher (Kandel) GmbH, Germany
	Palmac 750	Oleic Acid	Berg + Schmidt GmbH & Co. KG, Germany
	Palmac 98-16	Palmitic Acid	Berg + Schmidt GmbH & Co. KG, Germany
	Linoleic acid 60%, Tech.	Linoleic Acid	Acros Organics B.V.B.A, Belgium
	Arachidic acid 98%	Arachidic Acid	ABCR GmbH, Germany
surfactants	Amphoterge® W-2	Disodium Cocoamphoacetate	Lonza Group AG, Switzerland
	Axol® C62	Glyceryl Stearate Citrate	Evonik Nutrition & Care GmbH, Germany
	Dermofeel® G10L	Polyglyceryl-10 Laurate	Dr. Straetmans GmbH, Germany
	Kolliphor® P188	Poloxamer 188	BASF SE, Germany
	Kolliphor® P407	Poloxamer 407	BASF SE, Germany
	Lanette® E	Sodium Cetearyl Sulfate	BASF SE, Germany
	Lanette® N	Cetaryl alcohol and Sodium Cetearyl Sulfate	BASF SE, Germany
	MiranolUltra® C-32	Sodium Cocoamphoacetate	Solvay S.A., Belgium
	Plantacare® 810UP	Caprylyl/Capryl Glucoside	BASF SE, Germany
	Plantacare® 1200UP	Lauryl Glucoside	BASF SE, Germany
	Plantacare® 2000UP	Decyl-Glucoside	BASF SE, Germany

Tab. 1 (continued): Overview of materials used in this work.

surfactants	Plurol® Stearique WL 1009	Polyglyceryl-6 Distearate	Gattefossé SAS, France
	Polysorbate 80	Polysorbate-80	Caesar & Loretz GmbH, Germany
	Sabowax® WL	Cetearyl Alcohol and Sodium Lauryl Sulfate	SABO S.p.A., Italy
	Sisterna® L70-C	Sucrose Alkyl Ester	SISTERNA B.V., Netherlands
	Sisterna® PS750C	Sucrose Alkyl Ester	SISTERNA B.V., Netherlands
	Sodium dodecyl sulphate	Sodium Dodecyl Sulphate	VWR International GmbH, Germany
	TegoCare® 450	Polyglyceryl-3 Methylglucose Distearate	Evonik Nutrition & Care GmbH, Germany
	TegoCare® PSC 3	Polyglyceryl-3 Dicitrate/Stearate	Evonik Nutrition & Care GmbH, Germany
preservatives	Glycerol (plant) solution 87%	Glycerin	SERVA Electrophoresis GmbH, Germany
	Micocare® PEHG	Ethylhexyl Glycerine and Phenoxyethanol	Thor Personal Care SAS, France.
	1,2-Pentanediol	Pentylene Glycol	TCI EUROPE N.V., Belgium
	Propylenglycol 1,2 USP, Ph.Eur.	Propylene Glycol	CG Chemikalien GmbH & Co. KG, Germany
	Coenzym Q10	Ubiquinone	Dr. Rimpler GmbH, Germany

2.2.2. Methods

2.2.2.1. *Production of smartLipids 2nd skin*

All components of the natural skin lipids mixture were balanced in a beaker, co-melted at about 180 °C and stirred for 5 minutes forming a homogenous bulk lipid. 4.0 g of this bulk lipid were than heated up to 90 °C and merged with 36.0 g of a 1.5% solution of the respective surfactant with the same temperature. The raw emulsion was pre-homogenized for 30 sec at 8500 rpm using a rotor-stator homogenizer (Ultra-Turrax® T-25, IKA-Werke, Germany). The obtained pre-emulsion was then subsequently high-pressure homogenized for 3 cycles at 800 bars at 85 °C (Micron LAB 40, APV, Germany). The product was filled into glass vials, sealed and stored at room temperature.

For the long-term study, the product was again produced, additionally containing 20.0% glycerol, 1.0% Microcare PEHG, 3.0% pentylene glycol or 15% propylene glycol as preservative,

replacing water in the respective compositions. The other ingredients and production parameters remained the same.

For the loading experiment the smartLipids 2nd skin, each 10%, 20%, … up to 50% of the bulk lipid mixture was replaced by Ubiquinone. The other ingredients and production parameters remained the same.

2.2.2.2. *Characterization of smartLipids 2nd skin*

2.2.2.2.1 Production of smartLipids suspensions

The particle size was analyzed using a Mastersizer 2000 laser diffractometer and a Hydro 2000S dispersing unit (Malvern Instruments, UK). Slight aggregates were destroyed by applying ultrasound at 75% of the maximum power of the dispersing unit. As optical properties, a refractive index of 1.456 and an imaginary refractive index of 0.01 were used. Each measurement was performed 5 times and averaged. In addition, dynamic light scattering was performed using a Zetasizer Nano ZS (Malvern Instruments, UK). To prepare the sample, 10 µL of smartLipids 2nd skin were diluted to 10 mL using Milli-Q-water and a single-use-syringe. The samples were observed by microscopic images in a magnification of 100x, 400x and 1000x using a BA 210 microscope (Motic Deutschland GmbH, Germany) to evaluate the state of aggregation and to exclude the presence of micrometer-sized particles.

2.2.2.2.2 Melting behavior

For the differential scanning calorimetry measurements, between 3.0 and 3.5 mg of the smartLipids 2nd skin bulk mixture and its components were balanced into a 40 µL standard aluminum pan. A thermogram was taken on a Mettler Toledo DSC 1 (Mettler-Toledo International Inc., USA)., measuring between 10 °C and 90°C for the suspensions and 10 °C and 160 °C for the bulk lipids. The heating rate was 10 K/min. The thermograms of the smartLipids 2nd skin components were normalized to the balanced mass.

2.3. Results and Discussion

2.3.1. Composition of lipid mixture

The composition of natural skin lipids is a frequent topic in many publications. Qualitatively, the authors conclude that stratum corneum lipids consist mainly of ceramides, cholesterol and free fatty acids (Boncheva, 2014; van Smeden and Bouwstra, 2016; Weerheim and Ponec, 2001; Wertz, 2013). However, very different information can be found about the proportions, depending, e.g., on the solvent with which the lipids were extracted (Bonté et al., 1995), the analytics (Bonté et al., 1995), the age, sex and ethnicity of the subject (Jungersted et al., 2010), the examined body part (Weerheim and Ponec, 2001), the season and the depth of the skin (Weerheim and Ponec, 2001).

The strongest variation was found for ceramides with total contents of between 16% (Motta, 1994) and 70% (Deffond et al., 1986). For the smartLipids 2nd skin the highest content of 70% ceramides was selected, as their skin barrier strengthening property has already been proven (Evonik Nutrition & Care GmbH, 2019). According to van Smeden et al., the ratio of non-hydroxy-fatty acids ceramides to α-hydroxy- fatty acids ceramides in epidermis is 1 to 1.7 (van Smeden and Bouwstra, 2016). This ratio was adapted to the smartLipids 2nd skin with Ceramide IIIB as non-hydroxy-fatty acids ceramide and Ceramide VI as α-hydroxy- fatty acids ceramide. Besides the 70% ceramides, smartLipids 2nd skin was composed of 15% cholesterol and 15% free fatty acids. The quantitative composition of the free fatty acids was inspired by Nicollier et al. (Nicollier et al., 1986). This results in the following overall composition of smartLipids 2nd skin (Fig. 1): 44.1% Ceramide IIIB, 25.9% Ceramide VI,15.0% cholesterol, 3.3% stearic acid, 3.1% behenic acid, 2.7% oleic acid, 2.6% palmitic acid, 2.0% linoleic acid and 1.4% arachidic acid.

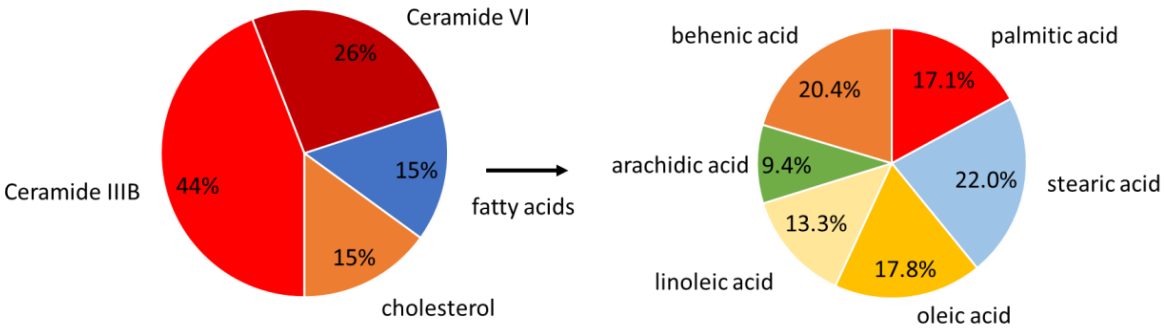

Fig. 1: Composition of the smartLipids 2nd skin derived from the composition of human stratum corneum lipids as it is described in literature.

Apart from the complex lipid matrix composition consisting of up to 10 components, smartLipids are characterized by their solid state at skin temperature, i.e. at 32 °C. Except for oleic and linoleic acid all components and thus 95.3 wt% have melting ranges above 60 °C (Fig. 2, upper). Melting the lipids to a single phase noticeably lowered the melting range, but the lipid mixture still exceeded the required limit of 32 °C (Fig. 2, lower). Thus, this lipid mixture fulfils all necessary criteria of the smartLipids technology.

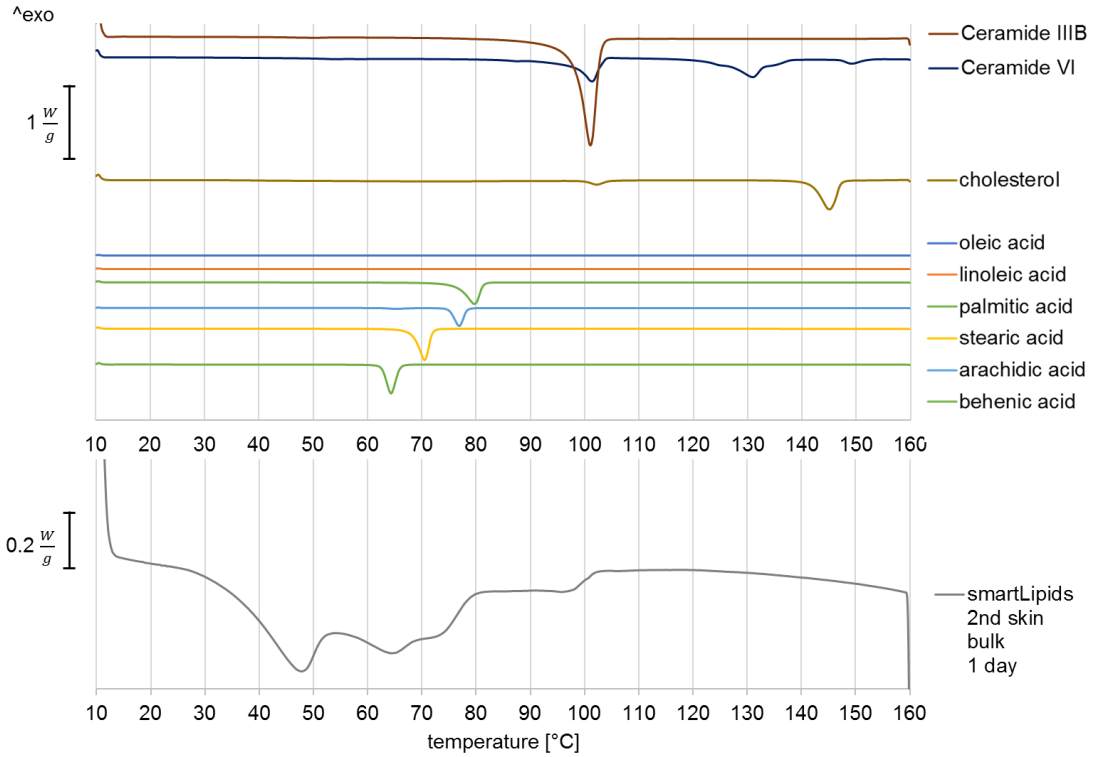

Fig. 2: DSC thermograms of all lipids individually (upper) and after co-melting and solidifying to a homogeneous lipid matrix (lower) both measured with a heating rate of 10 K/min from 10 °C to 160 °C.

2.3.2. Surfactant screening

As the lipid matrix consists of more than 9 different components, of which most show more or less pronounced surface activity, its physical stabilization in nanometer size range is a challenge. To stabilize the suspension 12 surfactants were selected with regard to their skin tolerability. Additionally 7 commonly used surfactants for lipid nanoparticles stabilization, e.g. Tween 80 were selected. For the screening, all surfactants were used at 1.5% and their stabilizing properties examined for a 10% particle suspension.

The result is described in Tab. 2. Already directly or just one day after production solidification and gelation of samples attributed to aggregation was observed (Fig. 3, lower, the right two

samples). Only 3 of the 19 prepared samples were still liquid after one week of storage at room temperature. These were stabilized with Miranol Ultra C-32, Lanette E and TegoCare 450. A rational relationship could not be established from the study. For instance, the calculated HLB values of the three surfactants are completely different (25, 37 and 12, respectively), as well as their chemical classification (amphoteric, anionic and non-ionic, respectively). What they all have in common is that all three are ECOCERT certified and are therefore organic ingredients.

Tab. 2: Macroscopic evaluation of all prepared samples 1 day after production, showing that only 3 out of 19 surfactants led to liquid suspensions without particles visible to the naked eye. Surfactants were classified in three categories (amphoteric, anionic and nonionic) and written in green if ECOCERT certified or red if not.

Type	Surfactant	Macroscopic Stability
Amphoteric	Amphoterge® W-2	gelled, visible particles
	Miranol Ultra® C-32	not gelled, no visible particles
Anionic	Axol® C62	not gelled, visible particles
	Lanette® E	not gelled, no visible particles
	Lanette® N	gelled, visible particles
	Sabowax WL	not gelled, visible particles
	Sodium Dodecyl Sulphate	gelled, visible particles
Nonionic	Dermofeel® G10L	gelled, visible particles
	Kolliphor® P188	not gelled, visible particles
	Kolliphor® P407	gelled, visible particles
	Plantacare® 810 UP	gelled, visible particles
	Plantacare® 1200 UP	gelled, visible particles
	Plantacare® 2000 UP	gelled, visible particles
	Plurol Stearique WL® 1009	not gelled, visible particles
	Sisterna L70-C	gelled, visible particles
	Sisterna PS750C	gelled, visible particles
	TegoCare® 450	not gelled, no visible particles
	TegoCare® PSC3	not gelled, visible particles
	Tween® 80	gelled, visible particles

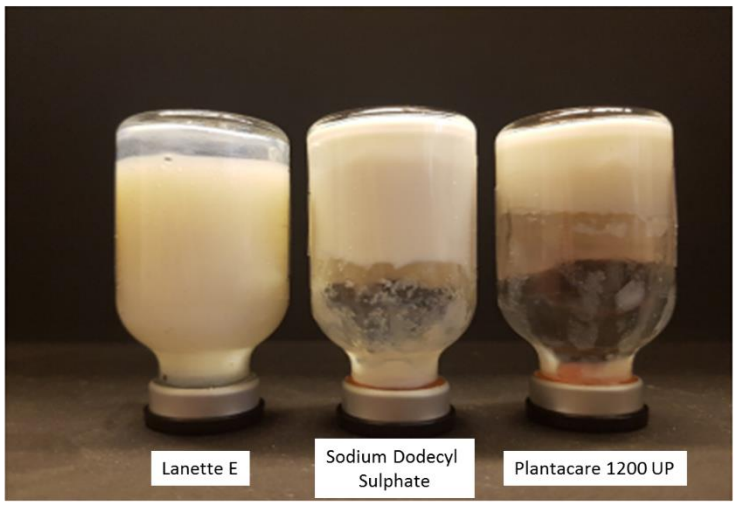

Fig. 3: Photos taken 1 day after production of a liquid sample stabilized with Lanette E (left), a gelled sample stabilized with Sodium Dodecyl Sulphate (middle) and a solidified sample stabilized with Plantacare 1200 UP (right).

The particle size and size distribution of these three liquid samples were analyzed on day 1 using PCS and LD (cf. chapter 2.2.2.1.). Lanette E and TegoCare 450 stabilized samples had a z-ave in the desired lower submicron range as well as a small polydispersity index (PdI) value of about 0.25 indicating a narrow particle size distribution. The LD90 value for the Lanette E sample is 310 nm and is therefore considerably smaller than for the TegoCare 450 sample with an LD90 diameter of 554 nm. In contrast to these two samples, the Miranol Ultra C-32 stabilized formulation had an LD90 value of 8 µm. The PdI value of the Miranol Ultra C-32 stabilized sample with 0.34 was also higher than the other two samples being in good agreement with the LD90 value in µm size range.

As expected, Miranol Ultra C-32 did not provide sufficient physical stabilization of smartLipids 2nd skin suspension. In addition to considerable particle growth visible under microscope, the sample completely gelled after 2 weeks. In contrast, the Lanette E and TegoCare 450 stabilized samples remained completely liquid after 2 months of storage and were therefore re-analyzed as most promising samples by PCS and LD. Both samples showed an increase in z-ave and PdI, but the values still remained in the lower submicron range, i.e. 211 nm and 329 nm, respectively. Also the LD90 values being below 600 nm are still in the submicron range. Unexpectedly, the TegoCare 450 stabilized formulation showed a strong increase in viscosity after 2 months and complete solidification after 3 months of storage.

Hence, Lanette E proved to be the most effective surfactant out of the screening and was therefore used in all subsequent investigations. The production of Lanette E stabilized smartLipids 2nd skin proved to be reproducible. Produced by 3 persons on 3 different days resulted in a z-ave of 156.8 nm ± 3 nm, PdI of 0.247 ± 0.006, LD50 of 316 nm ± 9 nm and LD90 of 614 nm ± 32 nm.

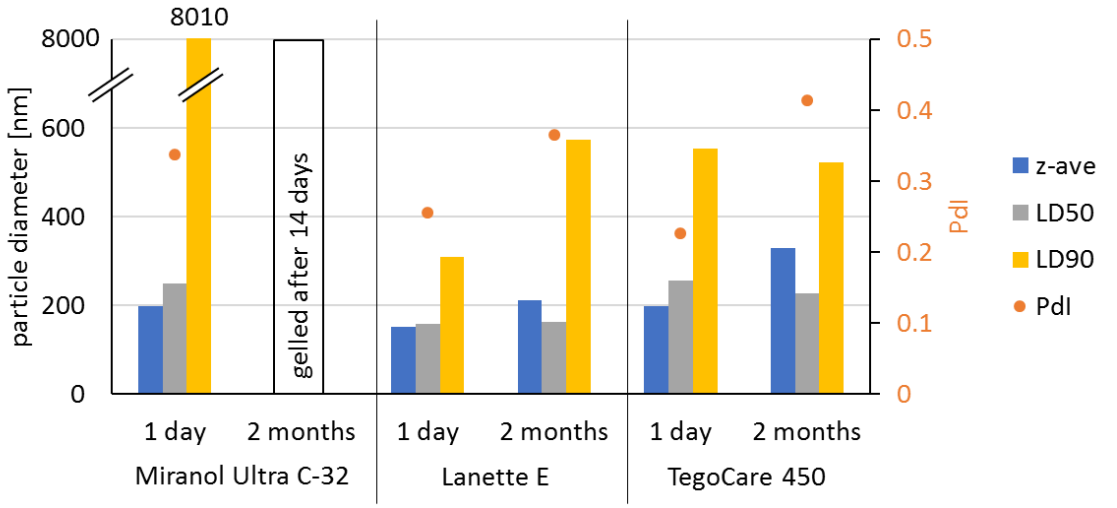

Fig. 4: Particle size (z-ave, LD50 and LD90) and polydispersity index (PdI) of smartLipids 2nd skin produced with the 3 best surfactants from the surfactant screening 1 day and 2 months after production.

2.3.3. Preservation of smartLipids 2nd skin

Since the smartLipids 2nd skin formulation is an aqueous suspension, preservation is needed. Therefore, 4 preservatives were added in their respective effective concentrations prior the homogenization step, and the influence in particle size, size distribution and storage stability was investigated. The addition of 3% pentylene glycole led to z-ave of 120 nm, PdI of 0.24 and LD90 of 240 nm, and thus to noticeably smaller particles compared to unpreserved formulation (Fig. 6). Hence, the addition of preservative pentylene glycole showed positive influence on suspension stability. In contrast, the addition of propylene glycol led to complete destabilization of the system visible by the beginning gelation 1 day after production. The addition of glycerol as a preservative resulted in larger particle diameters and a broader size distribution than in unpreserved suspensions with z-ave of 215 nm, PdI of 0.31 and LD90 of 499 nm. Microcare PEHG is a liquid blend of phenoxyethanol and ethylhexyl glycerine. Comparable to the pentylene glycole, Microcare PEHG led to suspension stabilization. The z-ave decreased from 157 to 140 nm and the LD90 value from 316 to 247 nm compared to the unpreserved formulation.

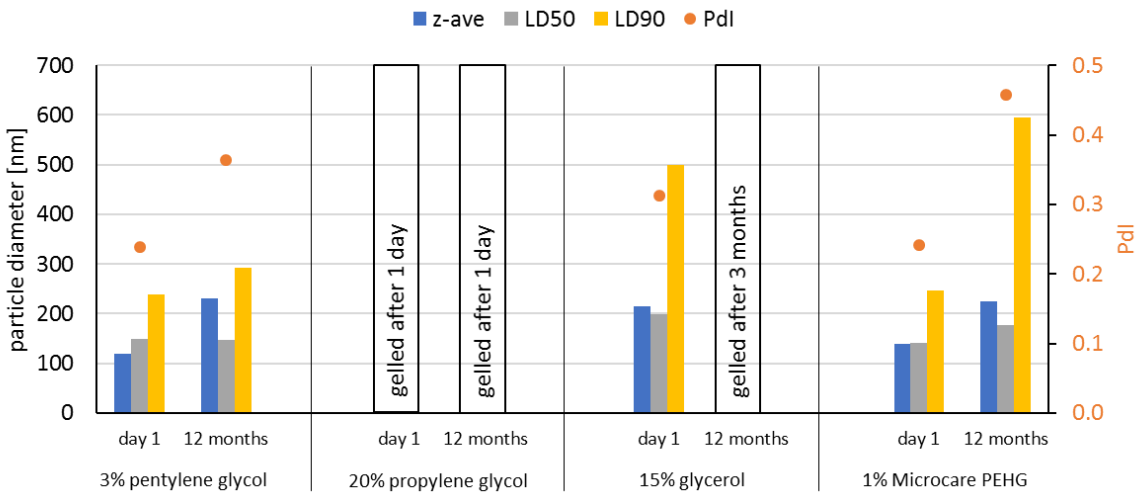

Fig. 6: Particle size (z-ave, LD50 and LD90) and polydispersity index of smartLipids 2nd skin stabilized with Lanette E and preserved by 4 different preservatives at their respective effective concentrations.

Storage of pentylene glycol and Microcare PEHG preserved formulation for 12 months did not result in gelation or solidification of the samples and both particle size and size distribution increased only slightly (Fig.6). With 231 nm and 225 nm, respectively, their z-aves were nearly the same. Considerable differences were found in their LD90 values. For pentylene glycole preserved sample the LD90 value was 292 nm and thus remained almost unchanged after 12 months, while for Microcare PEHG a significant increase from 247 nm to 595 nm was measured. Despite the increase in LD90 value the both preservatives resulted in storage-stable smartLipids 2nd skin formulations. Based on the narrower size distribution pentylene glycol should be preferred. In summary, a smartLipids 2nd skin formulation has been successfully developed that is preserved and exhibits physical storage stability over 12 months.

2.3.4. Loading with model active coenzyme Q10

Coenzyme Q10 is an effective antioxidant (Knott et al., 2015), naturally occurring in the human skin. It is commonly used in dermal products (Allemann and Baumann, 2008) due to its ability to scavenge UVA induced radicals (Zhou et al., 2010). This active matches well the smartLipids 2nd skin concept and was therefore loaded into the smartLipids as model active.

On the first day after production there was no noticeable difference between the samples with 30%, 40% and 50% coenzyme Q10 loading. The z-ave varied slightly and were between

156 nm (30%) and 140 nm (50%), where the LD50 and LD90 values were between 146 nm (30%) and 145 nm (50%) and 247 nm (30%) and 224 nm (50%), respectively.

Differences in stability became visible after storage of the samples. After 11 months the LD90 value increases to µm size range for samples with 30% and 40% coenzyme Q10 loadings. Most stable was the highest coenzyme Q10 loading of 50% with LD90 values of 278 nm. The increasing stability with increasing Q10 content can be explained by the fact that coenzyme Q10 has no surface active properties as the lipid mixture. Hence, coenzyme Q10 can be better stabilized by Lanette E.

It is noteworthy that a loading of 50% is possible. This is considerably higher compared to the loadings obtained in SLN (1st generation solid lipid nanoparticles) and NLC (2nd generation nanostructured lipid carriers) with 1.5% and 25%, and once again proves the advantages of smartLipids as the 3rd generation of solid lipid nanoparticles.

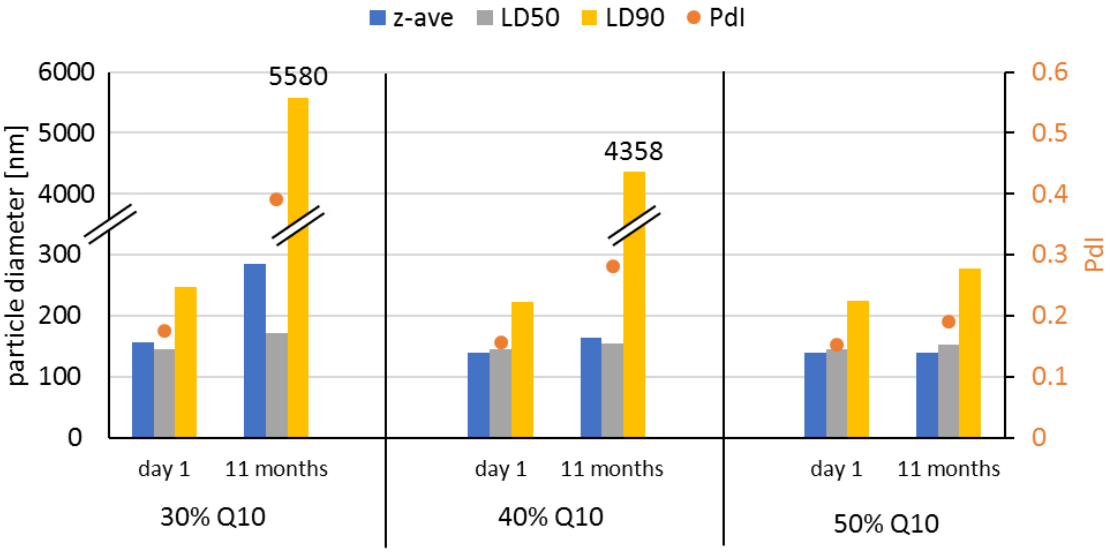

Fig. 7: Particle size (z-ave, LD50 and LD90) and polydispersity index (PdI) of smartLipids 2nd skin stabilized with Lanette E and loaded with 30%, 40% and 50% coenzyme Q10.

2.4. Conclusion

A smartLipids 2nd skin formulation was successfully developed. Its lipid phase composition was adapted from the natural skin lipid composition, i.e. consisted of 44.1% Ceramide IIIB, 25.9% Ceramide VI,15.0% cholesterol, 3.3% stearic acid, 3.1% behenic acid, 2.7% oleic acid, 2.6% palmitic acid, 2.0% linoleic acid and 1.4% arachidic acid. Among the 19 investigated surfactants, Lanette E, an ECOCERT certified surfactant at 1.5% proved to be most suitable for stabilizing a 10% suspension of this lipid mixture. The necessary preservation of the aqueous

smartLipids 2nd skin suspension was achieved by the addition of 3% pentylene glycol. This optimized formulation was physically storage stable for 12 months at room temperature by now. The smartLipids technology enabled a remarkably high loading of up to 50% coenzyme Q10 without affecting the storage stability. Thus a smartLipids 2nd skin formulation is now available for further investigations to demonstrate the concept of reinforcing impaired skin lipid barrier and enhancing the penetration of loaded actives.

2.5. References

Allemann, B., Baumann, L., 2008. Antioxidants used in skin care formulations. Skin Therapy Lett. 13 (7), 5–9.

Boncheva, M., 2014. The physical chemistry of the stratum corneum lipids. Int. J. Cosmet. Sci. 36 (6), 505–515.

Bonté, F., Pinguet, P., Chevalier, J.M., Meybeck, A., 1995. Analysis of all stratum corneum lipids by automated multiple development high-performance thin-layer chromatography. J. Chromatogr. B., Biomed. Appl. 664 (2), 311–316.

Brunekreef, B., Holgate, S.T., 2002. Air pollution and health. Lancet 360 (9341), 1233–1242.

Chamlin, S.L., Kao, J., Frieden, I.J., Sheu, M.Y., Fowler, A.J., Fluhr, J.W., Williams, M.L., Elias, P.M., 2002. Ceramide-dominant barrier repair lipids alleviate childhood atopic dermatitis: Changes in barrier function provide a sensitive indicator of disease activity. J. Am. Acad. Dermatol. 47 (2), 198–208.

Coderch, L., López, O., La Maza, A. de, Parra, J.L., 2003. Ceramides and skin function. Am. J. Clin. Dermatol. 4 (2), 107–129.

Cork, M.J., Danby, S.G., Vasilopoulos, Y., Hadgraft, J., Lane, M.E., Moustafa, M., Guy, R.H., Macgowan, A.L., Tazi-Ahnini, R., Ward, S.J., 2009. Epidermal barrier dysfunction in atopic dermatitis. J. Invest. Dermatol. 129 (8), 1892–1908.

Deffond, D., Saint Leger, D., Leveque, J.L., Agache P, 1986. In vivo measurement of epidermal lipids in man. Bioeng. Skin 2 (1), 71–85.

Dietrich, C., 2016. Antioxidant functions of the aryl hydrocarbon receptor. Stem Cells Int. 2016.

Ding, Y., Pyo, S.M., Müller, R.H., 2017. smartLipids®as third solid lipid nanoparticle generation - stabilization of retinol for dermal application. Pharmazie 72 (12), 728–735.

Elias, P.M., Menon, G.K., 1991. Structural and lipid biochemical correlates of the epidermal permeability barrier, in: Elias, P.M. (Ed.), Skin Lipids, vol. 24. Elsevier, pp. 1–26.

Essa, E.A., Bonner, M.C., Barry, B.W., 2003. Electroporation and ultradeformable liposomes; human skin barrier repair by phospholipid. J. Control. Release 92 (1-2), 163–172.

Evonik Nutrition & Care GmbH, 2019. Ceramide III / Ceramide IIIB technical information. https://www.ulprospector.com/de/eu/PersonalCare/Detail/1481/52000/Ceramide-III. Accessed 19 November 2019.

Feingold, K.R., 2012. Lamellar bodies: The key to cutaneous barrier function. J. Invest. Dermatol. 132 (8), 1951–1953.

Fujii-Kuriyama, Y., Mimura, J., 2005. Molecular mechanisms of AhR functions in the regulation of cytochrome P450 genes. Biochem. Biophys. Res. Commun. 338 (1), 311–317.

Gehring, W., Wenz, J., Gloor, M., 1997. Influence of topically applied ceramide/phospholipid mixture on the barrier function of intact skin, atopic skin and experimentally induced barrier damage. Int. J. Cosmetic Sci. 19 (4), 143–156.

Gelfand, J.M., Stern, R.S., Nijsten, T., Feldman, S.R., Thomas, J., Kist, J., Rolstad, T., Margolis, D.J., 2005. The prevalence of psoriasis in African Americans: Results from a population-based study. J. Am. Acad. Dermatol. 52 (1), 23–26.

Harding, C.R., 2004. The stratum corneum: Structure and function in health and disease. Dermatol. Ther. 17 Suppl 1, 6–15.

Jin, S.-P., Li, Z., Choi, E.K., Lee, S., Kim, Y.K., Seo, E.Y., Chung, J.H., Cho, S., 2018. Urban particulate matter in air pollution penetrates into the barrier-disrupted skin and produces ROS-dependent cutaneous inflammatory response in vivo. J. Dermatol. Sci. 91 (2), 175–183.

Jungersted, J.M., Høgh, J.K., Hellgren, L.I., Jemec, G.B.E., Agner, T., 2010. Ethnicity and stratum corneum ceramides. Br. J. Dermatol. 163 (6), 1169–1173.

Kim, K.E., Cho, D., Park, H.J., 2016. Air pollution and skin diseases: Adverse effects of airborne particulate matter on various skin diseases. Life Sci. 152, 126–134.

Knott, A., Achterberg, V., Smuda, C., Mielke, H., Sperling, G., Dunckelmann, K., Vogelsang, A., Krüger, A., Schwengler, H., Behtash, M., Kristof, S., Diekmann, H., Eisenberg, T., Berroth, A., Hildebrand, J., Siegner, R., Winnefeld, M., Teuber, F., Fey, S., Möbius, J., Retzer, D., Burkhardt, T., Lüttke, J., Blatt, T., 2015. Topical treatment with coenzyme Q10-containing formulas improves skin's Q10 level and provides antioxidative effects. Biofactors 41 (6), 383–390.

Li, X., Jin, L., Kan, H., 2019. Air pollution: A global problem needs local fixes. Nature 570 (7762), 437–439.

Mancebo, S.E., Wang, S.Q., 2015. Recognizing the impact of ambient air pollution on skin health. J. Eur. Acad. Dermatol. Venereol. 29 (12), 2326–2332.

Manojkumar, N., Srimuruganandam, B., 2019. Health effects of particulate matter in major Indian cities. Int. J. Environ. Health Res. 29 (6), 1–13.

Motta, S., 1994. Abnormality of water barrier function in psoriasis. Arch Dermatol 130 (4), 452.

Motta, S., Sesan, S., Monti, M., Giuliani, A., Caputo, R., 1994. Interlamellar lipid differences between normal and psoriatic stratum corneum. Acta. Derm. Venereol. Suppl. (Stockh.) (186), 131–132.

Müller, R.H., Olechowski, F., Köpke, D., Pyo, S.M., 2019. smartLipids: the third generation of solid submicron lipid particles for dermal delivery of actives, in: Cornier, J., Keck, C.M., van de Voorde, M. (Eds.), Nanocosmetics. From Ideas to Products, 1st ed., pp. 141–159.

Müller, R.H., Sinambela, P., Keck, C.M., 2013. NLC – the invisible dermal patch for moisturizing & skin protection. Euro Cosmetics 6, 20–22.

Ní Raghallaigh, S., Bender, K., Lacey, N., Brennan, L., Powell, F.C., 2012. The fatty acid profile of the skin surface lipid layer in papulopustular rosacea. Br. J. Dermatol. 166 (2), 279–287.

Nicollier, M., Massengo, T., Rémy-Martin, J.-P., Laurent, R., Adessi, G.-L., 1986. Free fatty acids and fatty acids of triacylglycerols in normal and hyperkeratotic human stratum corneum. J. Investig. Dermatol. 87 (1), 68–71.

Nutten, S., 2015. Atopic dermatitis: Global epidemiology and risk factors. Annals of nutrition & metabolism 66 Suppl 1, 8–16.

Pan, T.-L., Wang, P.-W., Aljuffali, I.A., Huang, C.-T., Lee, C.-W., Fang, J.-Y., 2015. The impact of urban particulate pollution on skin barrier function and the subsequent drug absorption. J. Dermatol. Sci. 78 (1), 51–60.

Pope, C.A., Burnett, R.T., Thun, M.J., Calle, E.E., Krewski, D., Ito, K., Thurston, G.D., 2002. Lung cancer, cardiopulmonary mortality, and long-term exposure to fine particulate air pollution. J Am. Med. Assoc. 287 (9), 1132–1141.

Puri, P., Nandar, S.K., Kathuria, S., Ramesh, V., 2017. Effects of air pollution on the skin: A review. Indian J. Dermatol. Venereol. Leprol. 83 (4), 415–423.

Rawlings, A.V., 2003. Trends in stratum corneum research and the management of dry skin conditions. Int. J. Cosmet. Sci. 25 (1-2), 63–95.

Ruick, R., 2015. smartLipids - die Neue Generation der Lipidnanopartikel nach SLN und NLC: Dissertation zur Erlangung des akademischen Grades des Doktors der Naturwissenschaften (Dr. rer. nat.). Freie Universiät Berlin.

Seaton, A., Godden, D., MacNee, W., Donaldson, K., 1995. Particulate air pollution and acute health effects. Lancet 345 (8943), 176–178.

van Smeden, J., Bouwstra, J.A., 2016. Stratum corneum lipids: Their role for the skin barrier function in healthy subjects and atopic dermatitis patients. Curr. Probl. Dermatol. 49, 8–26.

van Smeden, J., Janssens, M., Gooris, G.S., Bouwstra, J.A., 2014. The important role of stratum corneum lipids for the cutaneous barrier function. Biochim. Biophys. Acta. 1841 (3), 295–313.

Weerheim, A., Ponec, M., 2001. Determination of stratum corneum lipid profile by tape stripping in combination with high-performance thin-layer chromatography. Arch. Dermatol. Res. 293 (4), 191–199.

Wertz, P.W., 2013. Current understanding of skin biology pertinent to skin penetration: Skin biochemistry. Skin Pharmacol. Physiol. 26 (4-6), 217–226.

WHO, 2019. World Health Organization international website. WHO. https://www.who.int/airpollution/en/. Accessed 21 October 2019.

Yamamoto, A., Serizawa, S., Ito, M., Sato, Y., 1991. Stratum corneum lipid abnormalities in atopic dermatitis. Arch. Dermatol. Res. 283 (4), 219–223.

Zhou, H., Yue, Y., Liu, G., Li, Y., Zhang, J., Yan, Z., Duan, M., 2010. Characterisation and skin distribution of lecithin-based coenzyme Q10-loaded lipid nanocapsules. Nanoscale Res. Lett. 5 (10), 1561–1569.

3. Inverse loading method for the production of smartLipids loaded with whitening agent phenylethyl resorcinol

Abstract

Phenylethyl resorcinol (PER) is a highly effective tyrosinase inhibitor and therefore an interesting whitening agent in pharmacy and cosmetics. According to literature, the limitation of its use in dermal products because of low solubility and chemical instability can be significantly improved by nanostructured lipid carriers (NLC). Literature formulations, however, are not yet sufficiently developed for practical application. For example the PER loading and the total PER concentration in suspension are too low, and the physical storage stability of 3 months too short for a market product. Also, the feasibility of industrial large-scale production has not yet been proven. These points were elaborated in the present study with the aim of transforming the academic idea of PER lipid nanoparticles into a marketable product. In order to increase the PER loading in the lipid particles and PER concentration in total formulation smartLipids technology was combined with the inverse loading method. smartLipids are the further development of nanostructured lipid carriers (NLC). The increase in loading is the result of combining more than 10 different solid or solid and liquid lipids instead of using only 1 solid and 1 liquid lipid as in the NLC. The highest reported loading of PER in NLC of 25% in literature was successfully doubled to 50% by smartLipids technology. Mean particle size of 107 nm with polydispersity index of 0.15 was obtained by 3 cycles high pressure homogenization at 500 bar on Micron LAB 40. Lanette N was determined to be the best stabilizer. At 1.4%, 2.1% and 2.8% it enabled the stabilization of 10%, 15% and 20% PER smartLipids respectively for more than 14 months (mean particle size of 102 nm and polydispersity index of 0.17). The feasibility of industrial large-scale production has been demonstrated on a Micron LAB 60. Its high production volume of 60 kg/h enables the production PER smartLipids concentrate which is enough for a ton of effective skin whitening product. One passage on Micron LAB 60 at 400 bar led to stable PER smartLipids suspensions with 72% particles < 100 nm and a z-ave of 160 nm. If a product is desired that does not have to be declared as a nanoproduct, the production pressure can be reduced from to 300 bar, resulting in a suspension with only 44% particles < 100 nm and a z-ave of 183 nm. Thus, a marketable PER smartLipids formulation has been successfully developed with sufficient PER concentration, high storage stability and the possibility of large-scale production.

3.1. Introduction

Phenylethyl resorcinol (PER) is a synthetic compound inspired by pinosylvin, an antioxidative compound of the scotch pine bark (Hong et al., 2016). PER is reported to be a very potent whitening agent with a distinctly higher tyrosinase inhibition compared to the standards currently used, e.g. 100 times more inhibiting than β-arbutin (Kim et al., 2017), 50 times more than arbutin, 33 times more than hydroquinone (Kolbe et al., 2013), and 22 times more than kojic acid (Vielhaber et al., 2007). And clear decrease of skin pigmentation was proven in vivo already at the low PER concentration of 0.5% (Vielhaber et al., 2007). A major challenge in the development of PER-containing dermal products is PER's high sensitivity against oxygen and light (Fan et al., 2014b). The precise degradation mechanism is not yet clarified but an oily PER solution gets inactivated by > 30% already after 90 days of storage in natural daylight (Fan et al., 2014b). Furthermore, PER is poorly soluble in water (4.05 mg/g (Jeon et al., 2019)), which is the main component and outer phase in most dermal vehicles such as hydrogels, lotions and creams. This leads to the creation of a low concentration gradient between formulation and skin, resulting in insufficient skin penetration and poor performance of the formulation.

Therefore, various PER loaded dermal delivery systems have been developed to improve the chemical stability and skin penetration of PER, including microspheres (Jeon et al., 2019), liposomes (Fan et al., 2014a), ethosomes (Limsuwan et al., 2017), transferosomes, invasomes (Amnuaikit et al., 2018) and nanostructured lipid carriers (NLC) (Fan et al., 2014b). Only NLC was able to meet both, improved chemical stability and skin penetration simultaneously. The chemical stability of PER loaded in NLC could be increased by 29% compared to oily PER solution (Fan et al., 2014b), and efficacy of tyrosinase inhibition even by 67% compared to aqueous PER solution (Kim et al., 2017). Due to the occlusive effect of NLC on skin, penetration of loaded active can also be increased (Babaei et al., 2016; Li and Ge, 2012; Tofani et al., 2016). Further, NLC allow a sustained release of PER, alleviating irritative properties of PER (Fan et al., 2014b; Jia et al., 2016; Kim et al., 2017) as well as an increased cellular uptake (Kim et al., 2017). All these points make PER NLC a promising delivery system for skin whitening products. In order to transform this promising academic idea into a marketable product, the academic formulations still need improvements.

The PER lipid nanoparticles are dispersed in an aqueous surfactant solution and are therefore technically a suspension. In an already established dermal vehicle, PER lipid nanoparticles can

be incorporated by mixing this suspension under gentle stirring to a vehicle. With a dilution factor of 10 or higher, only minimal rheological changes are expected. Therefore, this factor is regarded as the limit value for industrial applicability of lipid nanoparticles. However, the formulations published so far do not contain enough PER and therefore fall below this limit. An improvement of the PER loading and increase of PER concentration in formulation is therefore necessary. Another point to be improved is the selection of the surfactant to stabilize the lipid nanoparticles in the suspension. In reported formulations, the surfactant used is either not skin-friendly or even incompatible with PER's phenolic structures, e.g. polyethylene glycol forming insoluble chelates. One point that has not yet been considered in PER lipid nanoparticle publications is the possibility of upscaling the production to industrial scale. So far, the production parameters have all been reported on laboratory scale.

In this article, all these 3 points were systematically elaborated with the aim of developing a marketable PER delivery system composed of skin-friendly ingredients, sufficiently high loading and concentration of PER, as well as the possibility of large-scale production.

3.2. Materials and methods

3.2.1. Materials

ACETEM 50-00 P MB (Acetylated Mono- and Diglycerides, Danisco Danisco Deutschland GmbH, Niebüll, Germany), castor oil (Caesar & Lorenz GmbH, Hilden, Germany), Cetiol® (Decyl Oleate, Caesar & Lorenz GmbH, Hilden, Germany), Compritol® 888 ATO (Glyceryl Behenate, Gattefossé Deutschland GmbH, Bad Krozingen, Germany), Cutina® CP(Cetyl Palmitate, BASF, Ludwigshafen, Germany), Cutina® HR (Hydrogenated Castor Oil, BASF,Ludwigshafen, Germany), Dynasan® 112 (Trilaurin), Dynasan® 114 (Trimyristin) and Dynasan® 118 (Tristearin) (IOI Oleo GmbH, Hamburg, Germany), isopropyl myristate (Merck Schuchard, Hohenbrunn, Germany), isopropyl palmitate (BASF, Ludwigshafen, Germany), isopropyl stearate (Fluka Chemika,Buchs, Switzerland), Lanette® N (Cetearyl Alcohol (and) Sodium Cetearyl Sulfate, BASF,Ludwigshafen, Germany), Lipocire™ A (C10-18 Triglycerides, Gattefossé Deutschland GmbH, Bad Krozingen, Germany), liquid paraffin (Caesar & Lorenz GmbH, Hilden, Germany), Miglyol® 812 (Caprylic/Capric Triglyceride, Caesar & Lorenz GmbH, Hilden, Germany), myristic acid (Carl Roth GmbH + Co. KG, Karlsruhe, Germany), Nafol 1822C (Behenyl Alcohol, Sasol Germany GmbH, Hamburg, Germany), octyl dodecanol (Caesar & Lorenz GmbH, Hilden, Germany), oleic acid (Caesar & Lorenz GmbH, Hilden, Germany), Oxynex® ST liquid

(Diethylhexyl Syringylidenemalonate (and) Caprylic/Capric Triglycerid, Merck KGaA, Darmstadt, Germany), Palmac 55-16 (Palmitic Acid, Berg + Schmidt GmbH & Co. KG, Hamburg, Germany), phenylethyl resorcinol (Watson International Ltd, Jiaungsu, China), Precirol® ATO 5 (Gattefossé Deutschland GmbH, Bad Krozingen, Germany), raffinate rapeseed oil (Caesar & Lorenz GmbH, Hilden, Germany), raffinate sesame oil (Caesar & Lorenz GmbH, Hilden, Germany), stearic acid (Sigma-Aldrich, St. Lois MO, USA), Sternoil 12-HSA (Hydroxystearic Acid, Berg + Schmidt GmbH & Co. KG, Hamburg, Germany), Tinosorb® S (Bis-Ethylhexyloxyphenol Methoxyphenyl Triazine, BASF, Ludwigshafen, Germany), Vegarol® 1698 (Cetyl Alcohol), Vegarol® 1898 (Stearyl Alcohol) and Vegarol® 2270(Behenyl Alcohol) (Berg + Schmidt GmbH & Co. KG, Hamburg, Germany), virgin linseed oil (Caesar & Lorenz GmbH, Hilden, Germany), virgin olive oil (Caesar & Lorenz GmbH, Hilden, Germany), Witepsol® H32 (C10-18 Triglycerides, IOI Oleo GmbH, Hamburg, Germany), Witepsol® W31 (C10-18 Triglycerides, Contensio Chemicals GmbH, Witten, Germany).

3.2.2. Lipid screening

The solubility of PER in various oils was determined by balancing 1.0 g PER in a 20 mL glass vial and adding oil in steps, corresponding to a PER solubility of 90%, 80%, 70%, 60%, 50%, 40%, 33%, 25%, 20% 10%, 5%, 1%, and 0.1% (w/w). After each oil addition, the sample was stirred for 30 minutes and complete dissolution of PER was examined both with the naked eye and under microscope (BA 210, Motic Deutschland GmbH, Wetzlar, Germany) at 100-fold magnification with a polarization filter.

3.2.3. Production of PER loaded lipid nanoparticles on lab scale

Lipid nanoparticle suspensions were produced by hot high pressure homogenization (Schwarz et al., 1994) using a Micron LAB 40 (APV Systems, Unna, Germany) having a production volume of 40 mL per batch. The lipid phase consisted of PER loaded to 50% and 80% in one of 23 solid lipids as well as Lanette N (INCI) at 1.4% for stabilizing 10% particles in aqueous suspension.
All lipophilic components, i.e. PER, solid lipids and Lanette N were heated to 85 °C and co-melted. Double distilled water was heated to the same temperature, added to the lipid phase, and pre-homogenized using a rotor-stator-homogenizer (Ultra-Turrax T 25, IKA-Werke, Staufen, Germany) for 30 seconds at 8000 rpm. The resulting pre-emulsion was then high pressure homogenized for 3 cycles at 500 bar and 85°C. In order to obtain nanosuspensions

from produced nanoemulsions, samples were slowly cooled to 20°C light protected at room temperature.

3.2.4. Production of PER loaded lipid nanoparticles on large scale

For upscaling the production, a Gaulin LAB 60 (APV Systems, Unna, Germany) equipped with two valves was used in discontinuous mode. 6 kg of PER smartLipids composed of 5% PER. 3% Lipocire A, 1% Oxynex ST liquid, 1% Tinosorb S, 1.4% Lanette N, and 88.6% double distilled water were produced on the Gaulin LAB 60. The pre-emulsion was prepared identical to lab scale production and passed once through the homogenizer with the pre-valve set to 20 bar, 30 bar and 40 bar, and the main valve set to 200 bar, 300 bar, and 400 bar, respectively. The obtained nanoemulsion was allowed to cool down slowly to a smartLipids suspension at room temperature and protected from light.

3.2.5. Particle size analysis

The particle size (z-ave) and polydispersity index (PdI) of prepared lipid nanoparticles were determined by photon correlation spectroscopy (PCS) using a Zetasizer Nano ZS (Malvern Instruments, Worcestershire, UK) having a measuring range of 0.1 nm to 10 µm. 10 µL of sample was diluted in 10 mL Milli-Q-water and measured for 10 times. The calculated averages are given as result. Further, samples were investigated by laser diffraction using a Mastersizer 2000 equipped with a Hydro 2000S dispersing unit (Malvern Instruments, Worcestershire, UK) to detect larger particles up to 2,000 µm exceeding the measuring range of PCS. Sample was added until an obscuration range of 4-6 % was reached. For dispersing the particles the stirrer unit was set to 1,750 rpm. Mie theory was used to calculate volume weighted diameters applying 1.456 as real and 0.01 as imaginary refractive index. Each sample was measured in triplicate and as result the calculated mean was used. In addition, the suspensions were examined with a light microscope (BA 210, Motic Deutschland GmbH, Wetzlar, Germany) at magnifications of 100, 400 and 1,000- fold to detect possible larger particles or aggregates in micrometer range.

3.2.6. Determination of encapsulation efficacy

The particles were precipitated by the addition of aqueous 1% NaCl solution and separated using a centrifugal filter with a nominal molecular weight cut-off of 3K (Modified PES 3K, 500

µl, VWR International GmbH, Darmstadt, Germany) at 8,000 x g for 30 minutes. To prevent the determination of incorrect results by the adsorption of PER on the filter membrane, these were saturated with 500 µL of an aqueous PER solution (250 mg/L) before use. PER concentration in filtrate was determined by UV-VIS analysis, and PER concentration in total formulation was determined after extraction in acetonitrile according to (Hong et al., 2016). Each sample was measured in triplicate and the mean was given as result.

The EE% was calculated after:

$$\mathrm{EE\%} = \frac{\text{PER total mass} - \text{PER mass in aqueous phase}}{\text{PER total mass}} * 100\%$$

3.3. Results and discussion

3.3.1. Definition of requirements to the new formulations

Prior to the development of novel PER NLC and smartLipids, the requirements to the formulations were precisely defined as follows:

a) Requirements to composition

The composition should only consist of skin-friendly ingredients. And raw materials that are certified as organic by e.g. ECOCERT should be preferred over synthetic raw materials if comparably stable formulations can be obtained. Most importantly, none of the ingredients should affect the efficacy of PER. For example, some lipid nanoparticle formulations in literature contain large amounts of surfactants containing polyethylene glycol in their structure (Fan et al., 2014b; Kim et al., 2017), e.g. Tween or steareth-21. PER with its phenolic structure shows the typical incompatibilities with polyethylene glycols (Fig. 1) (Fahr and Voigt, 2018; Roy and Moulik, 200). Phenolic structures are also not compatible with cellulose ether, e.g. methyl cellulose or hydroxypropyl methyl cellulose (Banks et al., 2014; Fahr and Voigt, 2018; Santa Cruz Biotechnology Inc., 2010). These raw materials must therefore be avoided in the novel formulation.

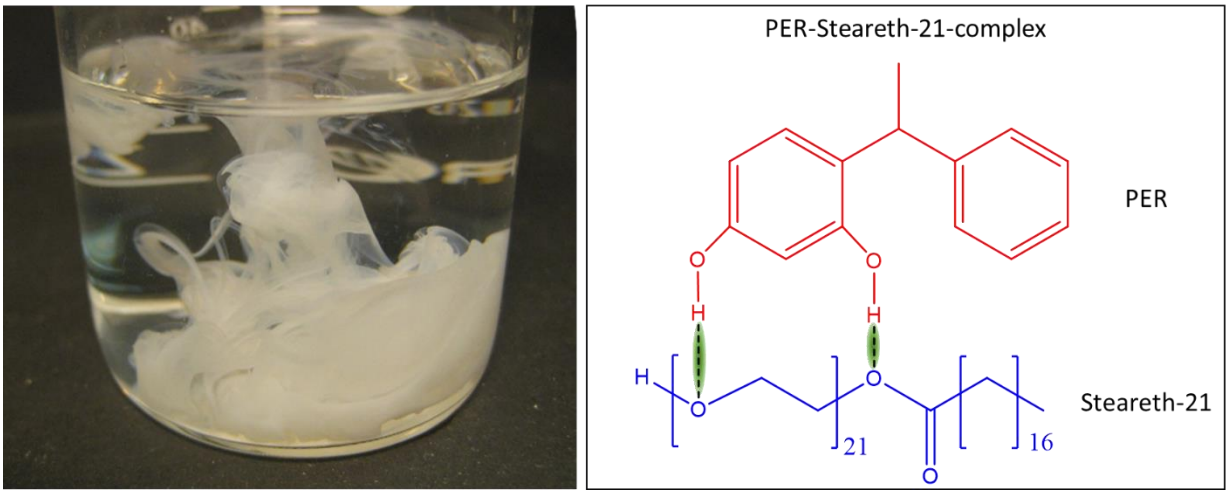

Fig. 1: Precipitation of white PER-steareth-21 complex after the addition of one drop 8% aqueous Steareth-21 solution to a PER saturated aqueous solution (left), and the molecular structure of the formed complex (right).

b) Requirements to PER loading and total PER concentration

Despite that many delivery systems were developed for PER, only very low loading capacities were achieved, e.g. 0.5-2.5% (related to the vehicle mass) in vesicular carriers (Amnuaikit et al., 2018; Fan et al., 2014a; Limsuwan et al., 2017). So far, highest PER loadings were achieved in NLC, being 20% (related to the particle mass) with total PER concentration in final suspension of 3% (Fan et al., 2014b), and 25% loading (particles) with a total concentration of 1% (product) (Jia et al., 2016). The reason for these low loadings is that PER is not only poorly soluble in water, but also only moderately soluble in lipids.

Like SLN and NLC, also smartLipids form an occlusive film on skin. The concentration gradient between this film and skin is directly proportional to the penetration rate. Hence, the higher the PER loading, the stronger the penetration. Also, the total PER concentration in suspension is of interest. Lipid nanoparticle suspensions are concentrates and can be incorporated to dermal vehicle, e.g. cream or lotion, by simple stirring. The higher the active concentration in the suspension, the less must be added to achieve the desired effective concentration in dermal vehicle. The industrially preferred dilution factor is 10 or higher, as in this case no changes to already established vehicles are necessary.

3.3.2. Lipid screening and inverse loading method

For the target dilution factor of ≥10, the suspension must have a minimum PER concentration of 5%. For a lipid nanoparticle suspension with a particle concentration of 10%, this would

correspond to a loading of 50% PER. Hence, a lipid mixture has to be created in which 50% PER can be dissolved. The solubility of solid active is higher in oils than in solid lipids why the appropriate oil is generally identified first in the development phase. To obtain the desired smartLipids properties such as chemical protection of loaded active, formation of an occlusive film, and increased adhesiveness, the lipid-active mixture has to be solid at skin temperature. Therefore, the melting point of the oily active solution is raised to over 32 °C in next step by adding solid lipids with high melting points.

Following the classical development steps, the solubility of PER was first investigated in 13 different oils approved for dermal application. Highest solubility of 33% was obtained in isopropyl myristate, isopropyl palmitate, and Miglyol 812 (Fig. 2). Since the melting point of the oily PER solution must be increased to 32 °C by the addition of high melting solid lipids, the PER concentration will drop from 33% to even lower values and the minimum required concentration will no longer be achieved. Thus, by the classical development process, it is consequently not possible to develop a PER formulation meeting the predefined requirements.

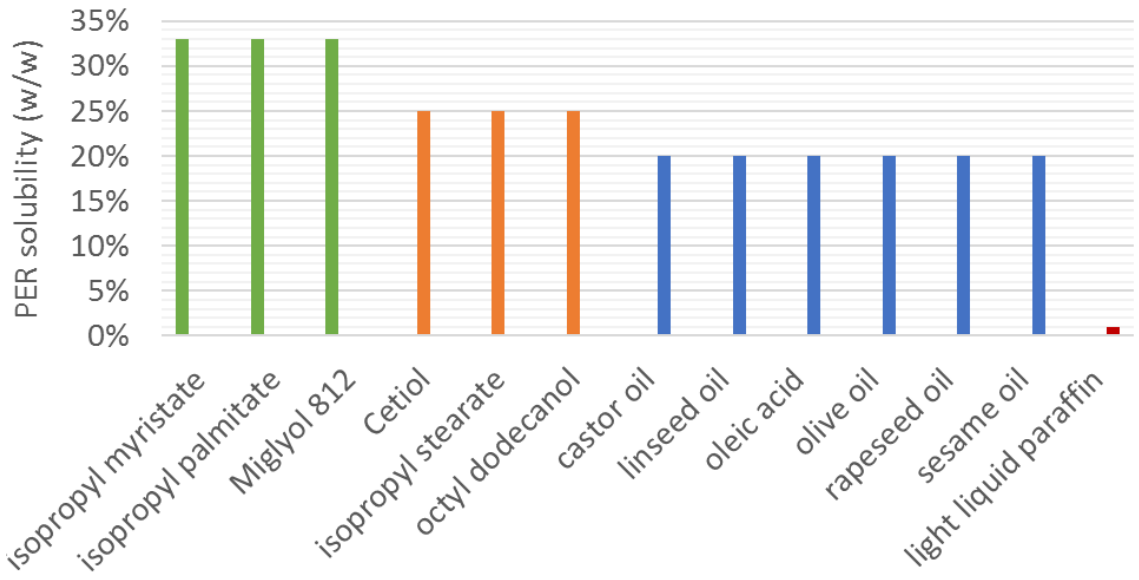

Fig. 2: Overview of PER solubilities in various oils determined at room temperature.

3.3.3. Inverse loading of PER into lipid matrices

In order to achieve a sufficiently high PER loading, a completely new approach was necessary. Fig. 3 schematically shows a phase diagram describing the homogeneous miscibility of a binary

system as a function of mass ratio and temperature. Blue areas represent a homogeneous mixture of the two components, whereas mixtures from the red area decompose into two phases.

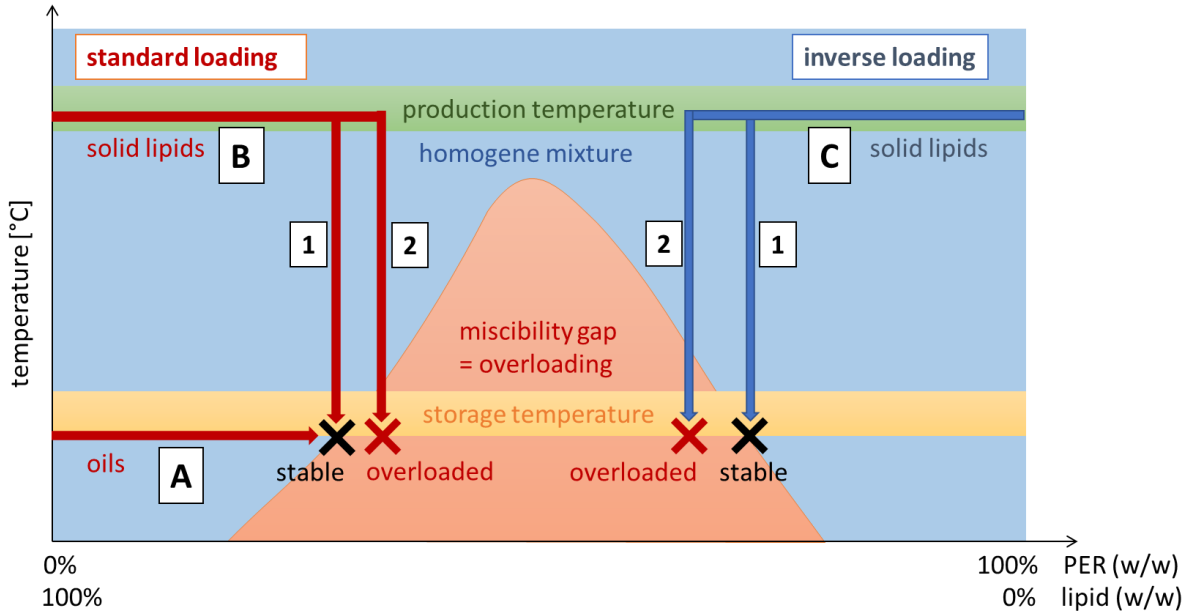

Fig. 3: Schematic illustration of a miscibility gap with upper critical solution temperature for a binary mixture of PER and lipid. Blue area: homogeneous mixture, red area: separation into two phases, green area: production temperature, yellow area: storage temperature. B1: maximum loading with standard method, B2: overloading inverse loading, C1: maximum loading with inverse method.

In the standard process for the galenic development of lipid nanoparticles, the solubility of the active is first examined in oils. This was done in section 3.2. by increasing the amount of PER in oil until a biphasic system was formed (Fig. 3, A). For the investigation of PER solubility in solid lipids, lipids were first melted at higher temperatures. In the melted state, however, it cannot be determined whether the mixture is suitable for the production of stable lipid nanoparticles. Even if the PER is completely soluble at the melting temperature of solid lipid, the solubility at room temperature may be different. This would lead to precipitation during cooling process (Fig. 3, B2). Therefore, a ratio must be found that is homogeneous for both production and storage temperature (Fig. 3, B1).

The special about PER is its melting point of 82 °C which is below the boiling point of water. Therefore, PER can be kept in melted state during entire production process allowing an inverse loading. Inverse loading means that instead of dissolving PER into a melted lipid (Fig.

3, B), the lipid can be dissolved in melted PER (Fig. 3, C). Particles with a very high PER content can therefore be achieved, still forming a homogenous PER-lipid mixture. (Fig. 3, C2).

A first miscibility test of PER at 85 °C with 20 pure lipids of the groups di-, and triglycerides, fatty acids, fatty alcohols, and waxes, and 3 lipid mixtures meeting the smartLipids principles was carried out. A narrower selection could not be made as all lipids were miscible with PER at a ratio of 50%, 65% and 80% at this temperature. Instead of melting each lipid with decreasing PER concentration and investigating the crystallinity or melting behavior of mixture after solidification, lipid nanoparticles were directly produced with the target PER loading of 50% and also at 80%. The overloading is much easier to detect in the suspension. With expulsion of active either the particles are cross-linked, and the suspension gelled, or PER crystals precipitate.

3.3.4. Production of PER lipid nanoparticles

Already after one day of storage, 13 of the 46 samples had to be excluded due to gelation (Fig. 4, left). Also, the viscosity of another 13 samples was already slightly increased on day 1, indicating an imminent gelation. For the remaining 20 liquid samples, the particle size was measured on day 1 (Tab. 1). There was no correlation to a certain lipid group, as at least one representative from each group had to be excluded from each group (Tab. 1). But a clear trend can be seen for the different loadings. While 8 of the 23 samples loaded at 50% had to be excluded already on day 1, it was only 5 for the samples loaded at 80%. This trend remains also for the evaluation after one week of storage with 14 vs. 10 excluded samples, respectively. This observation therefore confirms the theory of inverse loading. Another difference between the two loadings was the particle size. Distinctly smaller particle size was obtained for 80% loaded samples compared to respective 50% loaded samples except of Cutina CP sample, indicating a better interaction of Lanette N with PER than with the lipids. After 2 months of storage a further instability occurred in addition to gelling; the precipitation of large PER crystals in mm range (Fig. 4, middle). Therefore, 9 further samples had to be excluded.

After 3 months of storage only 3 out of 46 samples remained stable: Witepsol H32, Lipocire A, and Witepsol W31 with 50% PER loading (Fig. 4, right). What the three lipids have in common is that they are compliant to smartLipids technology. smartLipids represents the next and newest generation of lipid nanoparticles and is characterized by a lipid matrix consisting not

only of 1 solid and 1 liquid lipid, but of a complex mixture of up to 10 lipids. Due to its special lipid structure, retinol loading for example could be distinctly increased from 1% to 15%, and lidocaine loading from 15% to 40% (Ding et al., 2017; Keck et al., 2015; Müller et al., 2014; Müller et al., 2019; Ruick, 2015). The characteristic properties of lipid nanoparticles, e.g. chemical protection of loaded active (Ding et al., 2017), and formation of an occlusive film on skin, which increases the penetration of loaded actives (Müller et al., 2013), remain with smartLipids.

All three lipids Witepsol H32, Lipocire A, and Witepsol W31 are a very complex mixtures composed of C10 to C18 di- and triglycerides. Interestingly, only these three samples were against the trend that 80% is more stable than 50% loaded sample. This observation can only be explained by a differently shaped miscibility gap for these three lipids than the standard miscibility gap shown in Fig. 3. How exactly the miscibility gap is shaped for these three lipids cannot be estimated with the two measuring points. Important is, that complex lipid mixtures based to smartLipids technology enabled a PER loading of 50%, which physically storage stable for 14 months up to now.

Tab. 1: Macroscopic stability assessment (colors), and PCS particle size and polydispersity index of 50% and 80% loaded PER smartLipids with various lipids 1 day after production.

< 1 day ≤ 1 week ≤ 3 months ≥ 6 months

category	lipid	chemical identity	50% PER-loading z-ave [nm, d] PdI	80% PER-loading z-ave [nm, d] PdI
fatty acid	myristic acid	myristic acid	- -	- -
	Palmac 55-16	palm triple pressed acid	- -	- -
	palmitic acid	palmitic acid	- -	- -
	Stearic acid	stearic acid	384 ± 235 0.54 ± 0.13	- -
	Sternoil 12-HSA	12-hydroxystearic acid	- -	- -
fatty alcohol	Nafol 1822C	C18-C22 alcohol	- -	164 ± 4.2 0.32 ± 0.04
	Tetradecanol	myristylalcohol	517 ± 43.6 0.19 ± 0.03	265 ± 7.2 0.22 ± 0.03
	Vegarol 1698	cetylalcohol	655 ± 130 0.55 ± 0.11	250 ± 6.1 0.26 ± 0.04
	Vergarol 1898	stearylalcohol	- -	- -
	Vegarol 2270	behenylalcohol	232 ± 7.8 0.23 ± 0.03	157 ± 5.3 0.29 ± 0.03
diglyceride	Compritol 888 ATO	glyceryl dibehenate	- -	103 ± 1.5 0.21 ± 0.02
	Precirol ATO 5	glyceryl distearate	469 ± 8.7 0.33 ± 0.04	124 ± 26.2 0.17 ± 0.02
triglyceride	Cutina HR	hydrogenated castor oil	155 ± 2.4 0.17 ± 0.03	107 ± 1.9 0.22 ± 0.03
	Dynasan 112	trilaurin	114 ± 1.5 0.16 ± 0.03	90 ± 1.5 0.24 ± 0.04
	Dynasan 114	trimyrisin	102 ± 1.5 0.17 ± 0.03	89 ± 1.1 0.22 ± 0.02
	Dynasan 118	tristearin	- -	- -
	Softisan 154	hydrogenated palm oil	- -	- -
di- and triglyceride	Lipocire A	complex mixture of C10-C18 di- and triglycerides	107 ± 0.7 0.15 ± 0.02	92 ± 1.4 0.24 ± 0.01
	Witepsol H32		115 ± 1.9 0.17 ± 0.02	98 ± 3.9 0.30 ± 0.03
	Witepsol W31		107 ± 1.3 0.17 ± 0.02	92 ± 1.5 0.25 ± 0.02
wax	Apifil	bee wax	144 ± 10.6 0.30 ± 0.03	116 ± 3.3 0.26 ± 0.02
	carnauba wax	carnauba wax	- -	- -
	Cutina CP	cetylpalmitate	89 ± 1.4 0.18 ± 0.03	100 ± 1.9 0.26 ± 0.05

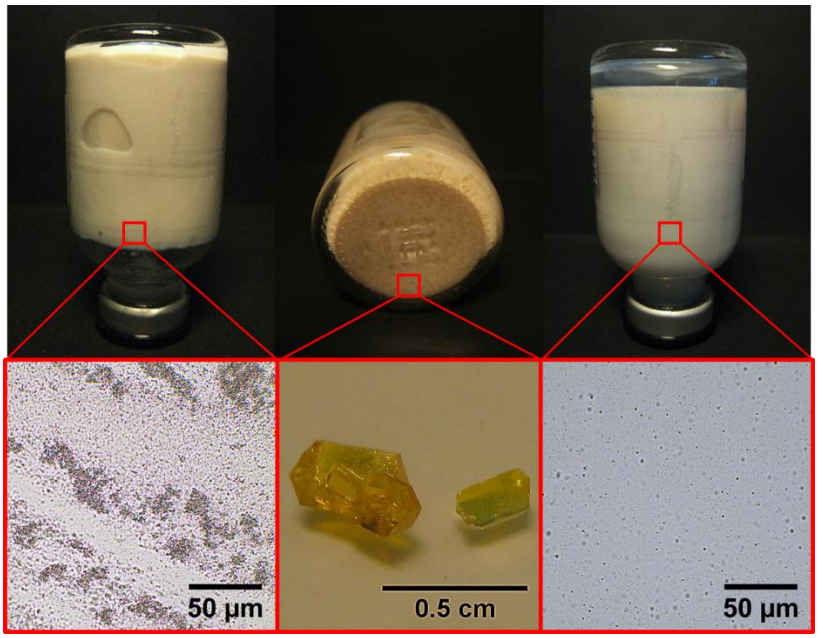

Fig. 4: Macroscopic (upper) and microscopic (lower) appearance of Sternoil-HSA (50% PER-loading) 1 day after production as an example for gelling formulations (left), of Cutina CP (50% PER-loading) 2 months after production as an example for formulations showing crystal growth (middle), and of Lipocire A (50% PER-loading) formulation as an example for stable formulations (right).

3.3.5. Characterisation of best 3 formulations

All three lipids lead to comparable PCS mean particle sizes of 107 nm - 115 nm and storage stabilities of 6 months (Fig. 5). Also, the encapsulation efficacy did not significantly differ, being 94.3% ± 0.2% for Lipocire A, 94.1% ± 0.2% for Witepsol W31 and 94.1% ± 0.2% for Witepsol H32, proving the firm inclusion of PER in lipid matrices. As Lipocire A, contrary to the two Witepsoles, has a dermal approval (Gattefossé, 2016), this formulation was selected for further investigations, i.e. long time storage stability assessment, increase of the particle concentration and large scale production.

One day after production, PER smartLipids at 50% produced with Lipocire A had PCS z-ave of 107 nm, LD D50 of 134 nm and D99 of 251 nm. These values remained practically unchanged over a period of 14 months with PCS z-ave of 102 nm, LD D50 of 136 nm and D99 of 254 nm. Compared to the maximum storage stability of 3 months found in literature, this new developed formulation with a storage stability of 14 months provides an almost fivefold extended shelf life.

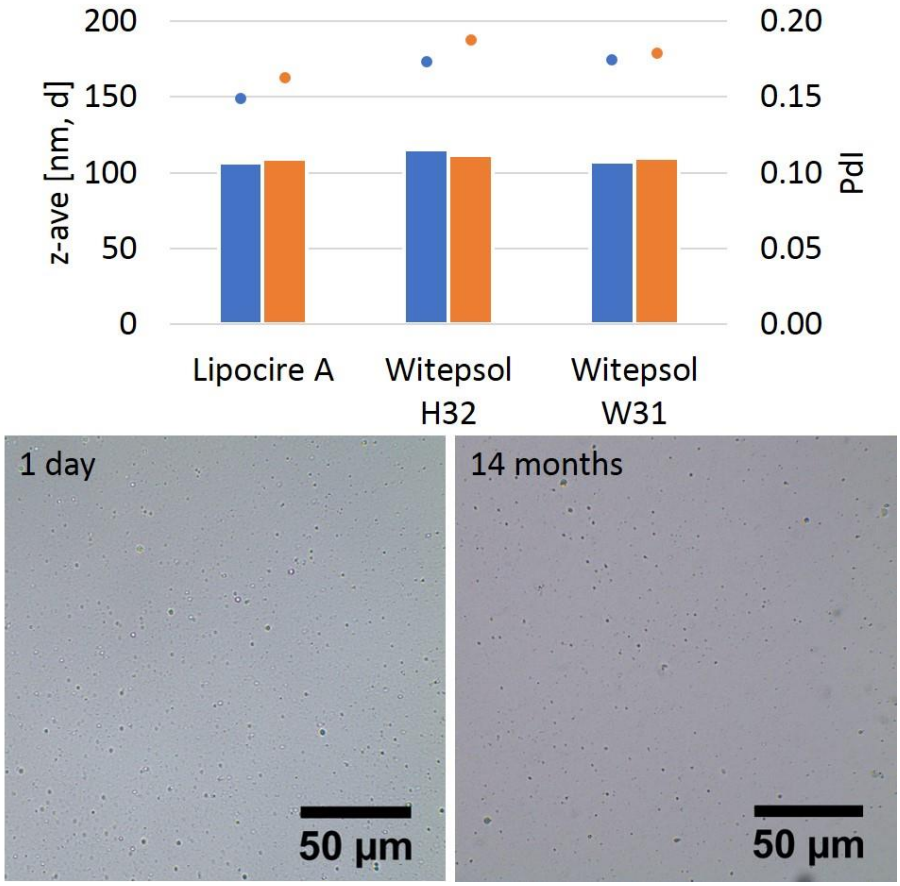

Fig. 5: PCS particle diameters (bars) and polydispersity indices (dots) of 50% loaded smartLipids containing Lipocire A, Witepsol H32 or W31 as complex solid lipid mixtures 1 day (blue) and 6 months (orange) after production (upper), and microscope images of Lipocire A formulation at 400-fold magnification (lower) at same times of investigation.

3.3.6. Increase of particle content

In addition to the loading, particle concentration of the suspension can also be increased to achieve a higher total concentration of PER in formulation. Therefore, PER smartLipids were produced again with particle contents of 15%, 20%, 25% and 30% corresponding to total PER concentration in formulation of 7.5%, 10.0%, 12.5%, and 15.0%. The surfactant concentration was adapted to 2.1%, 2.8%, 3.5% and 4.2%, respectively.

The use of same production parameters resulted in larger particles with increasing particle concentration. The mean particle size measured by PCS increased from 107 nm at 10% to 114 nm at 15%, 116 nm at 20%, 132 nm at 25%, and 148 nm at 30%. The LD D99 values were all comparable being in the range of 275-298 nm. The samples with 10%, 15% and 20% particle concentration remained physically stable for 14 months.

Thus, stable PER smartLipids with 50% loading and a particle concentration of 20% are possible, corresponding to a total PER-concentration of 10%. Hence, PER smartLipids can be diluted by factor 20, which meets the double of the targeted dilution factor of 10.

3.3.7. Establishment of large-scale production on LAB 60

The lab-scale production was carried out by a Micron LAB 40 with a total volume of 40 mL per production. For upscaling, the Micron LAB 60 was used having a production volume of 60 kg/h (Jenning et al., 2002). The final dermal product needs to contain 0.5% PER to be effective. Calculating with a 20% particle suspension and a PER loading of 50%, this corresponds to 50 kg of PER smartLipids concentrate per ton dermal product. Thus, about a ton of final dermal product can be produced within less than 1 h.

For lab scale production 3 cycles at 500 bar were applied. The LAB 60 has a different setup, why one passage on LAB 60 corresponds to 2 homogenization cycles (Fig. 6, right). The direct transfer of the cycle number from LAB 40 to LAB 60 is therefore not possible. In literature it is reported that fewer passages and less pressure are needed on LAB 60 to achieve comparable particle sizes to LAB 40, (Jenning et al., 2002). Therefore, production parameters were set to 1 passage at 200 bar, 300 bar and 400 bar, respectively. The particle size 1 day after production was measured to compare the results with the particle sizes of the LAB 40 production and also after 6 months to assess the physical stability of produced suspensions.

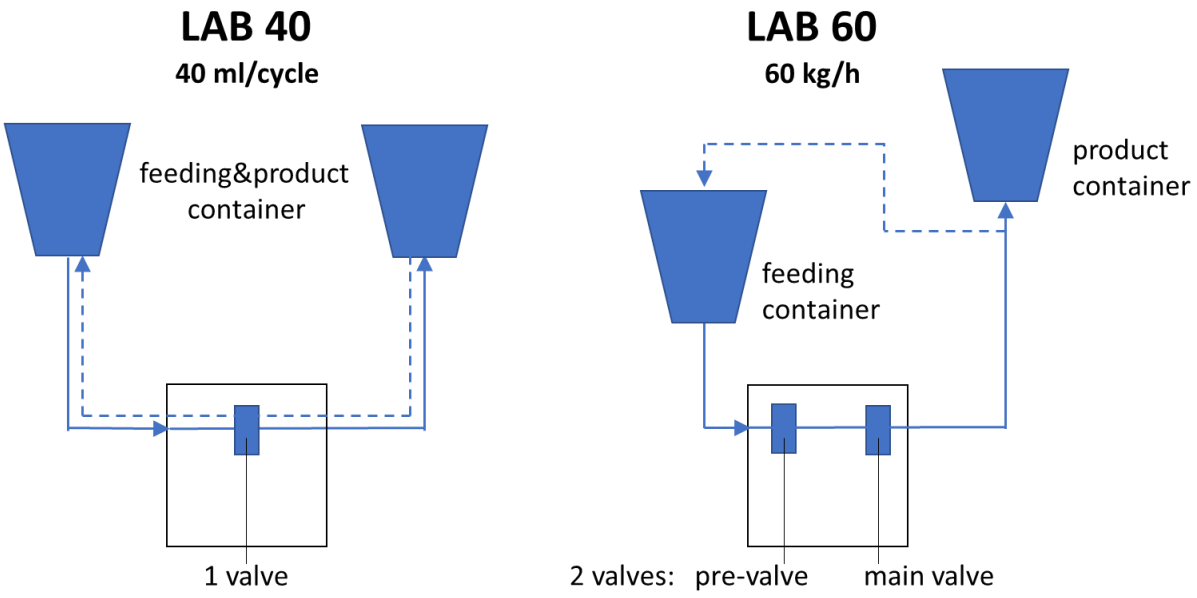

Fig. 6: Simplified illustration of an APV LAB 40 with one homogenization valve (left) and am APV Gaulin LAB 60 homogenizer with a pre- and a main homogenization valve (right).

Fig. 7 shows that both the particle size and the narrowness of the size distribution decrease with increasing pressure on LAB 60. The z-ave of the sample produced at 200 bar is 197 nm and decreases to 183 nm at 300 bar and 160 nm at 400 bar. The z-ave of 107 nm at 3x500 bar on LAB 40 is therefore not reached. However, the larger size can be advantageous for large scale production, especially for cosmetic applications. Consumers are increasingly concerned about nanoparticles, which is why manufacturers prefer products in the submicron range. These include particles with a diameter > 100 nm and < 1,000 nm - which still have the nano properties such as increased surface area, light scattering effects and dissolution properties - without having to be declared as nano.

The PCS z-aves are intensity weighted values but can be converted into number weighted mean diameters by Fourier transformation. The mean value of the 3x500 bar sample generated by LAB 40 is 64 nm, whereas 96.5% of the particles are < 100 nm. According to the legal definition of Regulation (EC) No 1223/2009, labelling as "nano" is required if 50% or more of the particles contained have a number weighted diameter of < 100 nm. This clearly applies to the 3x500 bar sample, which makes it a declarable nanoproduct. The sample produced on LAB 60 by one passage at 400 bar has a number weighted mean diameter of 104 nm where 71.6% of particles are < 100 nm, which also makes it legally a nanoproduct. In contrast, the samples produced at 300 bar and 200 bar do not have to be declared as nano. They each have a number weighted mean diameter of 135 nm and 145 nm with 32.2% and 44.2% particles < 100 nm, respectively.

What all three samples have in common is that they are physically highly stable and show almost no change in particle size and distribution after 6 months storage at room temperature. If PER with increased tyrosinase inhibition, improved chemical stability and controlled release is desired, but without being a nano declarable product, PER smartLipids in the submicron range of LAB 60 can be produced with 1 pass at 300 bar. If, on the other hand, the manufacturer wishes to emphasize his product as a nanoproduct, a suitable PER smartLipids suspension can be produced with 1 pass at 400 bar.

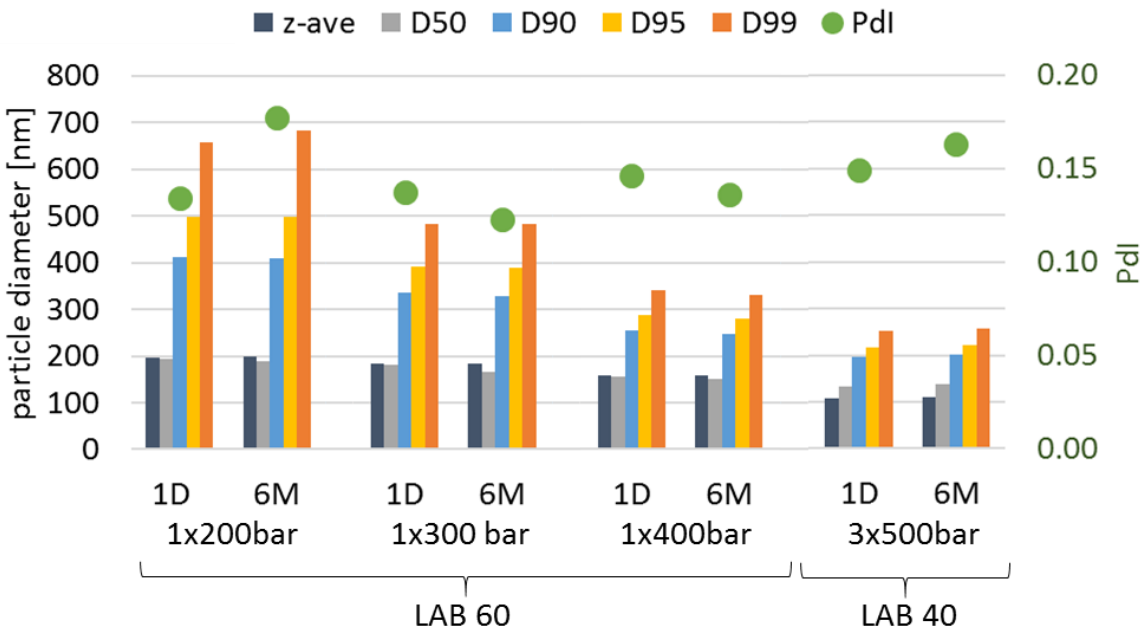

Fig. 7: PCS and LD particle diameters (bars) and polydispersity indices (dots) of 50% loaded PER smartLipids produced by LAB 60 applying 1 passage at 200, 300, and 400 bar, and LAB 40 applying 3 cycles at 500 bar after 1 day (1D) and 6 months (6M) of storage.

3.4. Conclusion

Using complex lipid mixtures complying to the smartLipids technology and applying the inverse loading method, PER lipid nanoparticles with a very high loading of 50% were obtained. The formulation consists only of components approved for dermal application. Furthermore, both the lipid mixture Lipocire A and the stabilizer Lanette N are ECOCERT certified as well tolerated organic compounds.

Applying 3 cycles at 500 bar led to particles with z-ave of 107 nm, polydispersity index of 0.15, LD D95 of 216 nm and D99 of 251 nm. Suspensions with 20% were physically stable at room temperature for 14 months up to now. This corresponds to a PER concentration of 10% in total formulation enabling the industrially required dilution factor of 20 for obtaining effective concentration of 0.5% in final dermal product. To demonstrate the possibility of upscaling, production was performed on a LAB 60 having a production volume of 60 kg/h. By varying the homogenization pressure, the particle size can be individually adjusted according to the individual needs of the consumer without compromising the storage stability of the suspension for at least 6 months (data by now). All together enables the practical application of promising PER lipid nanoparticles with improved tyrosinase inhibition and chemical stability.

3.5. References

Amnuaikit, T., Limsuwan, T., Khongkow, P., Boonme, P., 2018. Vesicular carriers containing phenylethyl resorcinol for topical delivery system; liposomes, transfersomes and invasomes. Asian J. Pharm. Sci. 13 (5), 472–484.

Babaei, S., Ghanbarzadeh, S., Adiba, Z.M., Kouhsoltani, M., Davaran, S., Hamishehkar, H., 2016. Enhanced skin penetration of lidocaine through encapsulation into nanoethosomes and nanostructured lipid carriers: a comparative study. Pharmazie 71, 247–251.

Banks, S.R., Pygall, S.R., Bajwa, G.S., Doughty, S.W., Timmins, P., Melia, C.D., 2014. The influence of substituted phenols on the sol:gel transition of hydroxypropyl methylcellulose (HPMC) aqueous solutions. Carbohyd. Polym. 101, 1198–1204.

Ding, Y., Pyo, S.M., Müller, R.H., 2017. smartLipids®as third solid lipid nanoparticle generation - stabilization of retinol for dermal application. Pharmazie 72 (12), 728–735.

Fahr, A., Voigt, R., 2018. Voigt's pharmaceutical technology, 12th ed. Wiley, Hoboken, NJ, 710 pp.

Fan, H., Li, Y., Huang, Y., Liu, G., Xia, Q., 2014a. Preparation and evaluation of phenylethyl resorcinol liposome. Integr. Ferroelectr. 151 (1), 89–98.

Fan, H., Liu, G., Huang, Y., Li, Y., Xia, Q., 2014b. Development of a nanostructured lipid carrier formulation for increasing photo-stability and water solubility of phenylethyl resorcinol. Appl. Surf. Sci. 288 (1), 193–200.

Gattefossé, 2016. Technical Data Sheet: Lipocire™ A Pellets, Lyon. https://cosmetics.specialchem.com/product/i-gattefosse-lipocire-a. Accessed 10 July 2019.

Hong, L., Han, D., Li, M.-X., Zhang, P., Liu, C.-G., 2016. Development and validation of an ultraviolet-visible (UV-Vis) spectrophotometric method for determination of phenylethyl resorcinol in new topical nanoemulsions. Int. J. Cosmet. Sci. 39 (3), 337–343.

Jenning, V., Lippacher, A., Gohla, S.H., 2002. Medium scale production of solid lipid nanoparticles (SLN) by high pressure homogenization. J. Microencapsul. 19 (1), 1–10.

Jeon, S.-H., Na, Y.-G., Lee, H.-K., Cho, C.-W., 2019. Hybrid polymeric microspheres for enhancing the encapsulation of phenylethyl resorcinol. J. Microencapsul. 36 (2), 130–139.

Jia, F., Gao, H., Jia, H., Zhang, W., 2016. Nanostructured lipid carriers with liquid crystal structure encapsulating phenylethyl resorcinol: Characterization and in vitro study. Mol. Cryst. Liq. Cryst. 633 (1), 1–13.

Keck, C.M., Lohan, S.B., Bauersachs, S., Ahlberg, S., Baisaeng, N., Müller, R.H., Witte, E., Wolk, K., Hackbarth, S., Röder, B., Lademann, J., Meinke, M.C., 2015. smartLipids Q10: highly effective protection from light as innovative anti-aging formulation for the skin. Menopause, Andropause, Anti-aging, Vienna, Vienna, 10.-12. Dezember 2015, 15.

Kim, B.-S., Na, Y.-G., Choi, J.-H., Kim, I., Lee, E., Kim, S.-Y., Lee, J.-Y., Cho, C.-W., 2017. The improvement of skin whitening of phenylethyl resorcinol by nanostructured lipid carriers. Nanomaterials (Basel) 7 (9), 241.

Kolbe, L., Mann, T., Gerwat, W., Batzer, J., Ahlheit, S., Scherner, C., Wenck, H., Stab, F., 2013. 4-n-butylresorcinol, a highly effective tyrosinase inhibitor for the topical treatment of hyperpigmentation. J. Eur. Acad. Dermatol. Venereol. 27 (1), 19–23.

Li, B., Ge, Z.-Q., 2012. Nanostructured lipid carriers improve skin permeation and chemical stability of idebenone. AAPS PharmSciTech 13 (1), 276–283.

Limsuwan, T., Boonme, P., Khongkow, P., Amnuaikit, T., 2017. Ethosomes of phenylethyl resorcinol as vesicular delivery system for skin lightening applications. Biomed. Res. Int. 2017, 8310979.

Müller, R.H., Olechowski, F., Köpke, D., Pyo, S.M., 2019. smartLipids: The third generation of solid submicron lipid particles for dermal delivery of actives, in: Cornier, J., Keck, C.M., van de Voorde, M. (Eds.), Nanocosmetics. From Ideas to Products, 1st ed., pp. 141–159.

Müller, R.H., Ruick, R., Keck, C.M., 2014. smartLipids - the next generation of lipid nanoparticles by optimized design of particle matrix. DPhG-Jahrestagung, Frankfurt, 24.-26. September 2014, PT.27.

Müller, R.H., Sinambela, P., Keck, C., 2013. NLC–the invisible dermal patch for moisturizing & skin protection. EuroCosmetics (6), 20–22.

Roy, B.K., Moulik, S.P., 200. Effect of hydrotropes on solution behavior of amphiphiles. Curr. Sci. 85 (8), 1148–1155.

Ruick, R., 2015. smartLipids - die neue Generation der Lipidnanopartikel nach SLN und NLC: Dissertation zur Erlangung des akademischen Grades des Doktors der Naturwissenschaften (Dr. rer. nat.). Freie Universiät Berlin.

Santa Cruz Biotechnology Inc., 2010. Material safety data sheet: hydroxypropyl cellulose, version sc-252897. http://datasheets.scbt.com/sc-252897.pdf. Accessed 10 July 2019.

Schwarz, C., Mehnert, W., Lucks, J.S., Müller, R.H., 1994. Solid lipid nanoparticles (SLN) for controlled drug delivery. I. Production, characterization and sterilization. J. Control. Release 30 (1), 83–96.

Tofani, R.P., Sumirtapura, Y.C., Darijanto, S.T., 2016. Formulation, characterisation, and in vitro skin diffusion of nanostructured lipid carriers for deoxyarbutin compared to a nanoemulsion and conventional cream. Sci. Pharm. 84 (4), 634–645.

Vielhaber, G., Schmaus, G., Jacobs, K., Franke, H., Lange, S., Herrmann, M., Joppe, H., Koch, O., 2007. 4-(1-Phenylethyl)1,3-Benzenediol: A hew, highly efficient lightening agent. Int. J. Cosmet. Sci. 29 (1), 65–66.

4. Phenylethyl resorcinol smartLipids for skin brightening – increased loading & chemical stability[2]

4.1. Abstract

Phenylethyl resorcinol (PER, 4-(1-phenylethyl)1,3-benzenediol) is a very potent tyrosinase inhibitor with clinically proven effectiveness at already 0.5%. A major challenge of incorporating PER into dermal products is its high sensitivity against light. Previously, by incorporating PER in nanostructured lipid carriers (NLC), chemical stability and tyrosinase activity could be increased by 29% and 67%, respectively. Despite this, degradation still occurred accompanied with reddish discoloration of the formulation – not acceptable for market products. In this study PER was incorporated into smartLipids, the 3rd generation of lipid carriers. Compared to NLC, the smartLipids formulation had a higher PER loading, was PEG-free and used ECOCERT-certified Lanette N. For PER stabilization, 14 additives from three groups were investigated: UV blockers, antioxidants and chelating agents. The UV blockers Tinosorb S and Oxynex ST liquid, as well as the chelating agents ethylenediaminetetraacetic acid and phytic acid completely prevented reddish discoloration under test conditions (3 months in the dark and 7 days at light exposure). Investigating the stabilizing mechanisms, UV absorbers with high absorption in UV-A range were most effective (Tinosorb S, Oxynex liquid). They showed good stabilization in dark and at light exposure. Chelating agents had mainly an effect via pH shift to pH 2, thus are not suitable for dermal products requiring pH around 5. Antioxidants were less effective. The antioxidants propyl gallate and BHT showed best stabilization at storage in dark and slightly less at light exposure, not impairing the physical stability. Some antioxidants even accelerated discoloration (e.g. Tinogard TT). In general, low standard electrode potential (<0.4 mV) seems to be favorable for PER stabilization. In conclusion, Tinosorb S proved to be the best stabilizer; combination with an antioxidant is optional. By combination of smartPearls technology and the Tinosorb S stabilization, PER market products without discoloration are feasible.

---

[2] This chapter has been published as:

Köpke, D.; Müller, R.H.; Pyo, S.M.; 2019. Phenylethyl resorcinol smartLipids for skin brightening – increased loading & chemical stability. European Journal of Pharmaceutical Sciences 137, 104992.

https://doi.org/10.1016/j.ejps.2019.104992

https://doi.org/10.1016/j.ejps.2019.104992

5. Determination of crystallinity of PER smartLipids

5.1. Introduction

The galenic development of PER smartLipids is described in Chapter 3 and 4. However, what has not yet been shown in the prior chapters is a proof of solid state of PER smartLipids. SLN and all the following generations of solid lipid nanoparticles have in common, that their particle matrix is solid at skin temperature. This feature allows an a priori better physical stability, better chemical protection and controlled release of incorporated actives and drugs (Müller et al., 2019). Further, solid lipid nanoparticles and their following generations are superior to nanoemulsions in terms of adhesiveness, durability on the skin as well as the extend of occlusion effect, which is required to the normalization of skin hydration and the increase in dermal penetration of the incorporated actives and drugs (Müller, R. H., Sinambela, P., Keck, C. M., 2013). Therefore, a solid state is crucial for the PER smartLipids to express the desired properties.

According to the used raw materials, it should be no problem, as all raw materials themselves have a melting point which is higher than 32°C (PER: 82.8 °C, Lipocire A 39.4 °C, Tinosorb S 82.8 °C, Lanette N 43.4 °C und 55.1 °C, Fig. 1). Thus, it has been expected that also the mixture of these substances will have a higher melting point than the single components. However, in the handling of PER, a characteristic phenomenon has been observed: After melting the raw drug powder, the active did not recrystallize at room temperature but remained in a liquid, highly viscous tar-like texture. Thus, the melting behavior was again simulated by DSC measurement confirming this observation: In the first heat up of PER (Fig. 1, straight blue line), a clear peak at 82.8 °C could be observed, whereas in the second heat up only a glass transition temperature with an onset of 3.6 °C and an endset of 6.7 °C was present (Fig. 1., dashed line). Thus, pure PER remains liquid at room themerature. Therefore, it is even more important to veryfy the PER smartLipids to remain solid at skin temperature. This was the aim of this chapter.

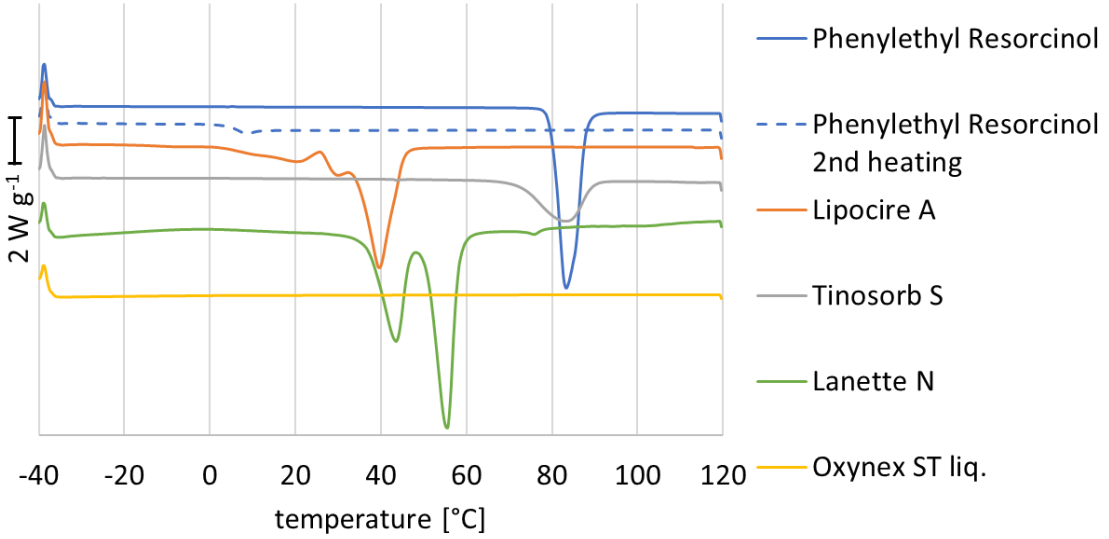

Fig. 1: DSC thermograms of all raw materials used for PER smartLipids from -40 °C to 120 °C at a heating rate of 20K/min showing melting peaks between 35 °C and 85 °C. In the 2nd heating, Phenylethyl Resorcinol remains liquid at room temperature and in the amorphous state at low temperature with a glass transition temperature of about 5°C. The thermograms were normalized to 1 g of substance. Exo Up.

5.2. Materials and methods

5.2.1. Materials

Phenylethyl resorcinol was purchased from Watson International Ltd, Jiaungsu, China, Lipocire A (C10-C18 triglycerides) from Gattefossé, France., Miglyol® 812 (caprylic/capric triglyceride) by Caesar & Loretz GmbH, Germany, Tinosorb® S (bemotrizinol) from Ciba AG, Switzerland, Oxynex ST liquid (diethylhexyl syringylidene malonate) from Merck KGaA, Germany, Lanette® N (emulsifying cetaryl alcohol) from BASF SE, Germany and locust bean floor (Ceratoniae Sem. pulv.) from ApoFit Arzneimittelvertrieb GmbH, Germany. Purified water was freshly obtained by a Milli-Q system from Merck KGaA, Germany.

5.2.2. Methods

5.2.2.1. *Production of analyzed materials*

PER smartLipids were produced as described in Chapter 3 and 4. For this, unstabilized PER smartLipids (PER 5 %, Lipocire A 5 %, Lanette N 1.4 %, purified ad 100 %) and stabilized PER smartLipids (PER 5 %, Lipocire A 3 %, Tinosorb S 1 %, Oxynex ST liquid 1 %, Lanette N 1.4 %, purified water ad 100 %) were produced. As negative reference for the X-ray crystallography (XRD), a nanoemulsion was produced in addition, being composed of PER 5 %, Miglyol 812 5 %, Lanette N 1.4 % and purified water ad 100 %, remaining all production parameters. The particle size was analyzed as described in Chapter 3 and 4. In addition, the respective bulk lipids, i.e. without Lanette N and water, were produced and investigated. The samples were stored in light-protected glass vials.

5.2.2.2. *Differential scanning calorimetry*

All materials were balanced into a 40 µL DSC standard aluminum pan. The respective samples were then analyzed using a Mettler Toledo DSC 1 (Mettler-Toledo International Inc., USA). As reference, an empty pan was used. To prevent oxidation of the samples, the furnace was flushed with nitrogen at a flow rate of 20 mL/min. Thermograms were taken from -40 °C to 120 °C at a heating rate of 20 K/min. This way, any endothermal (e.g. melting events) or exothermal process (e.g. crystallization events) can be recorded as a function of temperature. To avoid analytic and technical problems by freezing or boiling water, the smartLipids suspensions were analyzed from 10 °C to 90 °C only. The thermograms were displayed as heat flow normalized to the balanced mass as a function of the reference pan temperature. The thermograms were integrated using the STARe – software version 12.10. The crystallinity indices (CI) of the bulk materials were calculated using following equation:

$$Crystallinity\ index = \frac{melting\ enthalypy\ of\ the\ bulk\ lipid\ peak}{melting\ enthalpy\ of\ the\ raw\ drug\ powder * content\ in\ the\ bulk\ lipid}$$

5.2.2.3. *X-ray crystallography*

´The measurements were performed using an X-Ray-Diffractometer X'Pert Pro MDP (PANalytical/Philipps B.V., Netherlands). The X-Ray source was a Co-anode with an anode voltage of 40 kV and amperage of 35 mA. The resulting rays had a wavelength of 1,7903 Å. Detection was done in wide angle, i.e. between 10° and 110° and a scanning speed of 0,0263 °/s, i.e. 3827 measurement points all in all. The solid samples were measured directly in a thin layer. The liquid samples were thickend by the addition of 2% locust bean floor. The results were evaluated using the XRD software X'Pert HighScore Plus version 2.2.3.100 applying a curvature factor of 4, and after subtracting the background the results were illustrated as intensity (a.u.) as a function of diffraction angle.

5.3. Results and discussion

5.3.1. Differential scanning calorimetry

The starting temperature for the investigation of the thermal behavior of PER smartLipids was adapted to 10 °C to avoid freezing the water part of the sample. The end temperature was adapted to 90 °C to avoid the aluminum pans from burst and to avoid a “water belly” in the thermogram. However, the measurement showed only a highly intense peak at the very beginning of the experiment, which is caused by the high heat capacity of the sample. Between 20 °C and 90 °C, no thermal response could be observed. Only a small peak at 47.6 °C could be observed, which could be also interpreted as exothermal artifact. Also after 6 months and 9 months of storage at 25 °C, no thermal response could be observed (Fig. 2, dashed lines), except for minor exothermal peaks at 30.1 °C and 28.6 °C, respectively. This might be interpreted in 3 ways: a) PER smartLipids are a long-term stable nanoemulsion due to the formation of an eutectic mixture between PER and the bulk lipid, b) the particle matrix of PER smartLipids is solid but in the amorphous state and c) as a result from the comparatively low lipid content in the suspension (10 wt %), the DSC measurement of the PER smartLipids suspension is not sensitive enough to detect crystalline peaks.

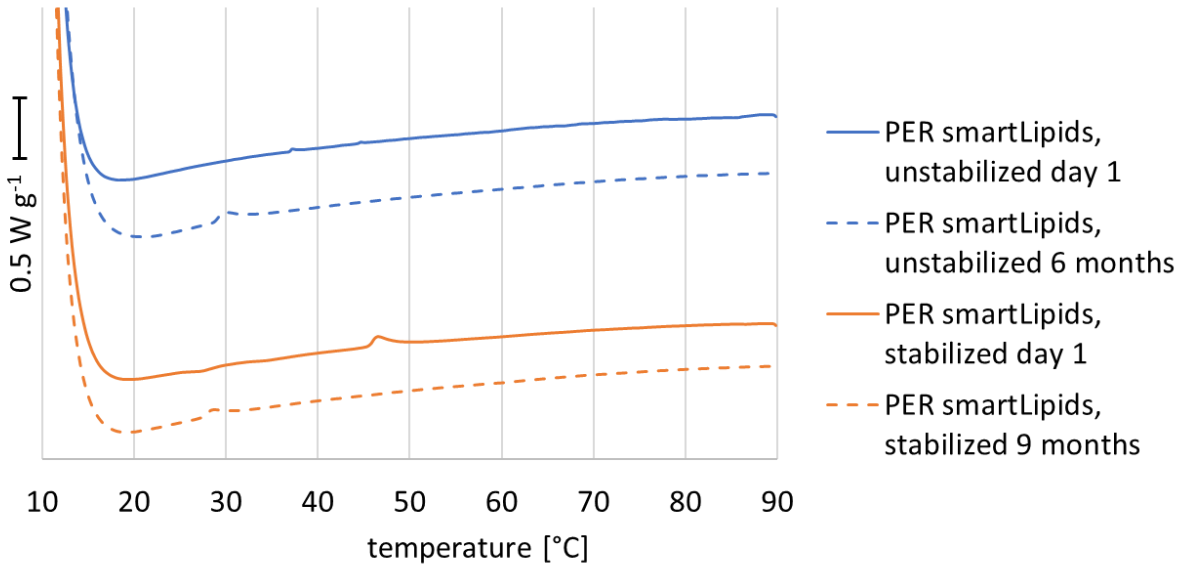

Fig. 2: DSC thermograms of PER smartLipids from 10 °C to 90 °C at a heating rate of 10K/min showing no thermo-response except for the initial peak which is caused by the high heat capacity of the sample. The thermograms were normalized to 1 gram of bulk lipid. Exo up.

As the next step, the bulk material, i.e. 100 % lipid mixture (50 % PER, 30-50 % Lipocire A and each 10 % Tinosorb S and Oxynex ST liquid for the stabilized lipid), was re-analyzed to increase the sensitivity of the method. The initial thermogram of PER smartLipids after 1 day (Fig. 3, straight blue line) shows melting peaks at , 3 °C and 15 °C, respectively. Between 32 °C and 120 °C, no thermal response could be observed. Thus, the PER smartLipids bulk material is liquid at room- and skin temperature. The same was the case for the stabilized bulk material (Fig. 3, orange straight line). But after short-term storage of 7 days (Fig. 3, dashed lines), both stabilized and unstabilized bulk material showed two peaks at about 35 °C and 80 °C. The unstabilized bulk lipid showed another small peak at about 60 °C. All of these peaks indicate the formation of crystalline structures with a melting point of > 32 °C and thus indicate a very slow solidification of PER smartLipids. After one year, the unstabilized bulk lipid showed increased peak intensity at 35 °C and 82 °C. One year stabilized bulk was not conducted.

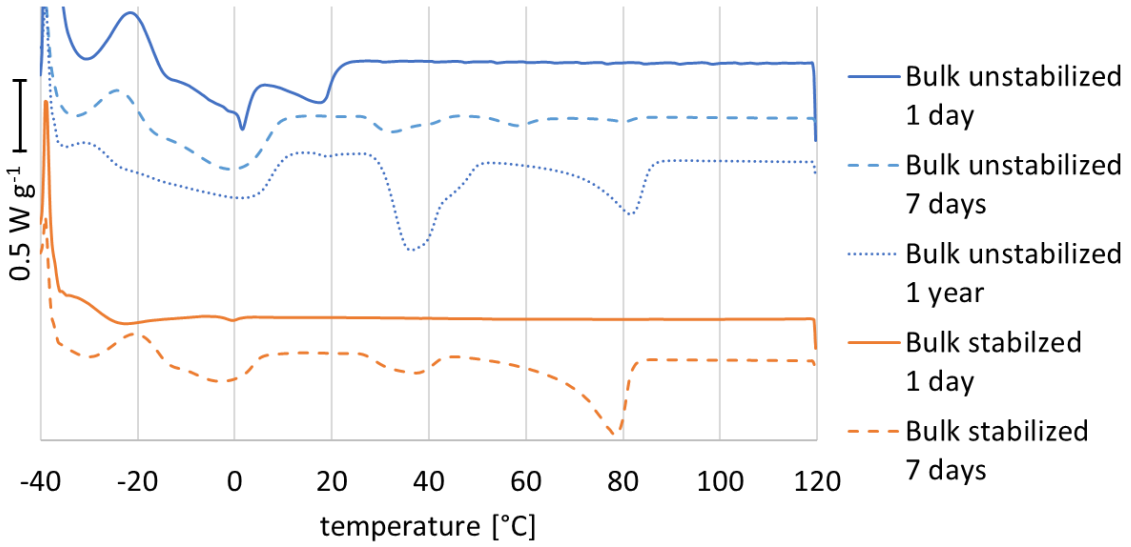

Fig. 3: DSC thermograms of PER smartLipids bulk lipid from -40 °C to 120 °C at a heating rate of 20K/min showing a slow solidifying process of the bulk material. The thermograms were normalized to 1 gram of bulk lipid. Exo up.

The crystallinity index (CI) of the presumable PER-peak, i.e. the peak at 80 °C, indicates a very small amount of PER (3.5 %) in the unstabilized bulk lipid being in the crystalline state after 7 days (Tab. 1). The majority of PER remains amorphous. Even after one year, only 27 % of the PER-amount appears in the crystalline form. In contrast, the CI of the stabilized bulk material is 42.2 %, already after 7 days. This area is probably overlapping with the area of recrystallized Tinosorb S, having the same melting point as PER. Therefore, a differentiation between the

two peaks cannot be done. Interestingly, the CI of the presumable Lipocire A peak (39 °C) is 39 % and 25 % after one week, when unstabilized and stabilized respectively, and almost completely (97 %) after one year. Therefore it can be concluded that PER smartLipids are a nanoemulsion directly after production. But already after one week, the particle matrix solidifies and shapes the desired solid PER smartLipids particles.

Tab. 1: melting temperatures (temp.), integrals and crystallinity indices (CI) of PER smartLipids raw and bulk materials and the respective raw materials.

	Peak near 39 °C			Peak near 82 °C		
	Temp. [°C]	Integral [mJ]	CI [%]	Temp. [°C]	Integral [mJ]	CI [%]
Phenylethyl Resorcinol	-	-	-	82.2	233.16	100.0
Lipocire A	39.4	209.71	100.0	-	-	-
PER smartLipids bulk unstabilized, day 1	-	-	-	-	-	-
PER smartLipids bulk unstabilized, day 7	32.1	41.02	39.1	80.0	4.11	3.5
PER smartLipids bulk unstabilized, 1 year	36.2	101.92	97.2	81.5	31.48	27.0
PER smartLipids bulk stabilized, day 1	-	-	-	-	-	-
PER smartLipids bulk stabilized, day 7	36.9	15.66	24.9	78.5	49.44	42.4

5.3.2. X-ray crystallography

For further differentiation, both PER smartLipids and the respective bulk lipids were analyzed by X-Ray crystallography. PER shows the most characteristic peaks at 17.2°, 19.2°, and 27.7°. The bulk material Lipocire A shows an amorphous fraction indicated by a broad peak between 20° and 30° as well as two characteristic crystalline peaks at 24.6° and 27.3°. Tinosorb S can be identified by a peak at 28.8° and Lanette N at 25.1° and 28.5° (Fig.4).

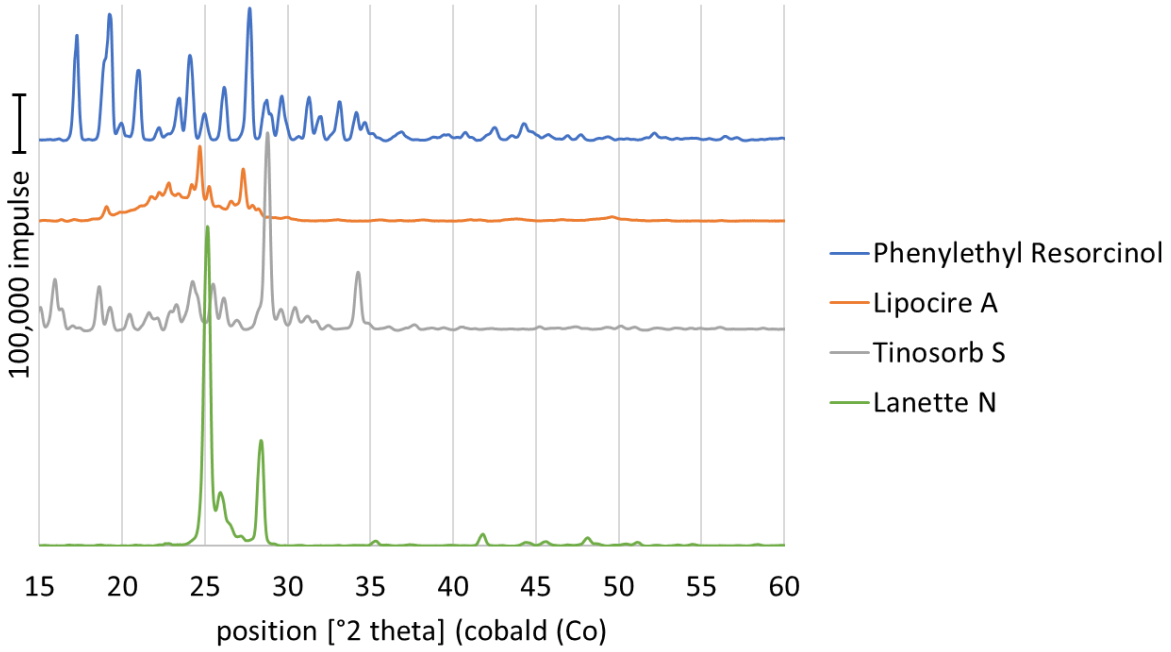

Fig. 4: X-ray diffractograms of all raw materials used for PER smartLipids showing characteristic peaks for PER, Lipocire A, Tinosorb S and Lanette N.

The results of the PER smartLipids suspensions corresponds to the DSC measurements: All measurements of the smartLipids suspensions show two broad peaks, one between 20° and 30° and the other between 25° and 40° (Fig. 5, blue and orange lines). The second peak obviously represents the locust bean floor (Fig. 5, black line). The first peak might represent the amorphous fraction of Lipocire A, but could also be caused by scattering of the X-rays on the surface of the particles. The latter is particularly plausible, since also the nanoemulsion shows a broad peak at this angle (Fig. 5, green line). The particle size (z-ave, PCS) of all samples was in the same magnitude, i.e. 107 nm for the unstabilized PER smartLipids, 160 nm for the stabilized PER smartLipids and 131 nm for the PER nanoemulsion. Besides a small neglectable peak at 25.4° in the nanoemulsion, which can be assigned to Lanette N, no crystalline peaks at all can be found in the spectra. This can be explained by the same 3 explanations like in the

DSC results (chapter 5.3.1), i.e. a) liquid state, b) amorphous state or c) a lag of sensitivity of the method. Therefore, these results do not allow a conclusion about the state of aggregation of the particles.

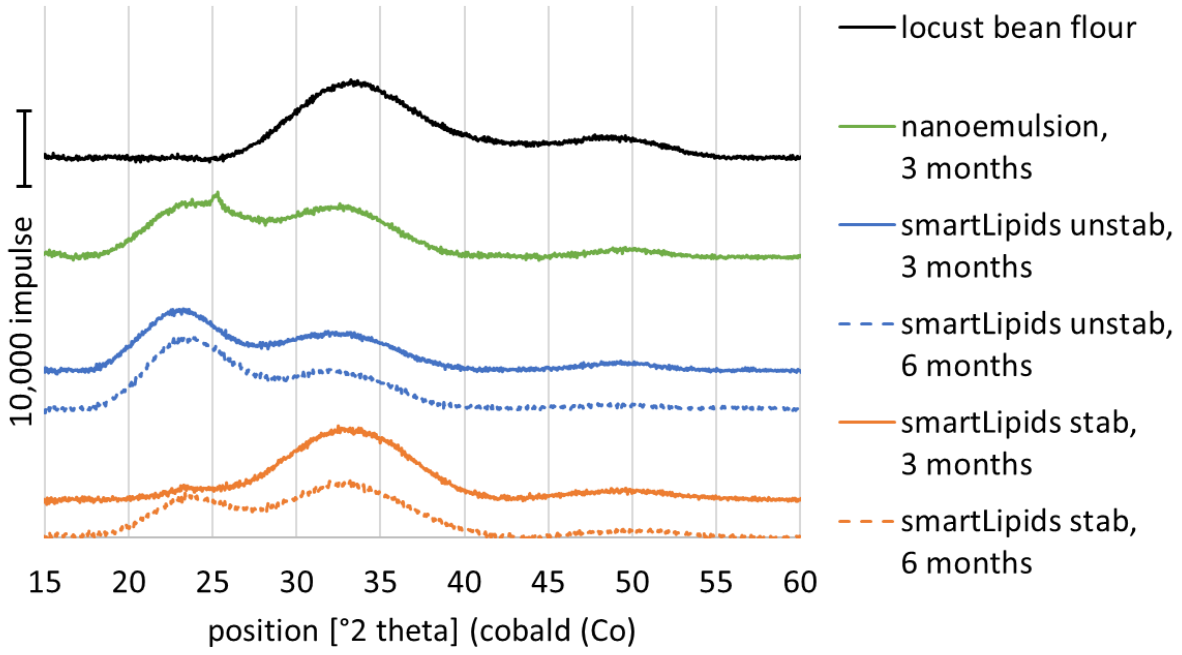

Fig. 5: X-ray diffractograms unstabilized (blue) and unstabilized (orange) PER smartLipids as well as PER nanoemulsion blank (green), thickened by 2 % locust bean floor (blank with water = black line) showing indifferent broad peaks that correlate to the locust bean floor- and nanoemulsion blanks.

To go further into detail, also the bulk lipids were investigated by XRD, as well. Both, the stabilized and unstabilized bulk lipids show characteristic peaks at 17.4°, 19.4° and 27.8°, i.e. they are close enough to be identified as PER-peaks (Fig. 6). Qualitatively there is no differences between the diffractograms of the stabilized and the unstabilized bulk lipid. Even though XRD is no quantitative method to determine the crystallinity of the samples, the peak heights of the bulk lipids (about 50,000 implulse at 27.8°) is much lower than in the respective PER RDP diffractogram (about 300,000 impulse). Considering a PER-content of 50 % in the bulk lipid, also in this experiment can be seen that the majority of PER (about two thirds) is not in the crystalline state. Thus, the magnitude of crystallinity determined by DSC could be confirmed.

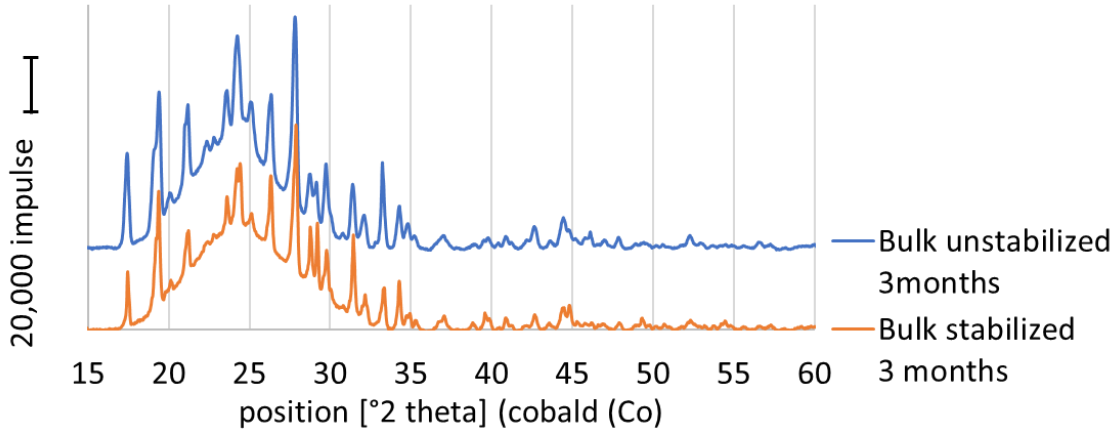

Fig. 6: X-ray diffractograms PER smartLipids bulk lipids show PER-characteristic peaks at 17.4°, 19.4° and 27.8°, proving the solid state of aggregation of PER smartLipids.

5.4. Conclusion

The DSC measurements of the PER smartLipids suspensions showed no thermal response between 20 °C and 90 °C due to a lag of sensitivity. The DSC analysis of the bulk material proofed the particles to remain in liquid state directly after production, but slowly solidifying within 7 days. These results could be confirmed by XRD measurements. Therefore, PER smartLipids are a suitable carrier system with delayed but occurring solidification of the particles. Thus, the typical smartLipids properties such as distinct occlusive effect and thus enhanced dermal penetration and reinforcement of the natural skin lipid barrier, high tissue adhesiveness and long durability on the skin can be expected.

5.5. References

Müller, R.H., Olechowski, F., Köpke, D., Pyo, S.M., 2019. smartLipids: The third generation of solid submicron lipid particles for dermal delivery of actives, in: Cornier, J., Keck, C.M., van de Voorde, M. (Eds.), Nanocosmetics. From Ideas to Products, 1st ed., pp. 141–159.

Müller, R. H., Sinambela, P., Keck, C. M., 2013. NLC – the invisible dermal patch for moisturizing & skin protection. Euro Cosmetics 6, 20–22.

6. Formulation of anti-pollution agent Symurban as smartCrystals for increased saturation solubility and improved dermal bioavailability[3]

6.1. Abstract

Several of most common dermatoses worldwide, e.g. psoriasis and atopic dermatitis are worsened in their clinical picture when the skin is regularly exposed to an increased air pollution level, e.g. particulate matter. This is explainable by the activation of the aryl hydrocarbon receptor (AhR) in the skin, which results in an increased release of proinflammatory cytokines and matrix metalloproteinases. Symurban is a competitive AhR antagonist and thus allows the effective protection of skin. In order to improve its dermal bioavailability as poorly soluble water active agent (0.25 µg/mL), smartCrystals were prepared and evaluated. smartCrystals are pure active crystals reduced in particle size to the submicron range of 100 nm to 1,000 nm. They feature the properties of nanocrystals, such as increased saturation solubility and dissolution velocity, without having to be declared as nanomaterial. Production methods and parameters were systematically investigated. Wet bead milling at 2,000 rpm for 30 minutes yielded the best results. A z-average of 280 nm was achieved for a 10% Symurban suspension with a polydispersity index of 0.20 indicated a narrow size distribution. For the long term stabilization of the smartCrystals suspension, the performance of 15 surfactants of different categories and HLB values was investigated and evaluated. It was found that non-ionic surfactants in general were better able to stabilize the system than anionic or amphoteric surfactants. Highest stability of over 12 months at 25 °C was achieved with 2% Plantacare 810 UP, an ECOCERT surfactant with high skin tolerance. The suspension was also chemically long term stable with > 97% of remaining Symurban over 12 months. The saturation solubility of Symurban was significantly increased from 0.25 µg/mL in raw drug powder in water to 2.9 µg/mL in Symurban smartCrystals, which corresponds to a factor of > 11 compared to raw drug powder. In a case study of one male volunteer with healthy skin conditions, penetration profiles of Symurban smartCrystals hydrogel and commercial anti-

[3]This chapter has been submitted for publication as:

Köpke, D., Pyo, S.M.; 2019. Formulation of anti-pollution agent Symurban as smartCrystals for increased saturation solubility and improved dermal bioavailability. International Journal of Pharmaceutics, *submitted [Manuscript ID: IJP-D-19-02592]*

pollution serum were determined and compared. After 20 minutes of exposure, the relative Symurban concentration in the deeper skin layers (tape 19-30) was more than 2 times higher when applied as smartCrystals hydrogel (16%) than the commercial serum (7%). These results suggest that smartCrystals is a promising delivery system for the poorly soluble anti-pollution agent Symurban.

6.2. Introduction

As a result of worldwide urbanization, the quality of air is constantly declining. According to WHO, 91% of urban population is exposed to air quality exceeding the limit of health concern (WHO, 2019). A correlation between air quality and diseases affecting the lungs and cardiovascular systems has already been proven with 29% of lung cancer, 25% of heart diseases, and 43% of lung diseases attributed to air pollution in 2016 (WHO, 2019). In recent years, increasingly the effect of air pollution on the largest organ exposed to the environment, the skin, have been studied (Kim et al., 2016; Mancebo and Wang, 2015; Puri et al., 2017). Air pollution is defined as the contamination of environment by any agent that modifies the natural characteristics of the atmosphere. After WHO, pollutants of major public health concern include particulate matter, carbon monoxide, ozone, nitrogen dioxide and sulfur dioxide (WHO, 2019). It was found that in particular the exposure of the skin to polycyclic aromatic hydrocarbons (PAH) and halogenated aromatic hydrocarbons (HAH) is harmful. They originate from incomplete burning of organic material and are primarily present in industrial exhaust gases, fuel burning, cigarette smoke, etc. and are transported by airborne fine dust particles (Alomirah et al., 2011). Penetrated into skin, the transcription factor aryl hydrocarbon receptor (AhR) is specifically activated (Denison and Heath-Pagliuso, 1998; Denison and Nagy, 2003; Hankinson, 1995; Marlowe and Puga, 2005) resulting in the upregulation of various pharmacological processes, e.g. enzymes of cytochrome P450 family (Fujii-Kuriyama and Mimura, 2005), melanogenesis (Luecke et al., 2010), cellular oxidant/antioxidant regulation (Dietrich, 2016), immune regulation (Esser et al., 2009; Stockinger et al., 2014; Veldhoen et al., 2008) and regulation of the epidermal barrier function (Haas et al., 2016) (Fig. 1). From this, the pathogenesis of various skin diseases are stimulated, such as vitiligo (Behfarjam and Jadali, 2018), psoriasis (Beránek et al., 2018; Kim et al., 2014) scleroderma (Noakes, 2017), neurodermatitis (Hidaka et al., 2017), acne vulgaris (Fabbrocini

et al., 2015). Further, the promotion of dermal carcinogenesis is discussed (Kolluri et al., 2017; Matsumoto et al., 2007; Xue et al., 2018).

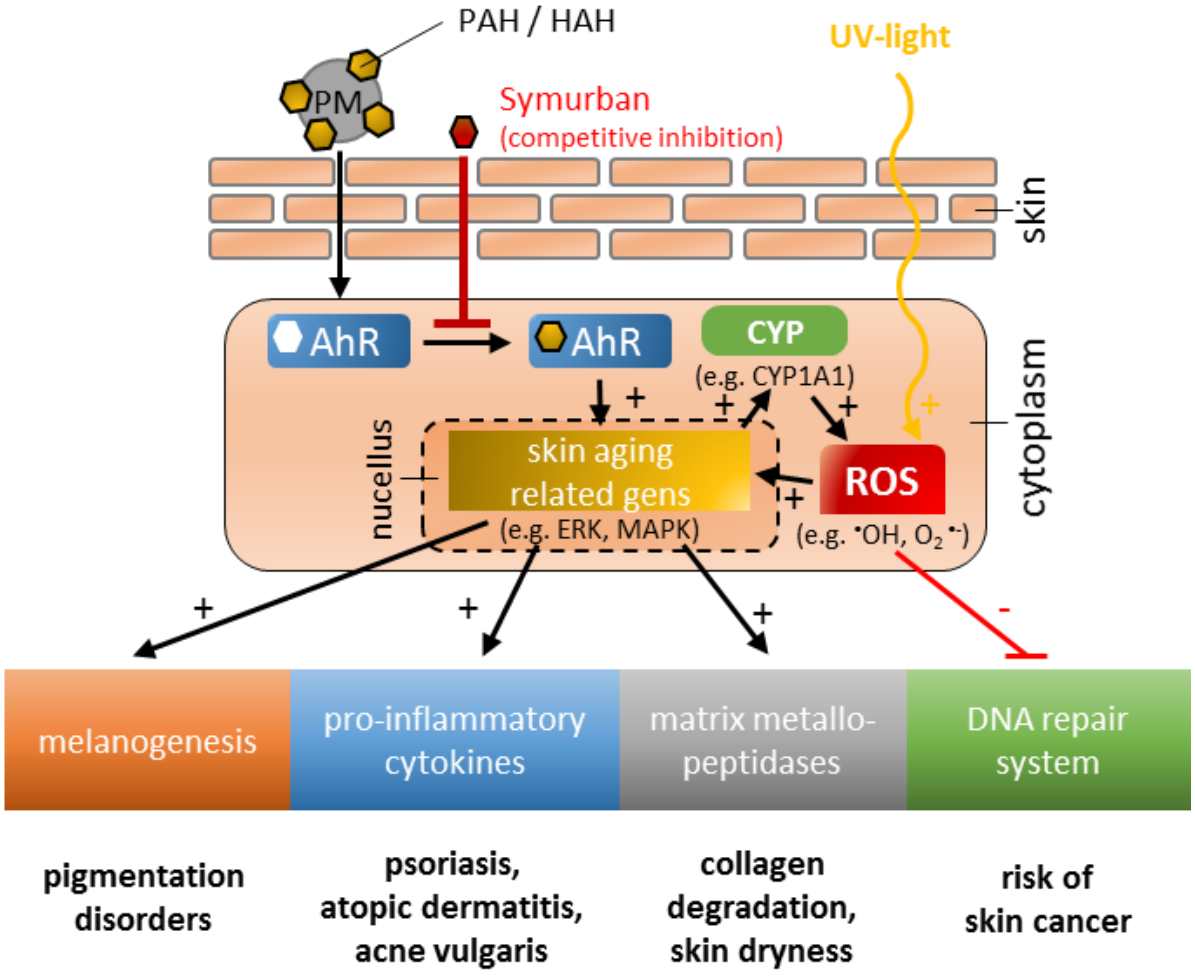

Fig. 1. Schematic illustration of impacts on skin caused by polycyclic aromatic hydrocarbons (PAH), hydrogenated aromatic hydrocarbons (HAH) adhere on the surface of particulate matter (PM), and UV-light exposure.

The concern about skin damages caused by air pollution is particularly evident in the personal care segment. The global anti-pollution skin care market is estimated to be 9 billion USD (2018), having an annual growth rate of 4.2% (Grandviewresearch.com, 2019). In 2016 Symurban (INCI: Benzylidene-Dimethoxydimethylindanone) was introduced to the market by the company Symrise as an anti-pollution active agent. As a competitive inhibitor of AhR Symurban can inhibit PAH/HAH induced effects (Haarmann-Stemmann et al., 2015; Qiao et al., 2017; Tigges et al., 2014). Originally, Symurban was introduced under the name SymHelios 1031 to the market 2009 with the main focus on protecting skin from UVB rays ("helios" -

Ancient Greek for “sun”). Its low solubility and resulting low penetration are advantageous as organic UV filter, but not as an anti-pollution active.

One physical approach for increasing the saturation solubility of actives and thereby their dermal bioavailability is the smartCrystals technology (Al Shaal et al., 2010; Hatahet et al., 2016; Pelikh et al., 2018; Pyo et al., 2016; Vidlářová et al., 2016). smartCrystals are pure active particles with sizes in the submicron range (100 nm – 1000 nm). What is special about particles in this size range is that they possess the properties of nanocrystals, such as distinctly increased saturation solubility (Hecq et al., 2005; Mauludin et al., 2009; Sun et al., 2012; Vidlářová et al., 2016) and a higher dissolution rate (Hatahet et al., 2016; Shegokar and Müller, 2010; Sun et al., 2012), compared to µm sized material without being declarable nanomaterials according to EU regulations (European Parliament, 2009). As a result, a greater concentration gradient is created between the formulation and the skin, enhancing the passive diffusion of the active ingredient into the skin. Due to the increased dissolution rate, the penetrated active agent molecules can then be quickly replaced, and the high concentration gradient can be maintained over a long period of time.

Aim of this work was to apply smartCrystals technology on Symurban to increase its solubility and thereby its skin penetration in order to obtain the full potency of Symurban as an anti-pollution agent *in vivo*.

6.3. Materials and methods

6.3.1. Materials

All materials used in this work are listed in Tab. 1 including trade name, INCI name and manufacturer/distributor. Milli-Q water was freshly produced using a Milli-Q system from Millipore GmbH (Darmstadt, Germany).

Tab. 1: Overview of materials used in this work.

	trade name	INCI/chemical description	manufacturer/distributor
active	Symurban®	Benzylidene Dimethoxydimethylindanone	Symrise AG, Germany
surfactants	Amphoterge® W-2	Disodium Cocoamphoacetate	Lonza Group AG, Switzerland
	Bergasoft SCG 22	Sodium Cocoyl Glycinate	Berg + Schmidt GmbH & Co. KG, Germany
	Dermofeel® G10L	Polyglyceryl-10 Laurate	Evonik Dr. Straetmans GmbH, Germany
	Eumulgin® SG	Sodium Stearoyl Glutamate	BASF SE, Germany
	Kolliphor® P407	Poloxamer 407	BASF SE, Germany
	Lanette® E	Cetaryl sulphate	BASF SE, Germany
	Miranol® Ultra C32	Sodium Cocoamphoacetate	Solvay S.A., Belgium
	Plantacare® 2000 UP	Decyl-Glucoside	BASF SE, Germany
	Plantacare® 810 UP	Coco-Glucoside	BASF SE, Germany
	Polyaldo® 10-1-CC	Polyglyceryl-10 Caprylate/Caprate	Lonza Group AG, Switzerland
	Sisterna® L70-C	Sucrose Alkyl Ester	Sisterna B.V., Netherlands
	Sisterna® SP70-C	Sucrose Alkyl Ester	Sisterna B.V., Netherlands
	SDS	Sodium Dodecyl Sulphate	VWR International LLC, USA
	Polysorbate 80	Polysorbate-80	Caesar & Loretz GmbH, Germany

Tab. 1 (continued): Overview of materials used in this work.

others	Microcare® PEHG (preservative)	Phenoxyethanol and Ethylhexylglycerin	Dr. Rimpler GmbH, Germany
	Carbopol® 981 NF (gelling agent)	Carbomer	Lubrizol Advanced Materials Europe BVBA, Belgium
GC materials	tert-Butyl methyl ether, HPLC grade, 99%+	Methyl tert-butyl ether 99%+	ThermoFischer (Kandel) GmbH, Germany
	Alphagaz™ 1 He	Helium 99,999%	AIR LIQUIDE Deutschland GmbH, Germany

6.3.2. Production of Symurban smartCrystals

6.3.2.1. *High pressure homogenization*

Symurban (10 wt%), Polysorbate 80 (2 wt%) and double distilled water (88 wt%) were pre-homogenized using a rotor-stator-homogenizer (Ultra-Turrax T25, IKA-Werke GmbH & Co. KG, Germany) at 8,500 rpm for 60 seconds. The so-obtained pre-suspension was subsequently high pressure homogenized in 3 steps: 2 cycles at 500 bar, 2 cycles at 1,000 bar and 15 cycles at 1,500 bar.

6.3.2.2. *Bead mill*

Symurban (10 wt%), surfactant (2 wt%) and double distilled water (88 wt%) were milled in a PML-2 pearl mill (Bühler AG, Switzerland) using SiLibeads type ZY-E 0.4-0.6 mm (Sigmund Lindner GmbH, Germany). Milling time was set to 30 minutes and the rotation speed to 2,000 rpm. Temperature during production was kept constant at 5 °C.

6.3.3. Particle characterization

6.3.3.1.1 Photon correlation spectroscopy (PCS)

The mean particle diameter and polydispersity index (PDI) of prepared smartCrystals were determined by dynamic light scattering using a Zetasizer Nano ZS (Malvern Instruments, Worcestershire, UK). Before measurement the samples were diluted 1:1,000 (vol%) in Milli-Q-water. Each sample was measured 10 times and the average was calculated and reported as z-average (z-ave).

6.3.3.1.2 Laser diffraction (LD)

The volume weighted particle diameter and distribution were measured by laser diffraction using a Mastersizer 2000 equipped with a Hydro 2000S dispersing unit (both Malvern Instruments, Worcestershire, UK). The refractive index used for Symurban was 1.610, which was determined prior LD measurement. As imaginary refractive index 0.01 was used. Sample was added to the dispersion unit until a laser obscuration between 4-6% was reached. Stirring speed was set to 1,750 rpm. Loose aggregates, if present, were re-dispersed by ultrasound at 25% to 75%.

6.3.3.1.3 Light microscopy

Samples were additionally examined by light microscopy using BA 210 (Motic Deutschland GmbH, Wetzlar, Germany) at 100-, 400-, and 1,000-times magnifications to detect possible particles and aggregates in µm-size.

6.3.4. Gas chromatography–mass spectrometry (GC-MS)

The Symurban concentration was determined by quantitative GC-MS analysis using an Agilent Technologies 7890A GC System paired with an Agilent Technologies 5975C quadrupole MS-detector. As column, an Agilent J&W GC column type 122-5532 G was used. At a heating rate of 20 K/min, the temperature was raised from 120 °C to 320 °C and maintained for 5 minutes. The flow rate of mobile phase He was set to 1 mL/min. For the measurement, 2 µL of sample were injected with a split-ratio of 1:10. The detector was used in SIM-mode at a molar mass of 293 M, being the main peak of mono-demethylated Symurban derivative, formed due to electron impact ionization. Symurban as E- and Z- isomer was detected at the retention times of 11.6 and 11.8 minutes, respectively. The total amount of Symurban was calculated as the sum of the two peaks. Each measurement was performed in duplicate and averaged. The method was calibrated by a 2^{nd} degree polynomial regression curve with a coefficient of determination of 0.9969. The limit of quantification was determined to be 0.25 µg/mL.

6.3.5. Determination of saturation solubility

For the investigation of saturation solubility, smartCrystals suspension was diluted in Milli-Q-water to a Symurban concentration of 1.0%. As reference, 1.0% Symurban raw drug powder (RDP) was dispersed in 0.4% aqueous Plantacare 810 UP solution to keep the surfactant concentration equal to the smartCrystals dilution. Both dilutions were then shaken for 24 hours in an Innova 4230 shaker (New Brunswick Scientific GmbH, Nürtingen, Germany) at 25 °C and 150 rpm. The undissolved Symurban crystals were removed by filtration using a 25 mm Cellulose Nitrate syringe-filter with a cutoff of 0.1 µm (GE Helathcare Life Sciences, Buckinghamshire, UK). Filtrates were diluted immediately 1:2 in aqueous 0.4% Plantacare 810 UP solution to avoid re-crystallization of supersaturated solution. Symurban concentration was then measured by GC-MS c.f. section 2.4. The determination of saturation solubility was done in triplicate. A Tuckey test was performed to determine significance ($p < 0.01$).

6.3.6. *in vivo* skin penetration study

The skin penetration of Symurban smartCrystals was determined in a case study on one volunteer using the tape stripping method (Jeong et al., 2010; Pellett et al., 1997). Symurban smartCrystals hydrogel at 0.25% was prepared using Carbopol 981 NF at 0.25% as gelling agent. On the inner forearm of the volunteer an area of 1.5 cm x 2 cm was treated with 45 mg of prepared hydrogel. After 20 minutes, the area was tape stripped 30 times using tesafilm® Kristallklar (tesa SE, Norderstedt, Germany). The by the adhesive tapes removed Symurban was extracted in 3.5 mL methyl tert-butyl ether and concentration in supernatant analyzed by GC-MS, c.f. section 2.4. As reference formulation a high-quality anti-pollution facial serum (80 € per 120 mL) with 0.25% Symurban (measured by GC-MS) and comparable viscosity to smartCrystals hydrogel was used.

6.4. Results and discussion

6.4.1. Production method of Symurban smartCrystals

For the production of Symurban smartCrystals, the two commonly applied top-down methods high pressure homogenization and bead milling were used. An aqueous Symurban suspension at 10% was prepared and processed, stabilized by 2.0% Polysorbate 80 being a commonly used surfactant for stabilizing nanosized suspensions. Unprocessed Symurban raw drug powder had a broad size distribution (0.4-800 µm) with a peak maximum at 25 µm (Fig. 2, upper red curve). Applying 5 cycles high pressure homogenization at 1,500 bar decreased considerably both the width of distribution (0.4-40 µm) and the peak maximum to 5.4 µm. However, after 10 cycles almost no change in size distribution and peak maximum was observed. Even after a total of 15 homogenization cycles, the peak maximum decreased only marginally to 4.1 µm (Fig. 2, light blue curve) and the desired nm range was not reached. Therefore, high pressure homogenization was considered to be unsuitable for the production of Symurban smartCrystals.

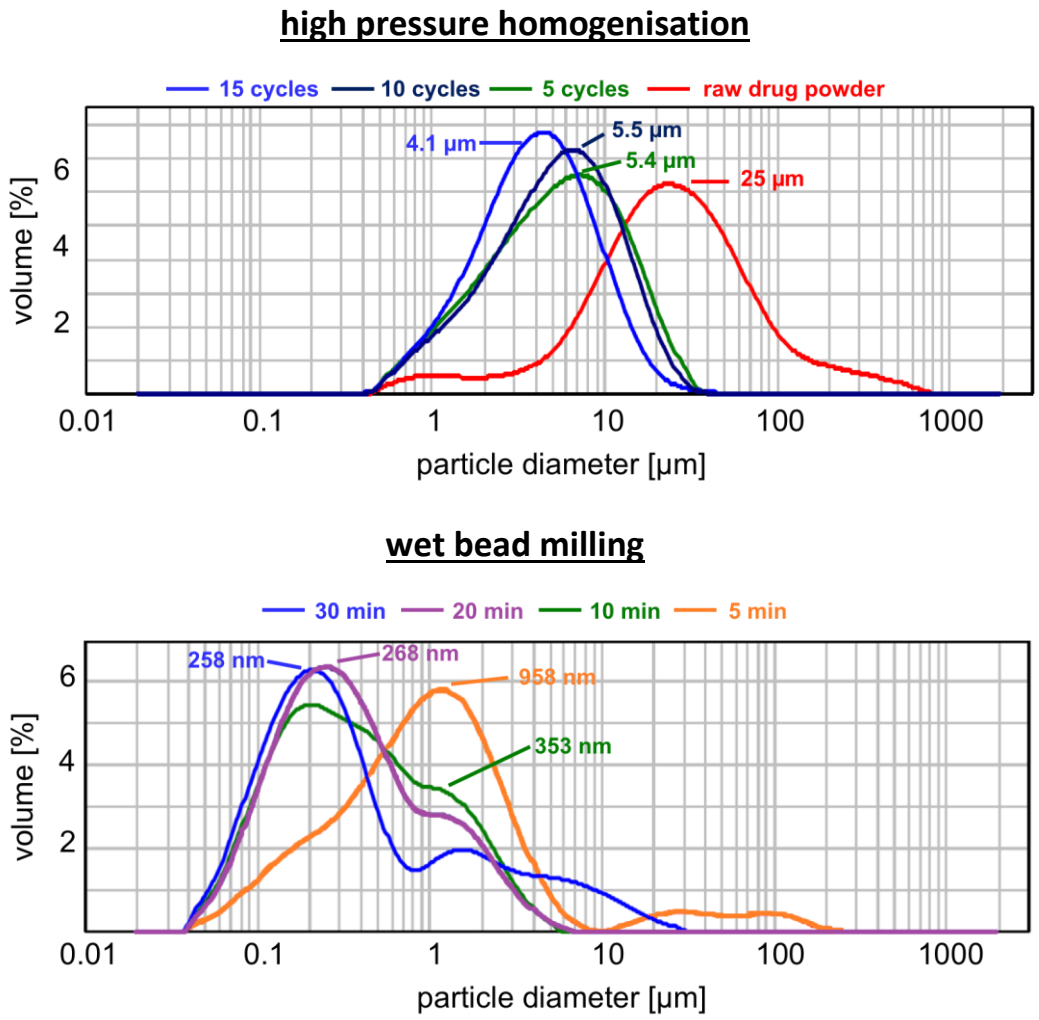

Fig. 2: LD particle size distribution of Symurban smartCrystals produced by high pressure homogenization (upper) and bead milling (lower), showing that only bead milling leads to appropriate size reduction of Symurban µm-crystals.

Besides the high pressure homogenization, bead milling is also a commonly used top-down method for the production of nm-sized particle suspensions. Already after a milling time of 5 minutes, the peak maximum of the RDP curve at 25 µm shifted to 0.95 µm being in the aimed nm-range. The particle size distribution is still broad, with the presence of a second particle fraction with sizes of 10-200 µm, which can be attributed to an unmilled fraction of sample. After 20 minutes of milling, the second fraction > 10 µm completely disappeared and the peak maximum is shifted to 268 nm. The increase of the milling time to 30 minutes leads to a so called “over-processing” of the suspension, visible in the further broadening of the particle distribution from 0.04-7 µm (20 minutes) to 0.04-30 µm (30 minutes). A narrow distribution is however essential for smartCrystals suspensions as storage stability is considerably higher

than for broad distributed suspensions whose small particles dissolve in favour of the large particles (Ostwald ripening, (Voorhees, 1985)).

In conclusion, Symurban smartCrystals at 10% can be obtained by bead milling. Optimal milling time was determined to be 20 minutes. Stabilized by Polysorbate 80 at 1.5% PCS z-ave of 295 nm with polydispersity index of 0.32 was achieved. These values are in good agreement with LD diameters LD50% of 0.26 µm, LD90% of 1.74 µm, and LD95% of 2.81 µm.

6.4.2. Screening of surfactants

A selection of 14 surfactants from different types (anionic, amphoteric, nonionic-PEG, nonionic-polyglyceryl and nonionic-glucoside) was used at 2.0% to stabilize 10.0% Symurban smartCrystals suspensions and compared to the results that were achieved with Polysorbate 80. The majority of the surfactants tested are ECOCERT certified and highlighted in green in Fig. 3. In addition, 4 surfactants were tested, which are not ECOCERT certified but commonly used for the production of nanosuspensions because of their good stabilizing properties. These surfactants are highlighted in red in Fig. 3.

All suspensions were examined under the microscope directly after production. Respective images are shown in Fig. 3 with their corresponding LD50% values (Fig. 3, left), zeta potentials (Fig. 3, middle) and PCS z-averages (Fig. 3, right). 6 of 15 surfactants, i.e. Bergasoft SCG 22, Eumulgin SG, Lanette E, Miranol Ultra C32, SDS and Sisterna SP70-C showed a pronounced tendency to form large aggregates visible to the naked eye already on the day of production. For these samples particle size and zeta potential were not determined (abbreviated as n.d. in Fig. 3).

Clear tendencies were visible by the surfactant screening. With anionic and amphoteric surfactants no stable Symurban smartCrystals suspension could be obtained showing all pronounced formation of aggregates. Also surfactants with high hydrophilic properties indicated by high HLB values > 20 proofed to be unsuitable for Symurban smartCrystals stabilization. Among the three subtypes of non-ionic surfactants (PEG, polyglyceryl and glucoside) no correlation could be found. In each of the 3 subtype groups both representatives can be found, one with high stabilizing properties in terms of particle size and size distribution and one showing pronounced aggregation (e.g. Plantacare 2000 UP leads to aggregation whereas Plantacare 810 UP remained stable – both are alkyl glucosides).

The 4 best-performing surfactants among tested 15 with regards to appearance (no aggregates), particle size (PCS mean particle size < 300 nm, LD50% < 300 nm), and size distribution (PdI < 0.35) were identified as Dermofeel G10L, Plantacare 810 UP, Polyaldo 10-1-CC, and Sisterna L70-C.

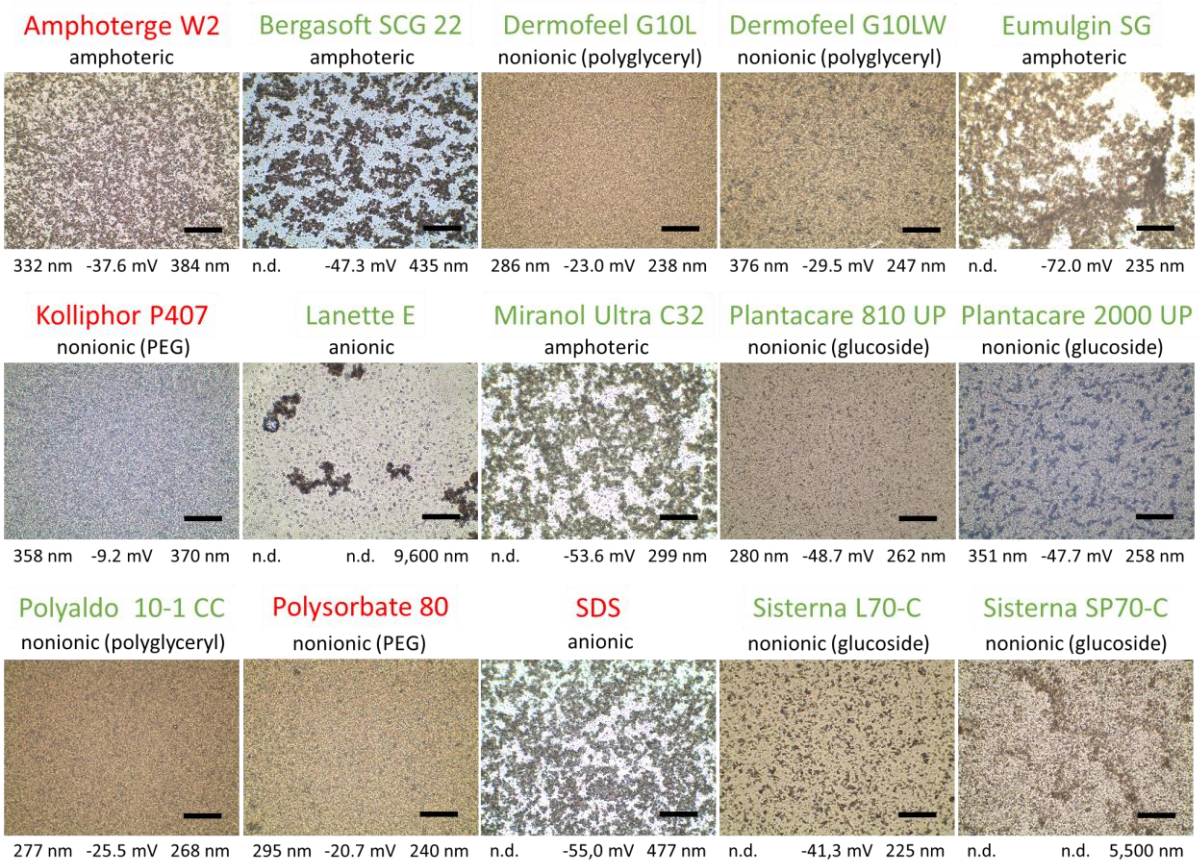

Fig. 3: Microscopic images at 400-fold magnification (scale bar 50 µm) for all produced samples with 2% surfactant, where ECOCERT surfactants are highlighted green and non-ECOCERT surfactants in red. The type of surfactant used is written above respective image, and LD50% value, zeta potential value, and z-average are written under the respective image from left to right.

6.4.3. Storage stability of Symurban smartCrystals

The four best formulations were stored at 25 °C, in the refrigerator at 4 °C and in the oven at 40 °C and their physical stability was re-analyzed after 1 month. After 1 month storage of Dermofeel G10L stabilized formulation at 25 °C, mean particle size and PdI clearly increased from 286 nm to 598 nm and 0.33 to 0.45 (Tab. 2). The LD90% value > 1.3 µm additionally confirms that this formulation is not storage stable. Comparable observations were made for the Sisterna L70-C stabilized formulation. With a z-ave of 522 nm, PdI of 0.5 and LD90% > 4 µm at the same storage conditions this formulation was not stable.

Both Plantacare 810 UP and the Polyaldo 10-1-CC stabilized formulation showed no noticeable changes under the microscope after 1 month storage at 25 °C. Both z-ave and PdI remained stable below 360 nm and 0.24, respectively. The only difference between the two was the LD95% and LD99% values. A higher storage stability was observed for the Plantacare 810 UP sample with an LD99% value of < 1 µm versus > 4 µm for the Polyaldo-10-1-CC sample. Also at the two other storage temperatures of 4 °C and 40 °C, the Plantacare 810 UP formulation is superior with smaller z-ave, PdI and LD99% values.

Both are nonionic surfactants sterically stabilizing the particles in the suspension. But in contrast to the Polyaldo-10-1-CC formulation, the Plantacare 810 UP formulation provides additional electrostatic stabilization based on the high zeta potential of -49 mV. This may explain the higher storage stability of the Plantacare 810 UP formulation. For this formulation, sufficient stability over 1 year was demonstrated at 25 °C, with a z-ave of 354 nm, a PdI of 0.20 and a LD95% value of < 1 µm (Fig. 4). The formulation also showed sufficient stability at 4 °C storage. Under stress conditions of 40 °C crystal growth was observed. This can be explained by increased solubility and decreased viscosity of formulation at higher temperature promoting Ostwald ripening.

In conclusion, Symurban smartCrystals at 10% stabilized with the ECOCERT certified Plantacare 810 UP at 2.0% proved to be storage stable for 1 year at both 4 °C and 25 °C.

Tab. 2: Particle size (PCS z-ave, LD D50, D90 and D95 all in [nm]) and polydispersity index of Symurban smartCrystals produced with 1.5% of the 4 best surfactants after 1 month storage at 4, 25 and 40 °C, showing that Plantacare 810 UP provides highest physical storage stability.

surfactant	1 month at 25 °C					1 month at 4 °C					1 month at 40 °C				
	PCS		LD			PCS		LD			PCS		LD		
	z-ave	PdI	D50	D90	D95	z-ave	PdI	D50	D90	D95	z-ave	PdI	D50	D90	D95
Dermofeel G10L	598	0.45	307	1,332	1,674	307	0.30	252	799	1,085	747	0.313	1,175	3,042	4,368
Plantacare 810 UP	270	0.21	231	449	523	263	0.20	257	569	708	345	0.200	295	758	3,342
Polyaldo 10-1-CC	357	0.24	315	1,206	1,988	286	0.20	249	622	815	532	0.275	428	3,371	27,401
Sisterna L70-C	522	0.50	2,028	4,353	5,191	263	0.34	268	2,454	3,243	1589	0.578	2,448	4,767	5,780

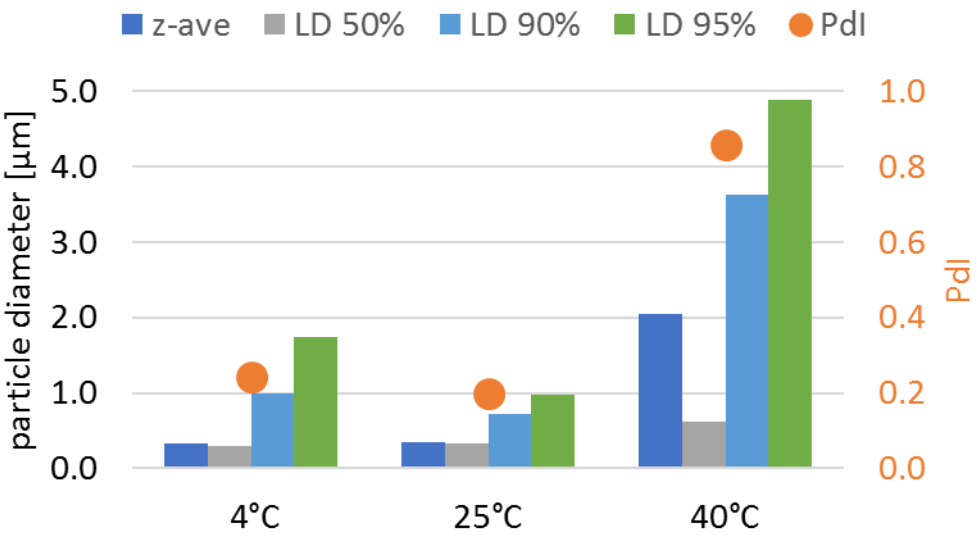

Fig. 4: Particle size and polydispersity index of Symurban smartCrystals stabilized with 2% Plantacare 810 UP after 12 months of storage at 4 °C, 25 °C and 40 °C. Best stability was achieved at 25 °C followed by 4 °C. Under stress conditions of 40 °C aggregation occurred.

Also chemically the formulation proofed to be stable. After 1 year of storage no significant reduction of Symurban concentration as smartCrystals suspensions was observed at any storage temperature, indicated by a remaining Symurban content of 100.1% at 4 °C, 97.5% at 25 °C and 100.9% at 40 °C.

All in all, the best formulation composed of 10% Symurban, 2% Plantacare 810 UP and 88% Milli-Q-water and produced by 30 minutes wet bead milling proofed to be physically and chemically highly stable. Recommended storage temperature was determined to be 25 °C, but also a storage at 4 °C was demonstrated to be feasible.

6.4.4. Saturation solubility

The increased dermal bioavailability of actives by smartCrystals technology is achieved through increased saturation solubility. Hence, the extent of saturation solubility increase of Symurban as smartCrystals was measured by GC (c.f. 2.4.) and compared to unprocessed µm-sized raw drug powder in water and in 0.2% aqueous Plantacare 810 UP solution (identical to the composition of smartCrystals composition).

Results of the saturation solubility study are presented in Fig. 5. The saturation solubility for smartCrystals formulation is significantly increased by a factor of > 15 for RDP in aqueous surfactant solution and > 11 for RDP in water from 0.19 ± 0.05 µg/mL and 0.25 ± 0.02 µg/mL to 2.86 ± 0.45 µg/mL, respectively.

As the penetration of actives into skin is a passive diffusion process, it is mainly dependent on the concentration gradient between formulation and skin and therefore on the saturation concentration of active in formulation (Hatahet et al., 2016; Pelikh et al., 2018; Vidlářová et al., 2016). By preparing Symurban as smartCrystals, an improved dermal bioavailability can therefore be predicted.

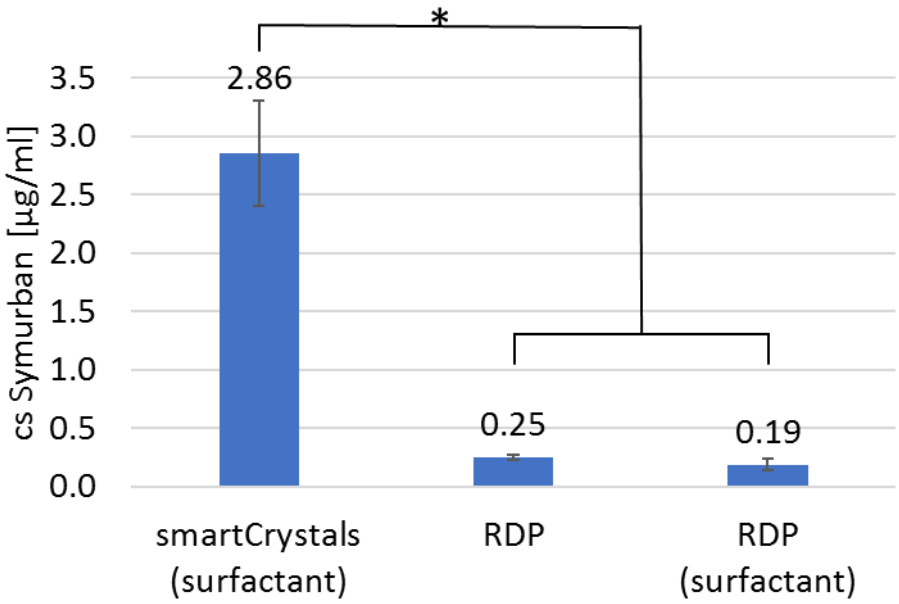

Fig. 5: Saturation solubility of Symurban as smartCrystals and raw drug powder (RDP) in water and in aqueous surfactant solution according to the composition of smartCrystals suspension demonstrating an at least 11-fold increased saturation solubility by smartCrystals technology. "" indicates statistically significant differences with $p < 0.01$.*

6.4.5. *In vivo* skin penetration profile

The assumption of improved dermal bioavailability by increasing saturation solubility was examined in a case study of one male volunteer by the tape stripping method. Instead of using a hydrogel with Symurban µm-crystals as a reference, the performance of smartCrystals hydrogel was compared to a Symurban containing market product of higher price level with an anti-pollution claim. The selection of a product being already optimized for the market was intended to challenge the smartCrystals as delivery system.

Both formulations had the same Symurban content of 0.25 wt%. Therefore, also the applied amount of formulation (45 mg) and size of skin area (1.5 cm x 1.5 cm) were kept identical. After 20 minutes of penetration each skin area was taped 30 times and the content of Symurban in the tapes were determined via GC (c.f. 2.4.) to create penetration profiles. The recovery rate of both formulations was comparable with 90.2% (reference product) and 92.3% (smartCyrstals gel) The loss of < 10% can be explained by the fact that the penetration is not only vertically but also horizontally oriented. The penetration depth exceeded the depth reached by 30 tapes and could therefore not be determined and compared. Clear differences can be seen in the distribution of the active ingredient in the skin (Fig. 6). The penetration profile of market product shows that 47% and therefore almost half of applied Symurban are located in the first 2 tapes. With 7% in the tapes 19-30, only a negligible amount reaches the deeper layers of skin. In contrast, smartCrystals hydrogel allows deeper penetration of larger amounts of Symurban, reflected by the Symurban content of only 26% in first 2 tapes and more than double in tapes 19-30. Symurban smartCrystals hydrogel therefore shows a more favourable distribution with higher concentrations in the deeper layers of the stratum corneum.

The present data confirm that by reducing the crystal size of Symurban into the submicron range its penetration can be improved. This result is consistent to data from literature showing superior skin penetration of submicron particles compared to raw drug powder (Al Shaal et al., 2010; Hatahet et al., 2016; Pelikh et al., 2018; Pyo et al., 2016; Vidlářová et al., 2016).

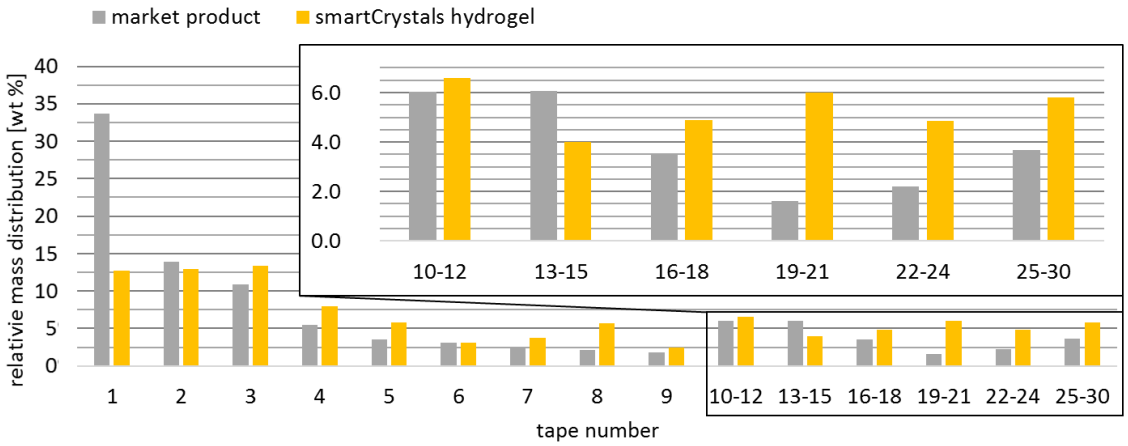

Fig. 6: Penetration profiles measured in vivo on the inner forearm of one volunteer with healthy skin conditions via tape stripping test after 20 minutes application of Symurban smartCrystals hydrogel (yellow bars) and a commercially available anti-pollution product (grey bars) with identical Symurban amount.

6.5. Conclusion

Symurban smartCrystals suspension at 10 wt% with mean particle size of 280 nm and PdI of 0.27 were obtained by wet bead milling at 2,000 rpm for 30 minutes. Generally, Symurban smartCrystals were better stabilized by nonionic surfactants compared to anionic surfactants. Highest physical and chemical storage stability among the 15 screened surfactants was obtained with 2 wt% Plantacare 810 UP, a skin friendly and as organic certified surfactant. No particle growth (z-ave of 354 nm and PdI of 0.20) nor chemical degradation (> 97%) was observed within 12 months at 4 °C and at room temperature. By smartCrystals technology, an increase in saturation solubility by a factor of > 11 was obtained leading to a favourable penetration profile with higher concentration of Symurban in deeper skin layers demonstrated *in vivo* by tape stripping test on the inner forearm of one volunteer. With this, smartCrystals can be seen as a highly promising system of poorly soluble Symurban.

6.6. References

Al Shaal, L., Müller, R.H., Shegokar, R., 2010. smartCrystal combination technology: scale up from lab to pilot scale and long term stability. Pharmazie 65 (12), 877–884.

Alomirah, H., Al-Zenki, S., Al-Hooti, S., Zaghloul, S., Sawaya, W., Ahmed, N., Kannan, K., 2011. Concentrations and dietary exposure to polycyclic aromatic hydrocarbons (PAHs) from grilled and smoked foods. Food Control 22 (12), 2028–2035.

Behfarjam, F., Jadali, Z., 2018. Vitiligo patients show significant up-regulation of aryl hydrocarbon receptor transcription factor. An. Bras. Dermatol. 93 (2), 302–303.

Beránek, M., Fiala, Z., Kremláček, J., Andrýs, C., Krejsek, J., Hamáková, K., Palička, V., Borská, L., 2018. Serum levels of aryl hydrocarbon receptor, cytochromes P450 1A1 and 1B1 in patients with exacerbated psoriasis vulgaris. Folia Biol. (Praha) 64 (3), 97–102.

Denison, M.S., Heath-Pagliuso, S., 1998. The Ah receptor: A regulator of the biochemical and toxicological actions of structurally diverse chemicals. Bull. Environ. Contam. Toxicol. 61 (5), 557–568.

Denison, M.S., Nagy, S.R., 2003. Activation of the aryl hydrocarbon receptor by structurally diverse exogenous and endogenous chemicals. Annu. Rev. Pharmacol. Toxicol. 43, 309–334.

Dietrich, C., 2016. Antioxidant functions of the aryl hydrocarbon receptor. Stem Cells Int. 2016.

Esser, C., Rannug, A., Stockinger, B., 2009. The aryl hydrocarbon receptor in immunity. Trends Immunol. 30 (9), 447–454.

European Parliament, 2009. Regulation (EC) No 1223/2009 of the European Parliament and of the Council of 30 November 2009 on cosmetic products: OJ L 342, 22.12.2009.

Fabbrocini, G., Kaya, G., Caseiro Silverio, P., Vita, V. de, Kaya, A., Fontao, F., Sorg, O., Saurat, J.-H., 2015. Aryl hydrocarbon receptor activation in acne vulgaris skin: A case series from the region of naples, Italy. Dermatology (Basel) 231 (4), 334–338.

Fujii-Kuriyama, Y., Mimura, J., 2005. Molecular mechanisms of AhR functions in the regulation of cytochrome P450 genes. Biochem. Biophys. Res. Commun. 338 (1), 311–317.

Grandviewresearch.com, 2019. Anti-pollution skincare products: market size, share & trends analysis report. https://www.grandviewresearch.com/industry-analysis/anti-pollution-skincare-products-market. Accessed 10 September 2019.

Haarmann-Stemmann, T., Esser, C., Krutmann, J., 2015. The janus-faced role of aryl hydrocarbon receptor signaling in the skin: Consequences for prevention and treatment of skin disorders. J. Invest. Dermatol. 135 (11), 2572–2576.

Haas, K., Weighardt, H., Deenen, R., Köhrer, K., Clausen, B., Zahner, S., Boukamp, P., Bloch, W., Krutmann, J., Esser, C., 2016. Aryl hydrocarbon receptor in keratinocytes is essential for murine skin barrier integrity. J. Invest. Dermatol. 136 (11), 2260–2269.

Hankinson, O., 1995. The aryl hydrocarbon receptor complex. Annu. Rev. Pharmacol. Toxicol. 35, 307–340.

Hatahet, T., Morille, M., Hommoss, A., Dorandeu, C., Müller, R.H., Bégu, S., 2016. Dermal quercetin smartCrystals®: Formulation development, antioxidant activity and cellular safety. Eur. J. Pharm. Biopharm. 102, 51–63.

Hecq, J., Deleers, M., Fanara, D., Vranckx, H., Amighi, K., 2005. Preparation and characterization of nanocrystals for solubility and dissolution rate enhancement of nifedipine. Int. J. Pharm. 299 (1-2), 167–177.

Hidaka, T., Ogawa, E., Kobayashi, E.H., Suzuki, T., Funayama, R., Nagashima, T., Fujimura, T., Aiba, S., Nakayama, K., Okuyama, R., Yamamoto, M., 2017. The aryl hydrocarbon receptor AhR links atopic dermatitis and air pollution via induction of the neurotrophic factor artemin. Nat. Immunol. 18 (1), 64.

Jeong, S.H., Kim, J.H., Yi, S.M., Lee, J.P., Kim, J.H., Sohn, K.H., Park, K.L., Kim, M.-K., Son, S.W., 2010. Assessment of penetration of quantum dots through in vitro and in vivo human skin using the human skin equivalent model and the tape stripping method. Biochem. Biophys. Res. Commun. 394 (3), 612–615.

Kim, H.O., Kim, J.H., Chung, B.Y., Choi, M.G., Park, C.W., 2014. Increased expression of the aryl hydrocarbon receptor in patients with chronic inflammatory skin diseases. Exp. Dermatol. 23 (4), 278–281.

Kim, K.E., Cho, D., Park, H.J., 2016. Air pollution and skin diseases: Adverse effects of airborne particulate matter on various skin diseases. Life Sci. 152, 126–134.

Kolluri, S.K., Jin, U.-H., Safe, S., 2017. Role of the aryl hydrocarbon receptor in carcinogenesis and potential as an anti-cancer drug target. Arch. Toxicol. 91 (7), 2497–2513.

Luecke, S., Backlund, M., Jux, B., Esser, C., Krutmann, J., Rannug, A., 2010. The aryl hydrocarbon receptor (AHR), a novel regulator of human melanogenesis. Pigment Cell Melanoma Res. 23 (6), 828–833.

Mancebo, S.E., Wang, S.Q., 2015. Recognizing the impact of ambient air pollution on skin health. J. Eur. Acad. Dermatol. Venereol. 29 (12), 2326–2332.

Marlowe, J.L., Puga, A., 2005. Aryl hydrocarbon receptor, cell cycle regulation, toxicity, and tumorigenesis. J. Cell. Biochem. 96 (6), 1174–1184.

Matsumoto, Y., Ide, F., Kishi, R., Akutagawa, T., Sakai, S., Nakamura, M., Ishikawa, T., Fujii-Kuriyama, Y., Nakatsuru, Y., 2007. Aryl hydrocarbon receptor plays a significant role in

mediating airborne particulate-induced carcinogenesis in mice. Environ. Sci. Technol. 41 (10), 3775–3780.

Mauludin, R., Müller, R.H., Keck, C.M., 2009. Kinetic solubility and dissolution velocity of rutin nanocrystals. Eur. J. Pharm. Sci. 36 (4-5), 502–510.

Noakes, R., 2017. Dissecting the enigma of scleroderma: Possible involvement of the kynurenine pathway. Pteridines 28 (2), 3172.

Pelikh, O., Stahr, P.-L., Huang, J., Gerst, M., Scholz, P., Dietrich, H., Geisel, N., Keck, C.M., 2018. Nanocrystals for improved dermal drug delivery. Eur. J. Pharm. Biopharm. 128, 170–178.

Pellett, M.A., Roberts, M.S., Hadgraft, J., 1997. Supersaturated solutions evaluated with an in vitro stratum corneum tape stripping technique. Int. J. Pharm. 151 (1), 91–98.

Puri, P., Nandar, S.K., Kathuria, S., Ramesh, V., 2017. Effects of air pollution on the skin: A review. Indian J. Dermatol. Venereol. Leprol. 83 (4), 415–423.

Pyo, S., Meinke, M., Keck, C., Müller, R., 2016. Rutin—Increased antioxidant activity and skin penetration by nanocrystal technology (smartCrystals). Cosmetics 3 (1), 9.

Qiao, Y., Li, Q., Du, H.-Y., Wang, Q.-W., Huang, Y., Liu, W., 2017. Airborne polycyclic aromatic hydrocarbons trigger human skin cells aging through aryl hydrocarbon receptor. Biochem. Biophys. Res. Commun. 488 (3), 445–452.

Shegokar, R., Müller, R.H., 2010. Nanocrystals: Industrially feasible multifunctional formulation technology for poorly soluble actives. Int. J. Pharm. 399 (1-2), 129–139.

Stockinger, B., Di Meglio, P., Gialitakis, M., Duarte, J.H., 2014. The aryl hydrocarbon receptor: multitasking in the immune system. Annu. Rev. Immunol. 32, 403–432.

Sun, J., Wang, F., Sui, Y., She, Z., Zhai, W., Wang, C., Deng, Y., 2012. Effect of particle size on solubility, dissolution rate, and oral bioavailability: Evaluation using coenzyme Q_{10} as naked nanocrystals. Int. J. Nanomedicine 7, 5733–5744.

Tigges, J., Haarmann-Stemmann, T., Vogel, C.F.A., Grindel, A., Hübenthal, U., Brenden, H., Grether-Beck, S., Vielhaber, G., Johncock, W., Krutmann, J., Fritsche, E., 2014. The new aryl hydrocarbon receptor antagonist E/Z-2-benzylindene-5,6-dimethoxy-3,3-dimethylindan-1-one protects against UVB-induced signal transduction. J. Invest. Dermatol. 134 (2), 556–559.

Veldhoen, M., Hirota, K., Westendorf, A.M., Buer, J., Dumoutier, L., Renauld, J.-C., Stockinger, B., 2008. The aryl hydrocarbon receptor links T_H17-cell-mediated autoimmunity to environmental toxins. Nature 453 (7191), 106.

Vidlářová, L., Romero, G.B., Hanuš, J., Štěpánek, F., Müller, R.H., 2016. Nanocrystals for dermal penetration enhancement - Effect of concentration and underlying mechanisms using curcumin as model. Eur. J. Pharm. Biopharm. 104, 216–225.

Voorhees, P.W., 1985. The theory of Ostwald ripening. J. Stat. Phys. 38 (1-2), 231–252.

WHO, 2019. World Health Organization international website. WHO. https://www.who.int/airpollution/en/. Accessed 21 October 2019.

Xue, P., Fu, J., Zhou, Y., 2018. The Aryl Hydrocarbon Receptor and Tumor Immunity. Front. Immunol. 9, 286.

7. Summary

Using smartLipids and smartCrystals technology, submicron formulations were developed enabling 4 different anti-pollution strategies: smartLipids 2nd skin provide skin barrier reinforcement, smartLipids 2nd skin Q10 allow improved dermal delivery of the skin-physiological antioxidant Q10. PER smartLipids improve the symptomatic treatment of pollution-induced pigmentation disorders and Symurban smartCrystals provide improved dermal delivery of the aryl hydrocarbon receptor antagonist Symurban.

The first aim of this thesis was the development of physically stable smartLipids 2nd skin (Chapter 2). In a surfactant screening 19 out of 16 surfactants lead to immediate aggregation of the formulations. Of the remaining 3 surfactants, only Lanette E proofed to provide long-term stability. After preservation by 3% pentylene glycol, a physical stabilization of the submicron suspension over 1 year could be achieved. The loading test with the model active ingredient coenzyme Q10 showed that the smartLipids 2nd skin could be loaded with up to 50% active ingredient with a storage stability of 11 months. The maximum loading capacity of the NLC formulations published so far (25%) has thus been doubled. Thus, the second aim of this thesis, to demonstrate the high loading capacity of smartLipids, was accomplished.

The third aim of this work was the development of physically stable PER smartLipids (Chapter 3). Searching for a suitable lipid, all tested cosmetic oils proofed to have insufficient solubility. Thereupon, so-called "inverse loading method" was developed, i.e. the smartLipids matrix lipid was dissolved in a molten active ingredient. This resulted in a loading of 50% phenylethyl resorcinol, increasing the previously published maximum load in NLC (20%) by factor 2.5. The best result was achieved with Lipocire A, a natural di- and triglyceride mixture, complying the smartLipids properties due to its complex composition. This was used to produce a physically stable suspension for 14 months. In addition, the production process was further developed in this chapter for industrial production-scale.

Despite the good chemical stability of PER in smartLipids, a reddish discoloration of the product was observed after several months of storage. This is probably caused by strongly colored degradation products of phenylethyl resorcinol. Therefore, the fourth aim of this

thesis was to optimize the color stability of PER smartLipids, which is described in Chapter 4 of this thesis. Tinosorb S and Oxynex ST liquid were the optimal stabilizers, remaining completely without discoloration in both, over 3 months under light protection and in a 7-day light stress test. The physical stability of the PER smartLipids remains unchanged. The verification of the solid state of the PER smartLipids could be carried out in Chapter 5 by differential scanning calorimetry and X-ray diffraction analysis, which was the fifth aim of this thesis.

The sixth aim of this thesis was the development of a long-term stable smartCrystals formulation with the aryl hydrocarbon receptor antagonist Symurban (Chapter 6). Wet bead milling proofed to be the most suitable process for the production of smartCrystals. Of the 15 surfactants tested, only Plantacare 810 UP showed sufficient stabilization of the smartCrystals suspension. With this surfactant, physical and chemical stability of the smartCrystals could be achieved for 1 year. The seventh and final aim of this thesis was to demonstrate the performance of Symurban smartCrystals concept. The saturation solubility of the Symurban raw drug powder could be increased almost fifteen fold from 0.2 µg/mL to 2.8 µg/mL by Symurban smartCrystals. In the dermal human case control penetration test, Symurban smartCrystals proofed to transport more than the twice amount of Symurban into deeper skin layers than a conventional cosmetic product.

All of the developed formulations provided physical and chemical stability of at least 11 months. Therefore, the overall aim of this thesis as well as all sub-aims could be accomplished.

8. Zusammenfassung

Unter Verwendung der smartLipids- der smartCrystals-Technologie wurden submikrone Formulierungen entwickelt, die 4 verschiedene Anti-Pollution Strategien ermöglichen: smartLipids 2nd skin liefert den Wiederaufbau der geschädigten Hautlipidbarriere, smartLipids 2nd skin Q10 ermöglicht eine verbesserte dermale Penetration des hautphysiologischen Antioxidans Q10. PER smartLipids verbessern die symptomatische Behandlung von durch Luftverschmutzung hervorgerufenen Pigmentierungsstörungen und Symurban smartCrystals bieten eine verbesserte dermale Penetration des Aryl-Hydrocarbon-Rezeptor-Antagonisten Symurban.

Das erste Ziel dieser Arbeit war die Entwicklung von physikalisch stabilen smartLipids 2nd skin (Kapitel 2). In einem Tensidscreening führten 19 von 16 Tensiden zu einer sofortigen Aggregation der Formulierung. Von den verbleibenden 3 Tensiden führte nur Lanette E zur Langzeitstabilität der Formulierung. Nach der Konservierung mit 3% Pentylenglykol konnte eine physikalische Stabilisierung der submikronen Lipidsuspension über 1 Jahr erreicht werden. Der Beladungstest mit dem Modellwirkstoff Coenzym Q10 zeigte, dass die smartLipids 2nd skin mit bis zu 50% Wirkstoff bei einer Lagerstabilität von 11 Monaten beladen werden können. Die maximale Beladbarkeit der bisher veröffentlichten NLC-Formulierungen (25%) wurde damit verdoppelt. Somit wurde auch das zweite Ziel dieser Arbeit erreicht.

Das dritte Ziel dieser Arbeit war die Entwicklung von physikalisch stabilen PER smartLipids (Kapitel 3). Auf der Suche nach einem geeigneten Lipid wurde eine unzureichende Löslichkeit in allen getesteten kosmetischen Ölen festgestellt. Daraufhin wurde das so genannte "inverse loading-Verfahren" entwickelt, d.h. das smartLipids-Matrix-Lipid wurde in dem geschmolzenen Wirkstoff gelöst. Dies führte zu einer Beladung von 50% Phenylethyl Resorcinol und erhöhte die zuvor veröffentlichte maximale Belastung in NLC (20%) um den Faktor 2,5. Das beste Ergebnis wurde mit Lipocire A erzielt, einer natürlichen Di- und Triglyceridmischung, die aufgrund ihrer komplexen Zusammensetzung das smartLipids-Konzept erfüllt. Mit diesem Lipid wurde eine physikalisch stabile PER smartLipids Suspension mit 14 Monaten Stabilität hergestellt. Darüber hinaus wurde in diesem Kapitel der Produktionsprozess für den industriellen Produktionsmaßstab weiterentwickelt.

Trotz der guten chemischen Stabilität von PER in smartLipids konnte nach mehrmonatiger Lagerung eine rötliche Verfärbung des Produkts beobachtet werden. Dies wird wahrscheinlich durch stark gefärbte Abbauprodukte von Phenylethyl Resorcinol verursacht. Daher war die Optimierung der Farbstabilität das vierte Ziel dieser Arbeit von PER smartLipids, die in Kapitel 4 dieser Arbeit beschrieben wird. Tinosorb S und Oxynex ST liquid waren die optimalen Stabilisatoren, die sowohl über 3 Monate unter Lichtschutz als auch in einem 7-tägigen Lichtstresstest ohne Verfärbung blieben. Die physikalische Stabilität der PER smartLipids bleibt unverändert. Das Vorliegen des festen Aggregatzustandes der PER smartLipids konnte in Kapitel 5 durch dynamische Differenzkalorimetrie und Röntgenbeugungsanalyse nachgewiesen werden, was das fünfte Ziel dieser Arbeit war.

Das sechste Ziel dieser Arbeit war die Entwicklung einer langzeitstabilen smartCrystals Formulierung mit dem Aryl-Hydrocarbon-Rezeptor-Antagonisten Symurban (Kapitel 6). Die Nassperlenmahlung hat sich als das am besten geeignete Verfahren zur Herstellung von smartCrystals erwiesen. Von den 15 getesteten Tensiden zeigte nur Plantacare 810 UP eine ausreichende Stabilisierung der smartCrystals Suspension. Mit diesem Tensid konnte die physikalische und chemische Stabilität der smartCrystals für 1 Jahr erreicht werden. Das siebte und letzte Ziel dieser Arbeit war es, die Eigenschaften des Symurban smartCrystals Konzepts zu demonstrieren. Die Sättigungslöslichkeit des Symurban unbehandelten Wirkstoffpulvers konnte durch Symurban smartCrystals fast um das Fünfzehnfache von 0,2 µg/ml auf 2,8 µg/ml erhöht werden. In einer Einzelfallstudie an Humanhaut zeigten Symurban smartCrystals mehr als die doppelte Menge Symurban in tieferen Hautschichten als ein konventionelles kosmetisches Produkt.

Alle entwickelten Formulierungen ermöglichten eine physikalische und chemische Stabilität von mindestens 11 Monaten. Daher könnte das übergeordnete Ziel dieser Arbeit sowie alle Teilziele erreicht werden.

9. Abbreviations

Abbreviation	Translation
AhR	aryl hydrocarbon receptor
BHT	butylated hydroxytoluene
BM	bead milling
CER	ceramide
etc.	et cetera
EU	European Union
GC-MS	gas chromatography with mass spectroscopy detection
GMP	good manufacturing practice
HAH	halogenated aromatic hydrocarbon
HPH	high pressure homogenization
IL	interleukin
INCI	International Nomenclature of Cosmetic Ingredients
LD	laser diffraction
LM	light microscopy
LNP	lipid nanoparticles
MMP	matrix metallopeptidase
NC	nanocrystals
NLC	nanostructured lipid carrier
NMBS	sodium metabisulfite
NSL	natural skin lipids
PAH	polycyclic aromatic hydrocarbon
PCS	photon correlation spectroscopy
PdI	polydispersity index
PEG	polyethylene glycol
PER	phenylethyl resorcinol
RI	refractive index
ROS	reactive oxygen species
rpm	revolutions per minute
SC	stratum corneum
SDS	sodium dodecyl sulphate
SLN	solid lipid nanoparticles
TEWL	transepithelial water loss
UK	United Kingdom
UV	ultraviolet radiation
WHO	world health organization
z-ave	z-average: PCS intensity weighted particle diameter

.

10. List of publications

Book chapters

(1) Müller, R.H, Olechowski, F., Köpke, D., Pyo, S.M., SmartLipids—The third generation of solid submicron lipid particles for dermal delivery of actives, , in: Cornier, J., Keck, C.M., van de Voorde, M. (Eds.), Nanocosmetics. From Ideas to Products, 1st ed., pp 141-159, 15 June 2019

Articles (peer-reviewed)

(1) Köpke, D., Müller, R.H., Pyo, S.M., Phenylethyl resorcinol smartLipids for skin brightening - Increased loading & chemical stability. Eur. J. Pharm. Sci., 104992. - doi: 10.1016/j.ejps.2019.10499

(2) Köpke, D., Pyo, S.M., Formulation of anti-pollution agent Symurban as smartCrystals for increased saturation solubility and improved dermal bioavailability. Int. J. Pharm., submitted [Manuscript ID: IJP-D-19-02592]

Proceedings

(1) Köpke, D., Schmidt, C., Müller, R. H., Reverse loading principle for higher loading of actives in SLN and NLC, Controlled Release Society (CRS) Local Chapter Germany, Marburg/Germany, 2.-3. March 2017

(2) Köpke, D., Pyo, S. M., Müller, R. H., smartLipids – superior loading capacity by chaotic lipid matrix of the whitening agent phenylethyl resorcinol, Controlled Release Society (CRS) Local Chapter Germany, Halle/Germany, 1.-2. March 2018

(3) Efkarpidou, A.-M., Köpke, D., Müller, R. H., Pyo, S. M., Anti-pollution skin care – 2nd formation by smartLipids from natural lipids, O10, Controlled Release Society (CRS) Local Chapter Germany, Leipzig/Germany, 7.-8. March 2019

(4) Köpke, D., Schmoll, J., Laufer, T., Pyo, S. M., Müller, R. H., Anti-pollution smartCrystals – submicron Symurban for enhanced dermal penetration, P34, Controlled Release Society (CRS) Local Chapter Germany, Leipzig/Germany, 7.-8. March 2019

(5) Pyo, S. M., Köpke, D., Efkarpidou, A.-M., Müller, R. H., Skin whitening – phenylethyl resorcinol smartLipids with improved loading capacity and chemical stability, P57, Controlled Release Society (CRS) Local Chapter Germany, Leipzig/Germany, 7.-8. March 2019

Abstracts

(1) Köpke, D., Chung, D., Türktüzün, T., Pyo, S. M., Müller, R. H., BergaCare SmartLipids – novel loading principle to increase the loading capacity of skin whiteners, T6041, American Association of Pharmaceutical Scientists (AAPS) Annual Meeting, San Diego/USA, 12.-15. November 2017

(2) Köpke, D., Pyo, S. M., Müller, R. H., smartCrystals – nano sized Symurban for innovative anti-pollution cosmetics, P 27, „Tag der Pharmazie“, local meeting of German Pharmaceutical Society (DPhG) Landesgruppe Berlin-Brandenburg, Berlin/Germany, 6. July 2018

(3) Köpke, D., Pyo, S. M., Müller, R. H., smartLipids – submicron industrial concentrate of phenylethyl resorcinol for skin whitening, POS.159, Annual meeting of German Pharmaceutical Society (DPhG), Hamburg/Germany, 2.-5. Oktober 2018

(4) Köpke, D., Pyo, S. M., Müller, R. H., BergaCare SmartLipids – Development of commercial concentrates of phenylethyl resorcinol for skin whitening, #508922, American Association of Pharmaceutical Scientists (AAPS) Annual Meeting, Washington DC/USA, 4.-7. November 2018

(5) Köpke, D., Pyo, S. M., Müller, R. H., Symurban smartCrystals – development of submicron suspension for enhanced dermal penetration of anti-pollution agents, #508945, American Association of Pharmaceutical Scientists (AAPS) Annual Meeting, Washington DC/USA, 4.-7. November 2018

(6) Köpke, D., Efkarpidou, A.-M., Pyo, S. M., Müller, R. H., Anti-pollution skin care – restoration of mechanical barrier by “smartLipids 2nd skin”, annual meeting of the Society for Dermopharmacy (GD), Düsseldorf/Germany, 25.-27. March 2019

(7) Almohsen, N., Köpke, D., Pyo S. M., Müller, R.H., Keck, C.M., Second-Skin SmartLipids® for advanced Corneotherapy, POS.119, annual meeting of German Pharmaceutical Society (DPhG), Heidelberg/Germany, 1.-4. September 2019.

(8) Köpke, D., Pyo, S. M., smartLipids 2nd skin – restoration and reinforcement of the skin's natural lipid film as anti-pollution strategy, POS.145, annual meeting of German Pharmaceutical Society (DPhG) Jahrestagung, Heidelberg/Germany, 1.-4. September 2019.

(9) Almohsen, N., Köpke, D., Pyo, S.M., Müller, R.H., Keck, C.M., Second Skin SmartLipids® an additional shield to the human body, 7th Galenus Workshop, Frankfurt am Main/Germany. 30. September-02. October 2019.

(10) Köpke, D., Müller, R. H., smartLipids 2nd skin Q10 – novel anti-pollution cosmetics by synergistic mechanical and molecular protection, # 713424, American Association of Pharmaceutical Scientists (AAPS) Annual Meeting, San Antonio, Texas/USA, 3.-6. November 2019

(11) Köpke, D., Olechowski, F. Müller, R. H., Pyo, S. M. Phenylethyl resorcinol smartLipids – improved chemical stability for color-stable skin brightening products, #689247, American Association of Pharmaceutical Scientists (AAPS) Annual Meeting, San Antonio/USA, Texas, 3.-6.November 2019

Acknowledgment

First of all I would like to express my gratitude to Prof. Dr. Rainer H. Müller for giving me this interesting topic, for the cherishing collaboration and for being ready to support me and always giving me the freedom to develop my own ideas at the same time.

Next I would like to thank Dr. Sung Min Pyo for co-supervision of this thesis, for her always open door and for being a steady source of mutual inspiration and a good friend.

I also would like to thank Prof. Dr. Cornelia M. Keck from the Department of Pharmaceutical Technology and Biopharmacy at the Phillips-Universität Marburg for the successful cooperation and for giving me the chance to perform my XRD experiments presented in this work. Special thanks also to Daniel Knoth, for his technical support in the performance of the XRD experiments.

I also appreciate and would like to thank Prof. Dr. Maria Kristina Parr for giving me the chance to use the GC-MS device and Dr. Jan Joseph for the technical support.

I also appreciate and would like to dignify the introduction into crucial lab techniques and administrative procedures that I received from Corinna Schmidt, Inge Volz and Gabriela Karsubke. I am grateful to all other my colleagues, first and foremost Dr. David Hespeler and Birthe Herziger, for co-inspiration, mutual support and their friendship.

And last but not least I would like to thank my friends and family. Special thanks to my girlfriend Juliana – I never found a love like yours before.

11. Curriculum Vitae

The curriculum vitae is not included in the online version for data protection reasons.